POSTGLACIAL RELATIVE SEA-LEVEL CHANGE ON THE ISLE OF SKYE AND IMPLICATIONS FOR EARLY HUMAN SETTLEMENT

Edward Rowan Jarvis Taylor

Submitted in accordance with the requirements for the degree of Master of Science by Research

The University of Leeds

School of Earth and Environment

August 2024

DECLARATION

I confirm that the work submitted is my own and that appropriate credit has been given where reference has been made to the work of others.

This copy has been supplied on the understanding that it is copyright material and that no quotation from the thesis may be published without proper acknowledgement.

The right of Edward Rowan Jarvis Taylor to be identified as Author of this work has been asserted by Edward Rowan Jarvis Taylor in accordance with the Copyright, Designs and Patents Act 1988.

ACKNOWLEDGEMENTS

ABSTRACT

Lithic artefacts found in the modern intertidal and coastal environments of northern Skye indicate Late Upper Palaeolithic human settlement in the area (Hardy et al., 2021) during the Loch Lomond Stadial. Changes in relative sea level during this period enabled the migration of these peoples around the ice margin on Skye, passing across land exposed by lower-than-present relative sea levels. Artefacts associated with these settlers have been found in amongst raised beach deposits at a site in northern Skye, some of which show evidence of reworking. Analysis is undertaken on sediment cores retrieved from an isolation basin behind the raised beach to reconstruct changes in relative sea level and palaeoenvironments, during the Postglacial and Holocene. The basal bedrock topography was mapped through a ground-penetrating radar (GPR) survey and utilised to identify suitable sites for sediment coring. The stratigraphy comprises lacustrine silts and clays at the base, followed by reed-rich clastic sediments, which are overlain by sphagnum peat. Diatom analysis reveals a distinct transition from freshwater to brackish conditions in the lacustrine deposits, dated to 8181 ± 144 years before present. Two new sea level index points and a terrestrial limiting data point are extracted from this isolation basin, the first such data from northern Skye. Bio-stratigraphic results reveal that this isolation basin was inundated by the highest tides for a sustained period during the mid-Holocene. Local patterns of relative sea level change reveal a strong possibility of a new submerged source for these reworked lithics on the shallow foreshore at the site. Additionally, data from large-scale reconstructions of relative sea levels and glacial ice extents of the Loch Lomond Stadial are used to identify possible migratory routes of these Late Upper Palaeolithic settlers.

TABLE OF CONTENTS

LIST OF FIGURES AND TABLES

ABBREVIATIONS

Abbreviation	
BIIS	British-Irish Ice Sheet
BNG	British National Grid
CD	Chart Datum
DEM	Digital earth model
dGPS	Differential Global Positioning System
EM	Early Mesolithic
GIA	Glacio-isostatic adjustment
GPR	Ground-penetrating radar
HAT	Highest Astronomic Tide
LAT	Lowest Astronomic Tide
LGM	Last Glacial Maximum
LM	Late Mesolithic
LLS	Loch Lomond Stadial
LOI	Loss on ignition
LUP	Late Upper Palaeolithic
MHWN	Mean High Water Neaps
MHWS	Mean High Water Springs
MLWN	Mean Low Water Neaps
MLWS	Mean Low Water Springs
MSL	Mean sea level
OD	Ordnance Datum
PPK	Post-processed kinematics
PSA	Particle size analysis
RSL	Relative sea level
RSS	Root sum of squares
RWL	Reference water level
SLIP	Sea level index point
TBM	Temporary benchmark
UKHO	United Kingdom Hydrographic Office

1. LITERATURE REVIEW

1.1 Introduction

The Postglacial and early Holocene witnessed major, rapid changes in relative sea level (RSL) that shaped the landscape of northwestern Scotland and the Isle of Skye (Shennan et al., 2018; Best et al., 2022). Providing quantitative constraints on the timing and elevation of RSL changes is fundamental to understanding the drivers of these changes, and how landscapes have evolved. This data can be produced by analysing coastal geomorphology and sediment stratigraphy from various landforms, in northwestern Scotland these are typically isolation basins (Shennan et al., 2006), salt marshes (Barlow et al., 2013) and coastal barrier systems (Selby and Smith, 2016). This project aims to provide new constraints on RSL and a detailed paleoenvironmental reconstruction for a site at South Cuidrach, Isle of Skye, Scotland (Figure 1.1).
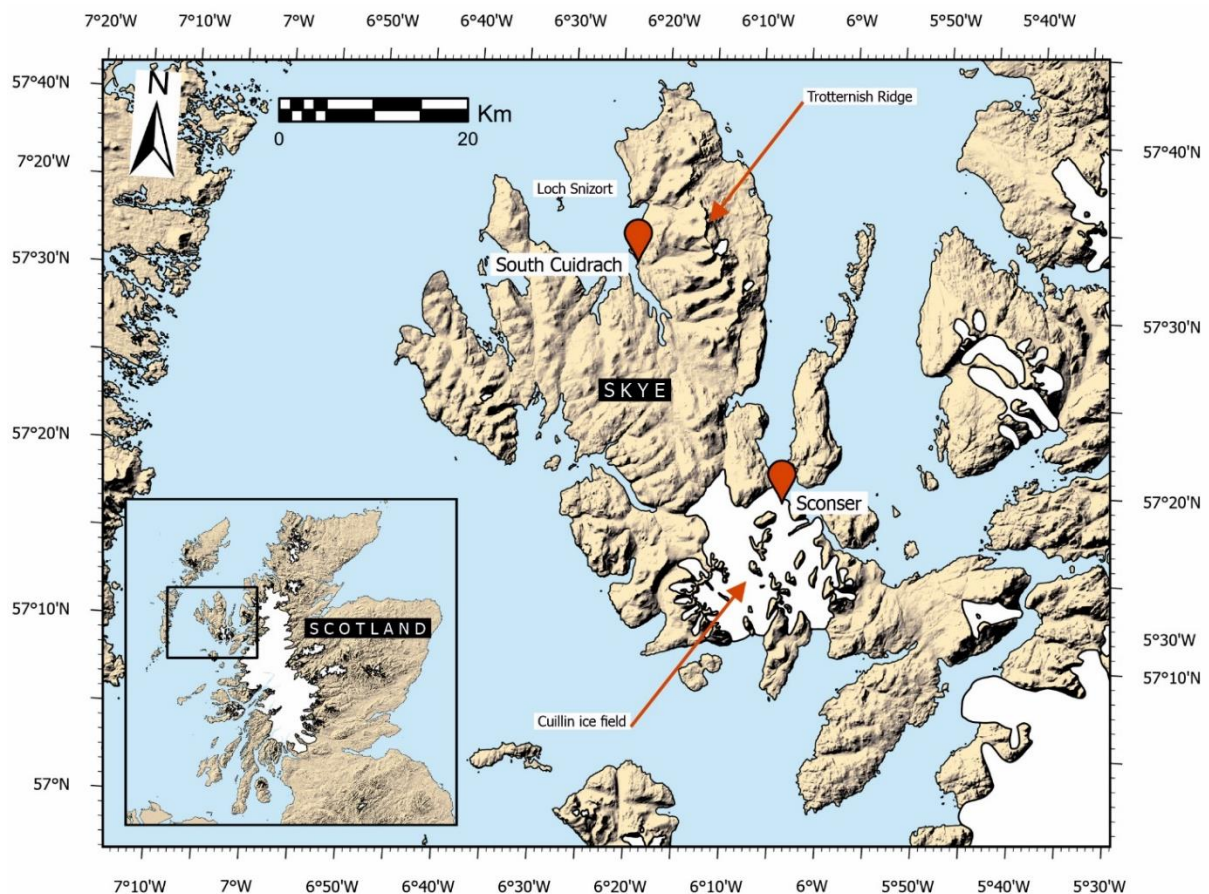
Figure 1.1. Two field sites at South Cuidrach and Sconser in the Isle of Skye, Scotland, UK. The maximum extents of the Loch Lomond Stadial ice sheet are shown in white (Bickerdike et al., 2018). Topography exaggerated 1.5X is sourced from Ordnance Survey (2024).

South Cuidrach is a small coastal site named after a nearby clachan. At this site, a Late Upper Palaeolithic (LUP) and Mesolithic archaeological presence has been identified in recent years (Hardy and Ballin, 2024). This site is a small coastal peatland fen at Loch Snizort in the north of the Isle of Skye, c. 6 km South of Uig. The site represents the northernmost presence of the Ahrensburgian LUP culture (Ballin and Saville, 2003), which inhabited much of northern Europe during the Younger Dryas (referred to in Scotland as the Loch Lomond Stadial (LLS)). Environmental and RSL changes impact the migrations and subsistence of pre-historic settlers, and so new findings at these sites will have far-reaching implications within archaeology. The integration of palaeoenvironmental data with archaeological evidence aims to build a more nuanced understanding of LUP and Mesolithic settlers at South Cuidrach. The LUP and Mesolithic periods hosted fundamental developments in the cultural evolution of humanity, which culminated in the Neolithic, whereafter hunter-gatherer lifestyles were replaced by agricultural food production (Hardy, 2016).

Stone circle artefacts with an unknown chronology or origin are investigated at a second site called Sconser, a large east-facing intertidal site c. 12 km south of Portree on Skye, first described by Hardy et al., (2021). These artefacts are intermittently submerged by the tides, creating a challenging environment for site investigations. Under the assumption that these artefacts were built above the high-tide mark, lower-than-present RSL may have enabled the construction of these artefacts. This project offers a trans-disciplinary approach to both these sites, where the interpretations of LUP and Mesolithic evidence on Skye are built upon palaeoenvironmental and RSL research outcomes.

1.2 Late-Upper Palaeolithic and Mesolithic Skye

The Late Upper Palaeolithic period (LUP) (c. 14 – 10.5 ka BP (Hardy and Ballin, 2024)) was the first in which human habitation can be identified in Scotland from archaeological records (Hardy et al., 2021), first appearing during the Bølling–Allerød post-glacial warming (c. 14.7 - 12.9 ka BP (Norris et al., 2021)). Lithics from various sites across Scotland (1.2.1) reveal details of the geographic dispersion of different people groups from this period, and their technological capabilities (Saville and Ballin, 2009; Saville et al., 2012; Ballin, 2017). On occasion in this thesis, the distinction is made between the Early Mesolithic and Late Mesolithic, the latter of which is much more widespread in Scotland and typified by more diverse and advanced technology (Lawson et al., 2023). In other instances, the overarching term (Mesolithic) is used to refer to both periods. There were various extensive Mesolithic (c. 10.5 – 5.5 ka BP (Hardy et al., 2024)) populations on the western seaboard of Scotland (Hardy and Wickham-Jones, 2002), a period with more widespread archaeological sites than the LUP in Scotland. The LUP

was typified by cold conditions during the LLS regional ice advance over northwest Scotland, whereas Mesolithic populations experienced a warming climate during the early Holocene; contrasting climatic and environmental conditions between the LLS and the early Holocene influenced the migrations and settlement of these cultures. At the beginning of the LLS, Scotland experienced a maximum drop in mean annual air temperatures of 10 °C (Golledge, 2010).

During these periods human populations appear to spread into habitable landscapes, and so the assumption is that environmental controls like terrestrial ice extent formed migratory barriers and partially determined where these people settled (Clark, 1936). If, for example, RSL were lower during the early Holocene, then it is likely that Mesolithic populations filled the available space. Equally, there is evidence that early Postglacial populations closely followed changing ice sheet margins (Wygal and Heidenreich, 2014). This thesis explores the palaeoenvironmental factors that might have controlled human migration and settlement during both the LUP and Mesolithic on the Isle of Skye.

Care must be taken when translating time-frame terminology between the disciplines of Quaternary science and archaeology, as this thesis does frequently. The Late Pleistocene is commonly defined as beginning at c. 129 ka, until the base of the Holocene (Head et al., 2021). Here, the term Postglacial is used to refer to the period following the Devensian glaciation up until the start of the Holocene. The Holocene is formally defined using the NGRIP2 Greenland ice core from 11,700 years b2k (before 2000 AD)/ 11.65 ka BP (BP = before 1950 AD), until the present day. The Early Holocene (Greenlandian stage) occurred from this date until 8.18 ka BP, 'the 8.2 ka cold event', observed using several proxies (e.g. δ^{18}O, δD) in the NGRIP1 ice record (Walker et al., 2018). The Late Upper Palaeolithic began around 14 ka BP and ended approximately at the Pleistocene/Holocene transition. The Palaeolithic/Mesolithic transition is typically defined as 11.8 ka BP (9800 BC) within archaeological literature (Ballin, 2017).

The Younger Dryas is a cold event which occurred in the northern hemisphere since the Devensian glacial period, from 12.9 to 11.7 ka in Britain. In Scotland, the Younger Dryas is known as the Loch Lomond Stadial (LLS) following Simpson (1934). During the LLS, large areas of northwestern Scotland experienced reglaciation, including the Isle of Skye. Evidence from geomorphological mapping reveals that cirque glaciers formed on the Trotternish ridge (Figure 1.1) (Ballantyne and Benn, 1994), whilst an ice field developed over southern and central Skye (Bickerdike et al., 2018) (Figure 1.1). For consistency, I quote dates as years ka BP (thousand years before present) or cal. BP (calibrated before present) for radiocarbon dates, throughout this thesis. When referencing archaeological groups, where appropriate, I use both years BC and ka BP. A table detailing the conversation between chronological periods can be found in Table 1 in the manuscript in Appendix A.

1.2.1 Late Upper Palaeolithic and Mesolithic Cultures

Continental Europe has a well-established record of LUP archaeology, where groups are differentiated by the type and shape of lithic artefacts they used (Terberger, 2006), referred to as 'industries' or 'lithic industries'. However, few of these industries had been identified in Scotland until recently (Saville and Ballin, 2009; Saville et al., 2012; Ballin, 2017; Hardy and Ballin, 2024). The migration of these peoples into northern Britain was the result of lower-than-present RSL across what is now the North Sea (Gaffney et al., 2008). Although sparse artefacts have been found over Doggerland, the main evidence of these migrations is from a series of sites in Scotland, occurring both before and during the LLS (Figure 1.2) (Saville and Ballin, 2009; Ballin, 2018; Hardy et al., 2021).
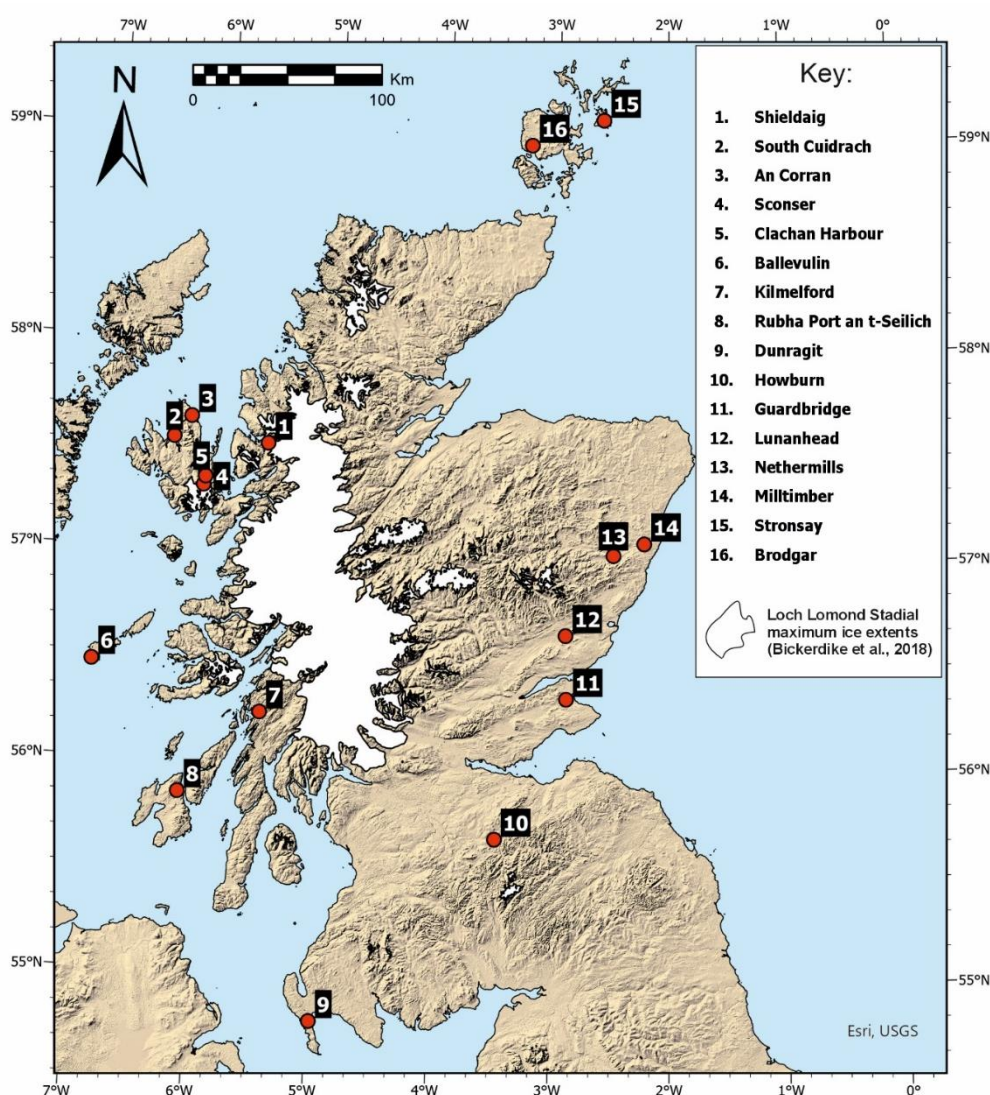
Figure 1.2. Late Upper Palaeolithic findspots in Scotland (adapted from manuscript in Appendix A). Includes maximum LLS ice extents from Bickerdike et al., (2018). Open-source topography from Ordnance Survey (2024).

Three major Late Upper Paleolithic (LUP) industries are found in Scotland. The earliest inhabitants evidenced in Scotland are the Hamburgian 'reindeer hunters,' who appear around 12,700 BC (14.65 ka BP) at Howburn, South Lanarkshire, in an extensive lithic assemblage corresponding to cultures from the same period in Denmark and Northern Germany (Ballin, 2018). The Federmesser-Gruppen culture is roughly contemporaneous with the Ahrensburgian culture, found at various sites, particularly coastal ones, in northwestern Scotland. The Federmesser-Gruppen culture (Saville and Ballin, 2009) appears earlier, with an onset around 12,000 BC (13.95 ka BP), than the Ahrensburgian culture (Ballin and Bjerck, 2016), which began around 10,800 BC (12.75 ka BP). Given this chronology, the later of these cultures was impacted by the rapid climate change at the start of the Younger Dryas. Hardy and Ballin (2024) state, "The severity and speed of these temperature changes were such that it would have required notable adaptive capabilities for populations in Scotland to survive." South Cuidrach represents the northernmost site in Britain where Ahrensburgian lithics have been found (Appendix A). The extent and timing of LUP habitation in Scotland remain unclear, as sites where artefacts are found are few and far between (Ballin et al., 2009, 2017, 2018).

At the start of the Holocene, a different array of cultures associated with the Mesolithic inhabited Scotland, reflected by a change in lithic technology. Younger lithics tend to be smaller in size and manufactured using different techniques (Ballin, 2018). These populations are known to have inhabited mainly coastal areas (Hardy and Wickham-Jones, 2002) and made many adaptations to their technology and dispersion in response to a rapidly changing climate (Walker and Lowe, 1990; Hardy et al., 2021). As with the LUP, research into the extent and the permanency of Mesolithic inhabitation in Scotland leaves much to be resolved (Hardy and Ballin, 2024). At South Cuidrach, there is an assemblage of lithics from multiple pre-historic periods.

1.2.2 South Cuidrach Archaeology

For some years before excavation, Late Mesolithic artefacts were found on the foreshore at South Cuidrach, a small embayment on the western side of the Trotternish Peninsula (Figure 1.1). Following the investigations by Hardy et al., (2021, 2024), lithic material representing various LUP and Mesolithic groups have been identified. These are differentiated by the forensic analysis of their size and shape, and by understanding their depositional and archaeological context. Varying technological uses of these lithics provide further data which also helps researchers to ascribe them to specific industries (Ballin, 2018).

Lithics were retrieved both from the surface of the modern beach and embedded within the raised beach deposits in front of the peat fen (this peatland is designated a 'fen' after (Joosten and Clarke,

2002)) (Figure 1.3). Within the raised beach, there are lithics associated with two different periods (Figure 1.4). The overlying poorly sorted, sand/clay matrix-supported section contains LUP artefacts, and the well-sorted, sand matrix-supported, well-rounded cobble section beneath contains Mesolithic artefacts (Hardy and Ballin, 2024). These researchers observed that the stratigraphy present at these locations is counter-intuitive, with older lithic artefacts embedded in the upper section of the raised beach, and younger artefacts embedded beneath (Figure 1.4). This photo of the sedimentary succession containing the lithics (Figure 1.4) was exposed by the digging of a farm track and can be located in Figure 1.3 amongst the 'Main lithic scatter'.

Figure 1.3. Aerial drone photo showing the main features of interest at the South Cuidrach (Figure 1.1) field site. Photo is from Hardy and Ballin (2024). Main archaeological lithic scatter (blue) within raised beach deposits (black). The peat fen (yellow) is the focus of the environmental reconstruction undertaken in this thesis.
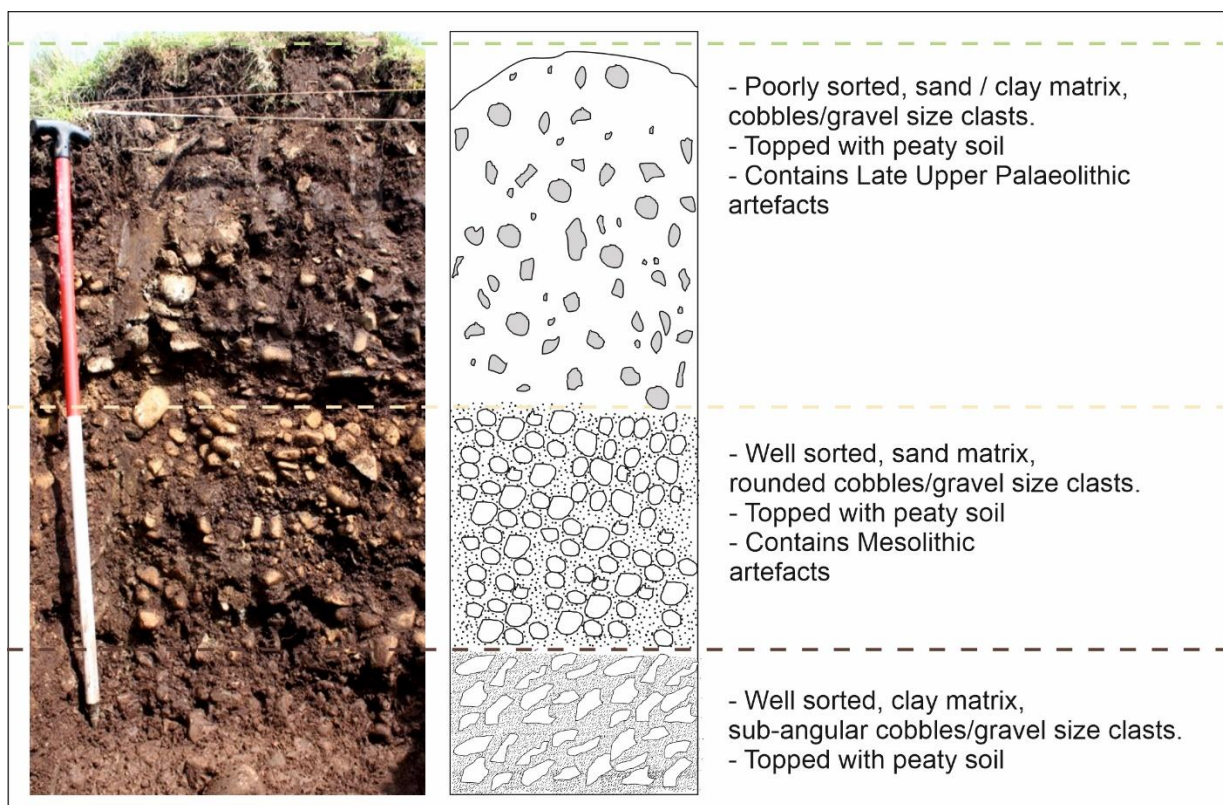
Figure 1.4. Lithological diagram adapted from unpublished field data from Professor Karen Hardy (Hardy et al., 2021). Shows a cross-section through a test pit within the raised beach at South Cuidrach. The location of this succession is noted 'main lithic scatter' in Figure 1.3.

The source material for these lithics is a baked mudstone, which was likely retrieved by LUP settlers from the nearby An Corran, in Staffin Bay (Figure 1.2). This is a headland on the Eastern side of the Trotternish peninsula, 15 km from South Cuidrach. This source material is a widely used material for toolmaking amongst Mesolithic settlers for its flaking properties (Hardy, 2016).

The LUP artefacts are found scattered along the modern foreshore and in the upper section of the raised beach deposits (Figure 1.4, and Figure 2 of the manuscript in Appendix A). The LUP lithics are distributed widely and are clearly not in situ (Hardy and Ballin, 2024). Some of the LUP lithics show evidence of rolling, which along with their distribution, has led researchers to conclude that they have been reworked from their original context. When placed in the context of RSL change on the Isle of Skye over the Postglacial and Holocene (1.4.4), Hardy and Ballin (2024) discuss the possibility that these artefacts have been transported from a now-submerged nearby site at a time of lower-than-present RSL. This was theorised when bathymetric data from the United Kingdom Hydrographic Office (UKHO) revealed a large gently sloping intertidal and sub-tidal zone at South Cuidrach (Figure 1.5).
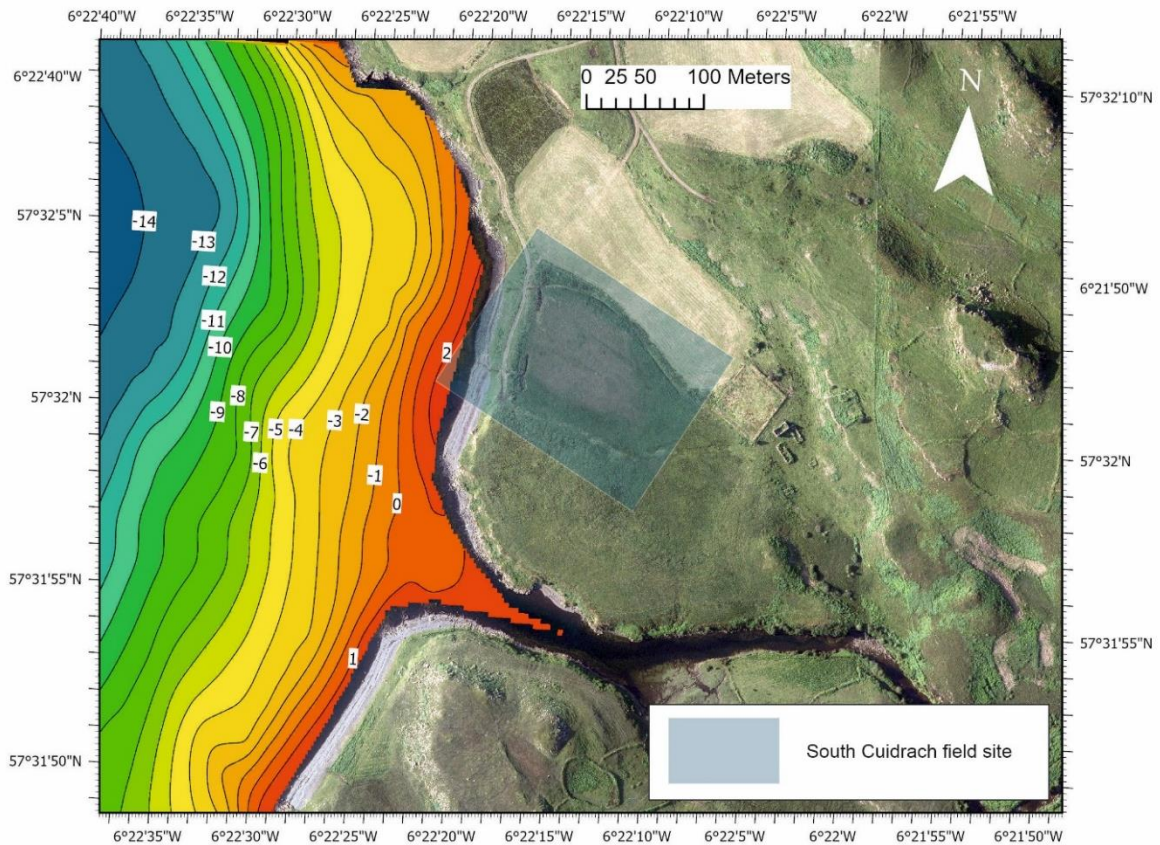
Figure 1.5. Gently sloping bathymetry at South Cuidrach. Aerial photography from © Getmapping Ltd (2024). Bathymetric data is converted to m OD (© British Crown and OceanWise (2024). All rights reserved. Licence No. EK001-20180802. Not to be used for Navigation).

1.3 The Glaciation of Northwestern Scotland and Skye

After first discussing the archaeological aspects of the South Cuidrach site, this section offers an overview of the glacial history of Scotland and the Isle of Skye, addressing a crucial element of the environmental and RSL changes that have taken place since the Last Glacial Maximum (LGM).

1.3.1 The British-Irish Ice Sheet

A complex pattern of climatic forcings including Earth orbital changes, greenhouse gas concentrations and ice sheet growth combined during Marine Isotope Stage (MIS)2, culminating in a maximum global mean cooling of between −6.5 and −5.7 °C at the LGM (Tierney et al., 2020) between 26 and 20 ka BP. The coalescing of the Fennoscandian and the British-Irish Ice Sheet (BIIS) resulted in an ice sheet which

engulfed most of northern Europe including Scotland at the LGM. The LGM occurred in Scotland at 26 - 24 ka BP (Clark et al., 2022) (Figure 1.6). During the growth of the BIIS in northwestern Scotland, the uplands of the inner Hebridean islands, including Skye, acted as centres of ice dispersal (Ballantyne and Small, 2019), diverting the flow of the BIIS which terminated at the edge of the continental shelf (Bradwell and Stoker, 2015). Subsequent deglaciation in NW Scotland corresponded with a global average temperature increase late in MIS2 at c. 19 ka BP (Clark et al., 2022). Northwestern Scotland lies where the BIIS accumulated its greatest thickness (>750 m) and mass (Bradley et al., 2011; Shennan et al., 2018; Clark et al., 2022),
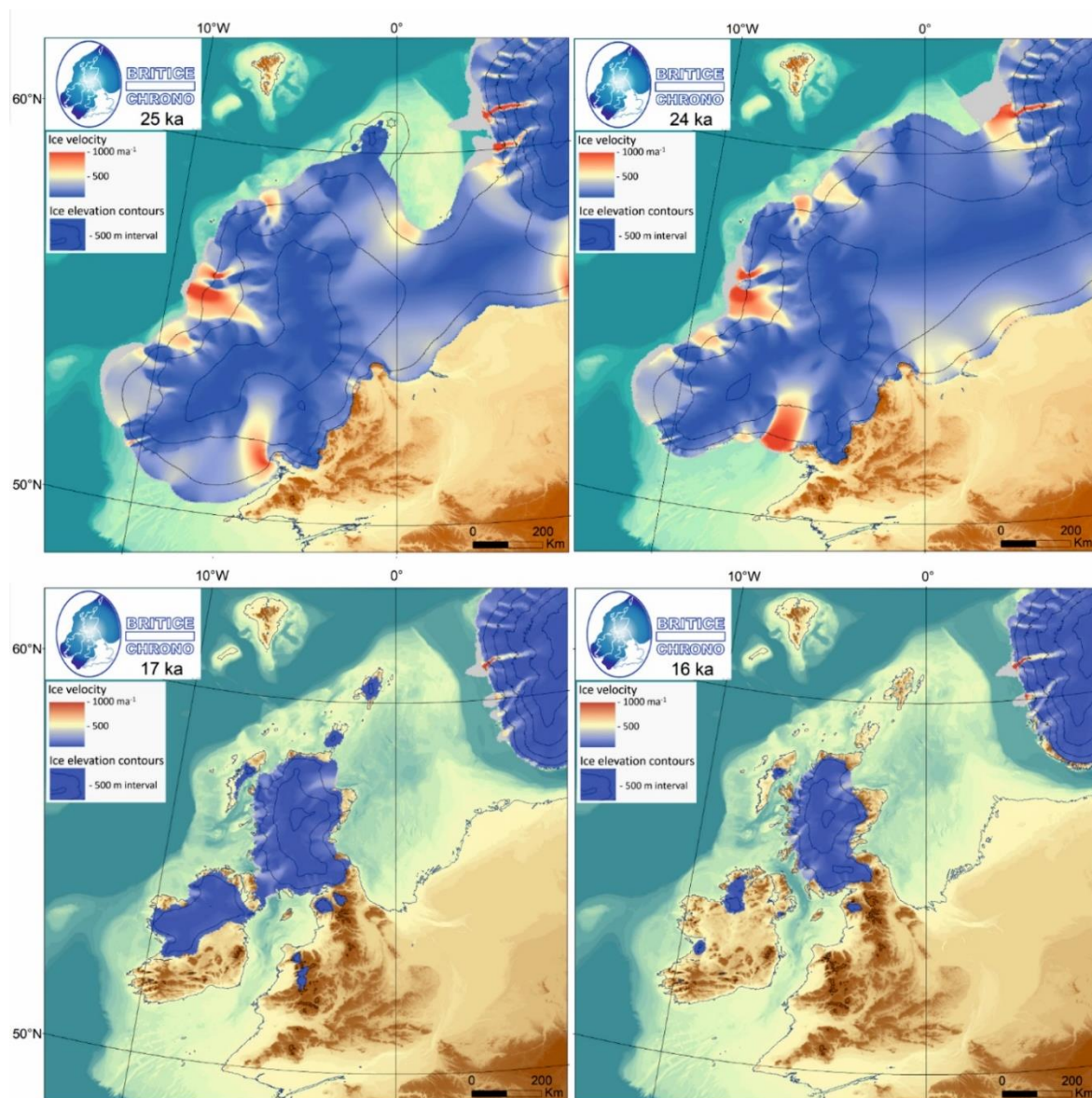
Figure 1.6. Reconstructions of; ice sheet extent; ice surface elevations; ice velocity; palaeotopography; and coastline position associated with the BIIS from the Britice-Chrono model (Clark et al., 2022) at 25, 24, 17 and 16 ka BP.

The deglaciation of Skye occurred at different times across the island. To the north and east of Skye, rapid ice sheet retreat of the Minch Ice Stream occurred between 17.6 and 16.4 ka (Figure 1.6), in part controlled by changes in RSL (Simms et al., 2022). The Trotternish peninsula, particularly on its west coast, experienced deglaciation earlier than in the southern and eastern upland areas of Skye (Figure 1.6). The Trotternish Peninsula was likely ice-free as early as 18.5 ka (Bradwell et al., 2021). Mainland ice from the BIIS was deflected by an independent ice dome forming around the Cuillins in the south and centre of the island (Bickerdike et al., 2018). During the period following the LGM and up until the Holocene, referred to here as the Postglacial, climatic fluctuations resulted in further patterns of glacial advance and retreat in Scotland.

1.3.2 Younger Dryas (the Loch Lomond Stadial)

Following the Bølling-Allerød interstadial warming (14.7 – 12.9 ka BP) (Naughton et al., 2023), the LLS hosted the development of an icefield on Skye (Figure 1.1), which covered an area of 150 km^2 (Bickerdike et al., 2018). Skye remained a persistent and independent centre for cold-based ice after deglaciation following the BIIS (Ballantyne and Small, 2019), but was free of ice-sheet cover by 15 ka (Clark et al., 2022). A wide range of geomorphological and sedimentological evidence exists which supports the re-glaciation of the Cuillin mountains and the Kyleakin Hills during the LLS (Ballantyne, 1989) (Figure 1.1). Although, chronological constraints on the precise timing of the LLS on Skye are limited. Revised [10]Be ages for a glacial erratic at Coire Fearchair (10 km southeast of Sconser) suggest the cirque was glaciated at 12.5 ± 0.3 ka BP (Bromley et al., 2023). Figure 1.1 shows the LLS cirque glaciers on the Trotternish peninsula, to the east of the Trotternish ridge at c. 11 – 10 ka (Ballantyne, 1990). Nevertheless, most northern and western areas of Skye, which are characterised by lower elevation compared with the Cuillins and Trotternish ridge, remained ice-free, and there were no ice caps in these areas.

Over the mainland, the Western Highland Glacier complex would have been a significant barrier to human migration across Scotland during the LLS (Hardy et al., 2024), stretching c. 200 km from north to south (inset Figure 1.1), covering an area of over 9000 km^2 (Bickerdike et al., 2017). Glaciation of different areas of Scotland during the LLS is unlikely to have occurred simultaneously and at the same rate (Palmer et al., 2020). The growth and retreat of Scotland's ice sheets during the LGM and Postglacial contributed to a complex pattern of RSL change in the region.

1.4 Postglacial and Holocene Relative Sea-Level changes

1.4.1 Drivers of Relative Sea Level Change

Following the LGM, local and global changes in terrestrial ice mass resulted in a complex pattern of RSL change in Scotland and across the Isle of Skye (Shennan et al., 2018; Best et al., 2022; Simms et al., 2022). Rising global barystatic (formerly termed eustatic) sea level resulting from the melting of far-field ice sheets (Fairbanks, 1989) occurred alongside glacio- and hydro-isostatic adjustment of the Earth's crust due to the redistribution of mass from melting ice sheets (Peltier and Andrews, 1976). Changes in the earth's gravity field also due to redistribution of mass from melting ice sheets further impact RSL patterns in Scotland (Peltier, 1998).

Global ocean volume increases (or decreases in the opposite case) due to the addition of water which has been redistributed from terrestrial ice masses or stored on land (or in the atmosphere in comparatively tiny amounts) is known as the barystatic component of RSL (Gregory et al., 2019). Barystacy, along with the thermal expansion of ocean water due to increasing temperatures (Llovel et al., 2023), is a main cause of contemporary increases in global mean sea level (Chen et al., 2017). Widespread deglaciation following the LGM (1.4.4) resulted in an increase in global ocean volume (Lambeck et al., 2014). However, RSL patterns over this period at near-field sites are usually non-monotonic since the LGM because of perturbations to the lithosphere and mantle.

Perturbations in the solid Earth in response to the loading and unloading of ice masses, termed glacio-isostatic adjustment (GIA), create vertical land movement which causes changes in RSL (Bradley et al., 2011; Shennan et al., 2018; Simms et al., 2022). Isostasy refers to the concept that deformation occurs to return the solid Earth to a state of equilibrium in response to glacial ice-mass changes (Gregory et al., 2019). The elastic properties of the Earth's crust result in rapid recovery following these ice-mass changes (Khan et al., 2015). In contrast, the viscoelastic upper mantle returns to an equilibrium over much larger, typically millennial timescales (Farrell and Clark, 1976). As distance increases from the sites of glaciation centres, the effects of GIA on RSL are decreased, particularly the direct effects of ice mass change. As a result, records of RSL change in equatorial regions show a lesser impact of GIA compared with higher latitudes (Woodroffe and Horton, 2005; Milne et al., 2005). RSL change at lower latitudes since the LGM is also characterised by a gradual fall in the ocean surface due to 'equatorial ocean syphoning', which is the loading of ocean basins following an increase in global ocean volume from glacial meltwater (Milne and Mitrovica, 2008). Isostatic deformation of the solid Earth can result in lateral flow of the mantle, causing subsidence in near-field locations, and uplift around the periphery

of the ice load (intermediate field locations) during ice loading, and the reverse during deglaciation (Figure 1.7) (Kemp et al., 2013; Khan et al., 2015).

Another key component of RSL change is gravitational change. The sea surface is instantaneously coincident with the global geoid; an equipotential surface of the gravitational field, and so RSL changes occur in response to large-scale displacements of the solid Earth (Peltier, 1998; Shennan et al., 2018). These changes are termed 'deformation of the ocean geoid' and are important on both short and long time scales.
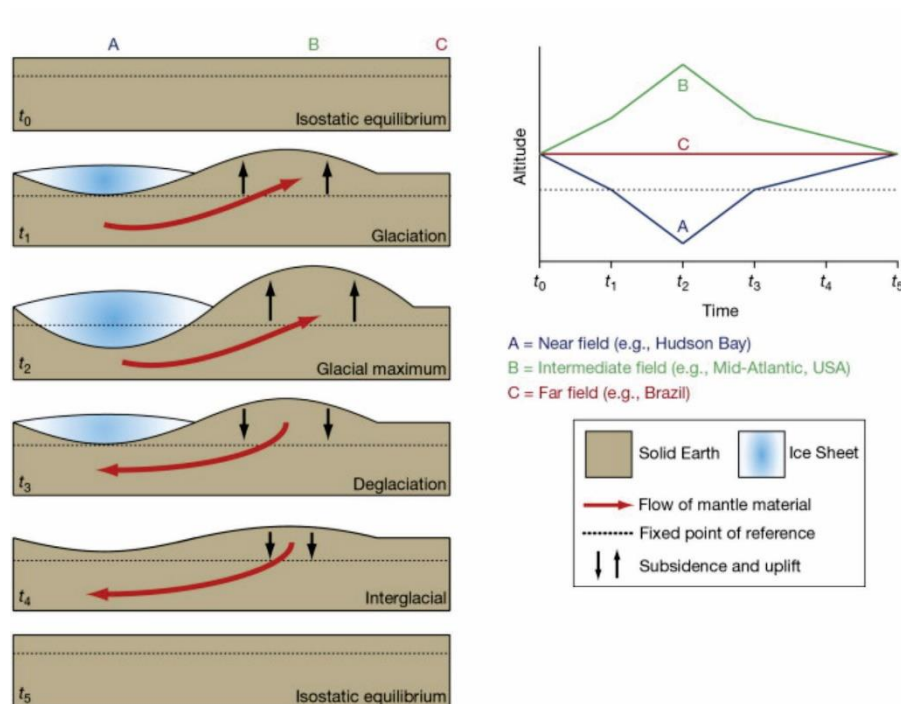
Figure 1.7. Schematic diagram of the glacio-isostatic adjustment caused by continental ice sheets at near, intermediate, and far-field locations. Adapted from Figure 1 of Kemp et al., (2013).

1.4.2 Reconstructing Relative Sea Level

Processes which act at the modern shoreline around the globe are currently creating a geological record of modern mean sea level (MSL). A change in RSL, driven by the processes described above, can sometimes be inferred by investigating similar features of the geological record which appear at a higher or lower elevation from present sea levels (Rovere et al., 2016). Indicators of past sea levels can arise from geomorphic, sedimentary, archaeological, or biological features. Mechanical wave action, chemical and biological weathering can produce notches which serve as sea level indicators in rocky

shorelines (Long, 2001). Coastal sediment stratigraphy often preserves changes between terrestrial and marine depositional environments, and bio-stratigraphic indicators of sea-level change such as diatoms and foraminifera (Long et al., 2011). Coralline microatolls have been used extensively in RSL research, and are particularly effective at delineating RSL change in the tropics over the Late Holocene (Hallmann et al., 2020). Submerged archaeological artefacts can also provide time or elevation constraints on RSL changes under certain conditions (Benjamin et al., 2017).

Indicators to be used as a proxy for RSL should have an indicative meaning, which includes a reference water level, an indicative range, an elevation and an age (all with associated uncertainties) (Shennan and Horton, 2002). The indicative range is 'The vertical range over which the indicator occurs at present' (Shennan, 2015). The indicative meaning is often determined using a modern analogue, such as the position in which a geomorphological feature is found in the modern environment with respect to modern tidal levels (e.g. Shennan et al., 1994). However, tidal ranges will have changed in the past and one of the ongoing challenges in RSL research is to incorporate palaeo-tidal data into RSL reconstructions (Ward et al., 2016). Methods for dating RSL changes depend on the age range and context of the reconstruction in question. Radiocarbon is typically used to build chronologies in settings where a suitable carbon source is found and up to an age of ~50,000 years, making it very suitable in the Postglacial and Holocene (Woodroffe et al., 2015).
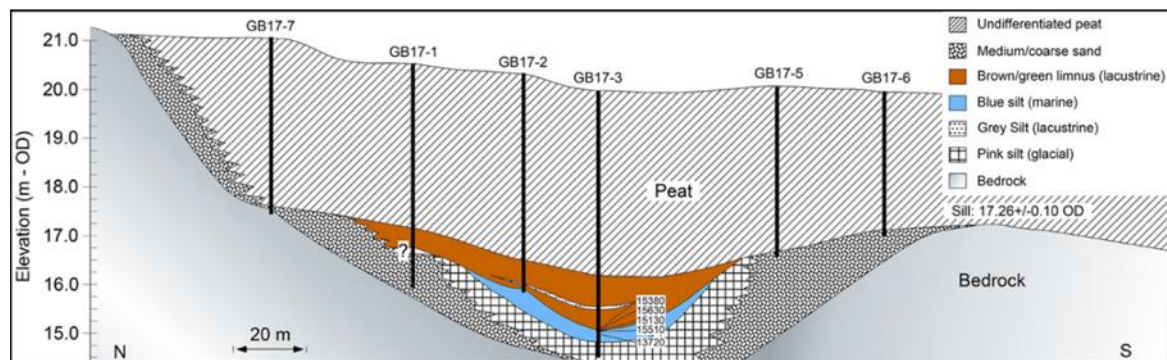
Figure 1.8. A schematic showing typical stratigraphy of an isolation basin from NW Scotland, and the elevation of the sill (the ingression point of the isolation basin) on the right. Adjusted from Simms et al., (2022), Figure 3.

In northwestern Scotland, some of the best records of past sea levels come from isolation basins (Figure 1.8). These are topographic depressions where the internal sediment stratigraphy contains an archive of past sea level changes, due to having been inundated one or more times in the past (Shennan et al., 2005; Selby and Smith, 2016; Smith et al., 2019). High-resolution records of RSL change since the LGM in Scotland have been achieved using mainly data from isolation basins at sites like

Arisaig in Inverness-shire (Shennan et al., 1993, 1994, 1999, 2000, 2005). These features are easily measured against a vertical datum because their ingression and isolation from the sea are controlled by the minimum elevation of the bedrock at the sill/point of ingression, making them highly effective in providing spatial and temporal constraints on RSL change (Long et al., 2011).

A marine regression for example, driven by a fall in RSL, might result in the following sedimentary sequence within an isolation basin (Figure 1.8). Firstly, there is a period of continuous marine influence in the basin characterised by deposits of marine clays/sands. Water conditions are saline, and this is reflected in the biostratigraphy through diatom and foraminifera species. Subsequently, as RSL falls, the basin becomes intertidal, and the marine deposits become intermittent. Water conditions become brackish and support respective biostratigraphy, as the basin is only inundated during the highest tides or storms. Finally, an isolation basin may have only freshwater input, preserved through terrestrial lacustrine sedimentology and freshwater indicator species in the biostratigraphy. Similar sequences have been found in isolation basins from various regions which were glaciated during the last glacial period with favourable hard-rock bedrock topography, such as Scotland, Norway and Greenland (Shennan et al., 1994; Long et al., 2011; Simms et al., 2022). Indicators such as isolation basins have been fundamental to building large-scale simulations of GIA (Bradley et al., 2011).

1.4.3 Glacio-Isostatic Adjustment Modelling

The first quantitative models of sea-level change were pioneered in the 1970s (Farrell and Clark, 1976; Peltier and Andrews, 1976) providing the foundation for GIA modelling today. In Britain and Ireland, several recent GIA models have made improvements to the field of research, building on the wealth of RSL data points associated with the advance and retreat of the BIIS as well as global ice sheet changes (Bradley et al., 2011; Clark et al., 2022). GIA models use either empirical reconstructions of ice sheet change or physics-based numerical models and iteratively alter them to fit RSL data points (Bradley et al., 2011; Kuchar et al., 2012). More recent research has attempted to end the circularity of this approach by testing different scenarios of ice-sheet extent and thickness from large-scale ice-sheet reconstructions (Clark et al., 2022) against RSL databases (Bradley et al., 2023).

The variety and quantity of RSL data points have greatly improved as this field of research has grown in recent years (Shennan et al., 2018). Improvements in the quality of new RSL data points come from technical advancements in different fields. For example, microfossil-based transfer functions which enable researchers to quantitatively reconstruct palaeo-marsh elevations and their uncertainties (e.g. Barlow et al., 2013). The chronologies of various RSL data points have been refined over time through advancements in methodologies, such as the shift from bulk to accelerator mass spectrometer (AMS)

[14]C dating, along with updated age calibration models (Reimer et al., 2020), leading to further improvements. Large uncertainties remain in past global and regional ice volumes (Pollard et al., 2023) which are a key input to GIA models, and improvements to the future of GIA modelling will come from the incorporation of improved ice-sheet reconstructions like the BRITICE-CHRONO reconstruction (Clark et al., 2022). GIA modelling has been used to improve understanding of the rheological properties of the solid Earth (e.g. Lloyd et al., 2024), but the complex structure of the lithosphere means that future GIA modelling should incorporate Earth models which account for, for example, lateral variations in the thickness of the lithosphere (Nield et al., 2018). Most GIA models have typically included earth models which consider only vertical changes in the thickness of the lithosphere (Whitehouse, 2018). Such improvements may result in better data-model fit and constraints on the drivers of RSL change.

1.4.4 Relative Sea Level Patterns at South Cuidrach and Sconser

Different processes dominate at different points in time to cause RSL changes on Skye, resulting in a highly non-monotonic pattern of RSL change (Shennan et al., 2018). Data from the BRADLEY2011 GIA model (Bradley et al., 2011) is shown in Figure 1.9 which illustrates the main patterns of RSL changes expected by the GIA model at the two study sites in this thesis. The model outputs in Figure 1.9 reflect the interplay between the global meltwater influx and glacio-isostatic rebound on the Isle of Skye. This GIA model has a high grid resolution of 70 km^2 (Bradley et al., 2011), however, it is tested against very few data points from northern areas of Skye. The results above are mostly constrained by data from southern Skye (e.g. Selby and Smith, 2016) and an RSL curve for Skye based on empirical data is a key target for future research (Best et al., 2022).

Several key events which are incorporated into the BRADLEY2011 model are observed in the RSL outputs for Sconser and South Cuidrach (Figure 1.9). When the BIIS retreated from northern Skye at c. 17 ka (Clark et al., 2022), a sharp drop in RSL of c. 15 m occurred, such that RSL fell below 0 at both sites in Figure 1.9. The period of low RSL between c. 15 – 10 ka is punctuated by a spike following 14 ka in both model outputs. This is because the barystatic curve incorporated into the model includes the meltwater pulse 1A (MWP1A) event at c. 14 ka (Clark et al., 1996), which outpaces the rate of isostatic land-level uplift at both sites. The sharp increase in global meltwater discharge of MWP1A is well documented in far-field sites (Deschamps et al., 2012), but its magnitude and source have been disputed over the years (Fairbanks, 1989; Peltier, 2005; Gregoire et al., 2016; Lin et al., 2021) although it has long since been widely associated with a global trend of deglaciation caused by the Bølling warming at 14.6 ka BP (Fairbanks, 1989). Although isolation basin records in Scotland show limited detail in the evidence for the RSL rise associated with MWP1A, they do provide an upper limit of the

magnitude of these changes (Bradley et al., 2011; Shennan et al., 2018; Best et al., 2022). Lin et al., (2021) suggest there is a high likelihood that MWP1A is caused by a rapid increase in meltwater from northern hemispheric ice sheets. Further empirical field data from northwest Scotland is needed to evaluate the magnitude of the MWP1A RSL event on Skye (Best et al., 2022).
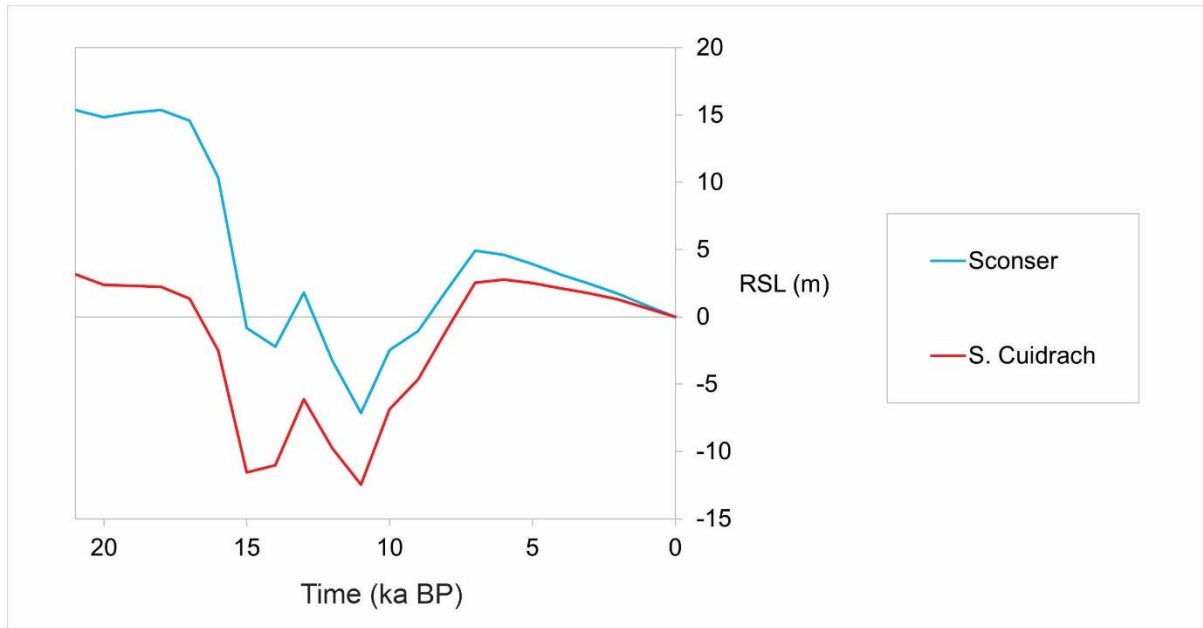
Figure 1.9. GIA model predictions of RSL change over the last 21 ka for two sites on Skye, which are the subject of this study; Sconser (57°18'51"N, 006°05'25"W) and South Cuidrach (57°32'01"N, 006°22'19"W). These are identified in Figure 1.1. Data was exported using the PALTIDE tool (Ward et al., 2016; Scourse et al., 2024) into which the GIA model from Bradley et al., (2011) is incorporated.

The increased global meltwater input associated with the 8.2 ka climate event (Daley et al., 2011) also contributed to the start of rapid mid-Holocene barystatic sea-level rise. North Atlantic cooling disrupted the Atlantic meridional overturning circulation, resulting in reduced heat transport to the northern Atlantic (Barber et al., 1999). This meltwater input occurred due to several key meltwater events during the ablation of the Laurentide ice sheet (Rush et al., 2023) and resulted in rapid global sea-level rises. The GIA model shows that RSL rose above present levels in the mid-Holocene at both sites in Figure 1.9. This was caused by a period in which barystatic RSL rise from ice melt outpaced the GIA process, rising to a high stand which peaked at c. 6 – 7 ka BP (the mid-Holocene highstand). GIA models (Figure 1.9) predict that global meltwater input continued to decline following the mid-Holocene highstand (Shennan et al., 2018), but the main driver of RSL change on Skye following this

highstand is the GIA process, as following c. 6 ka, RSL in Skye falls driven by glacio-isostatic uplift (Selby and Smith, 2016; Shennan et al., 2018).

Sconser is closer to the mainland and south Skye glaciation centres than South Cuidrach (Figure 1.1), and as with other sites closer to the main ice load centres of the mainland and Cuillin mountain range, such as Arisaig (Shennan et al., 1994). This results in higher RSL at Sconser than at South Cuidrach, and more rapid GIA response following the LGM and following the LLS. This GIA model (Figure 1.9) estimates that RSL at Sconser regressed c. 22 m following deglaciation until the lowstand at 11 ka, compared with c. 15 m at South Cuidrach (Bradley et al., 2011). These data offer useful insights into the likely trajectory of RSL changes at both sites over the Postglacial and Holocene, however as previously stated modelled RSL in northern Skye has significant limitations. New empirical data from South Cuidrach may offer insights into both RSL changes and archaeology.

1.5 Research Objectives

This project aims to provide context for the archaeological artefacts at South Cuidrach, analysing the sedimentary succession within the peat fen to produce a palaeoenvironmental reconstruction of landscape and coastal changes. To understand the conditions which enabled the migration of LUP and Mesolithic populations to the site I aim to gain a holistic picture of their environmental setting. This is achieved using a multiproxy approach which couples the sea level reconstruction with subsidiary data about local vegetation changes. RSL changes may have been key to facilitating LUP and Mesolithic migrations to and from the site (Appendix A), and their inhabitation of South Cuidrach. Accurate constraints on RSL change at South Cuidrach aim to improve our understanding of these migrations/settlements. Intertidal artefacts may be able to offer approximate constraints on RSL changes at the site. Conversely, RSL reconstructions from GIA modelling may be useful in understanding the time frame in which these artefacts were built.

The background outlined in this chapter has led to the formation of the following overarching research question, which this thesis aims to answer: **How did relative sea level and environmental changes on the Isle of Skye affect the migrations of Late Upper Palaeolithic and Mesolithic humans?** I address this question through three main research objectives:

1. Reconstruct changes in RSL during the Postglacial and Holocene at South Cuidrach.

RSL changes in northern Skye are poorly constrained (Best et al., 2022), and therefore this thesis aims to address this spatial data gap. Diatom assemblages within sediment cores taken from the peat fen at

South Cuidrach will be analysed to understand changes in salinity throughout the sedimentary succession, with the aim of reconstructing changes in RSL. A dGPS survey of the site will define geomorphological features against Ordnance Datum, so that any changes can be compared to modern mean sea level. Analysing Loss on Ignition (LOI) and pollen assemblages from sediment cores also aims to identify RSL changes, relying on a chronology from radiocarbon dates. Ground-Penetrating-Radar (GPR) and dGPS elevation survey techniques will be used to understand the geomorphology, and precisely measure the elevations of features.

2. Investigate how the environment has changed over the Postglacial and Holocene at South Cuidrach.

By conducting a pollen analysis on a sediment core retrieved from the peat fen at South Cuidrach I aim to describe local vegetation changes. Inferences of changes in climate and RSL may also be made from these data. Skye has a well-established pollen record for the Postglacial and Holocene, so abundances of specific taxa may provide further chronological information for the peat fen. Vegetation changes will be considered alongside analysis of the lithology within the sediment core. Once key events are identified from the biostratigraphic analysis of the sediment cores, radiocarbon dating will provide absolute ages for events.

3. Determine how changes in RSL impacted the construction of currently intertidal artefacts at Sconser, Isle of Skye.

Presently intertidal archaeological structures (currently, dates for the building of these artefacts are unknown) must have been constructed during a period in which they were not inundated by the tide (Hardy et al., 2021). RSL reconstructions may be used to provide an approximate chronology for their construction. The artefacts may act as a limiting point in RSL under the assumption that these artefacts were built above the highest tides at that time (approximate HAT). A dGPS survey provides precise elevations for these artefacts (relative to OD) for comparison with present sea levels and RSL predictions for the Postglacial and Holocene in northern Skye.

To conclude this chapter, the necessary background and literary context for this research has been laid out, along with key research aims to address. The following chapter outlines the methodology used to study South Cuidrach, whereas the methodology/results from Sconser are found in Chapter 4.

2. METHODOLOGY

This chapter outlines the methods used in this study to identify RSL and reconstruct environmental change at South Cuidrach. It includes descriptions of each field and lab technique used in this project.

2.1 South Cuidrach Fieldwork

2.1.1 South Cuidrach Site Description

The South Cuidrach field site is situated above a small bay adjoining Loch Snizort; just north of the mouth of the Hinnisdal River, at which the Glen Hinnisdal ends (Figure 2.1). Loch Snizort is a tidal sea loch in the northwestern corner of the Isle of Skye with a maximum depth of c. 100 m, lying between the Trotternish peninsula and the Waternish Peninsula. The loch joins onto the Lower Minch to the northwest, a strait that separates the Inner and Outer Hebrides. The seaward side of the South Cuidrach field site faces northwest. It consists of 1.2 hectares of roughly level peat fen that is elevated above the vegetation/modern beach transition mark and situated behind a cobble beach. Glen Hinnisdal lies between the site and the Trotternish ridge, which runs north to south along the Trotternish peninsula. The site is surrounded by cattle-grazed farmland, although the peat fen itself is too wet for agricultural use. The peat fen is fed by a small stream which drains directly into Loch Snizort. There are exposed bedrock crags 100 m to the east of the fen. A small farm track runs along the shoreline side of the raised beach, which was used to access the site (Figure 2.2).

The vegetation in the surrounding grazed farmland is coastal grassland typical of Skye's temperate climate, including various species of grasses and sedges. The peat fen within the topographic depression (or bedrock basin) at South Cuidrach is covered with sphagnum mosses, which contribute to the formation of peat (Langdon et al., 2005), and are visible in Figure 2.2. The site is not presently a woodland, although sparse trees and shrubs are found close by, particularly gorse and heathers. The temperate, maritime climate is characterised by mild temperatures and abundant rainfall. Moderated by the North Atlantic, Skye experiences average winter temperatures of 1 – 7 °C, and summer temperatures of 10 – 15 °C. Annual precipitation averages 1700 mm (Met Office, 2024). Loch Snizort is described as macrotidal as the mean spring range is between 4 and 6 m. The current mean sea level (MSL) at Uig is 3.03 m Chart Datum (CD) (0.33 m Ordnance Datum (OD)) and the spring tidal range is 4.6 m (Table 2.1).
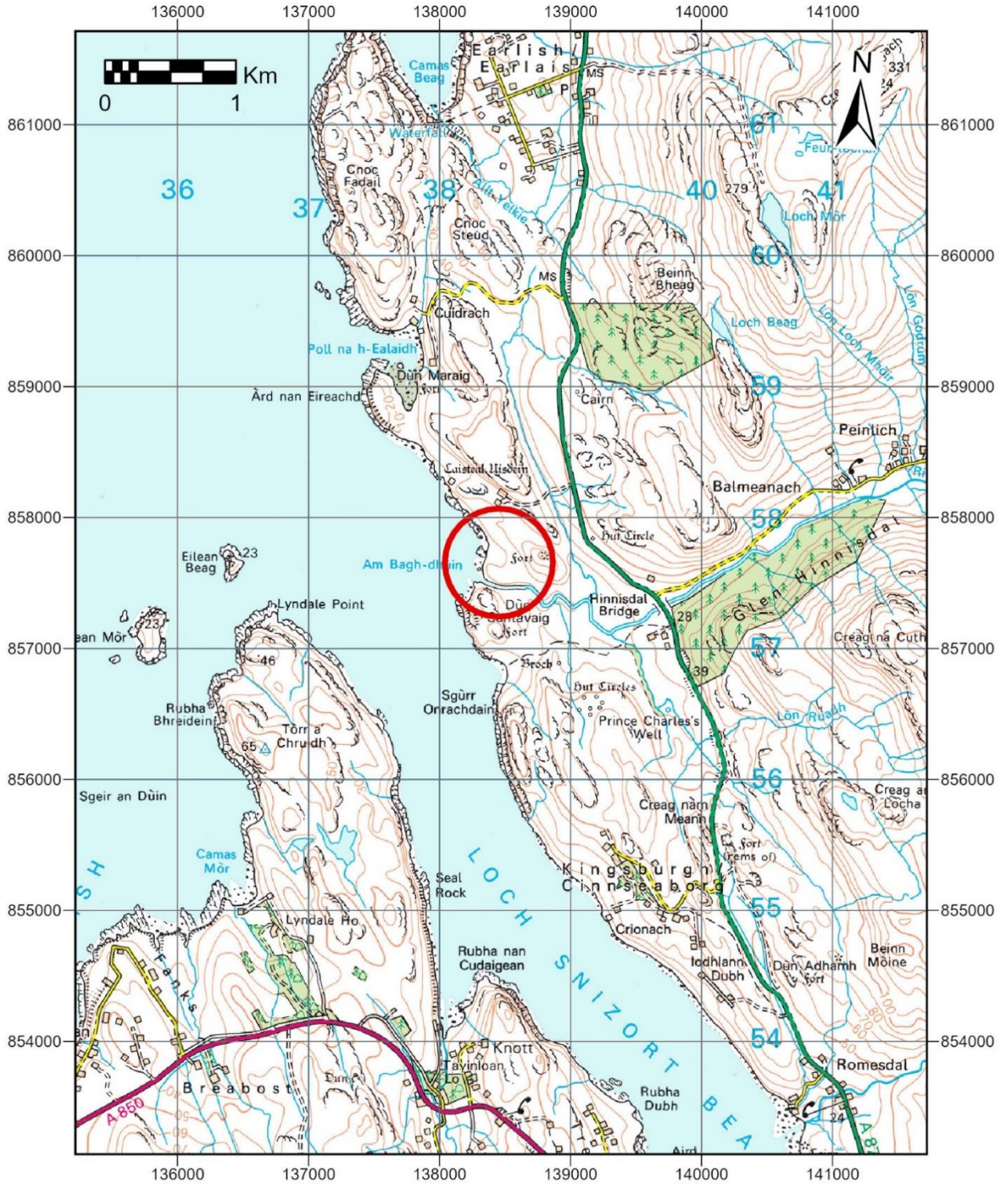
Figure 2.1. Ordnance Survey map showing location of South Cuidrach study site. Projected British National Grid (BNG) and displaying BNG coordinate system (Ordnance Survey, 2024).

Table 2.1. Nearest available empirical tidal data to field sites South Cuidrach and Sconser. All units are meters. From United Kingdom Hydrographic Office Admiralty Tide Charts (UKHO, 1993). CD = Chart Datum, OD = Ordnance Datum.

Location	Mean Level (m CD)	HAT	MHWS	MHWN	MLWN	MLWS	LAT	Range (MHWS-MLWS)	Correction to OD (Newlyn) (m)
Ullapool	3	5.8	5.2	3.9	2.1	0.7	0	4.5	-2.75
Loch Snizort (near S. Cuidrach) (± Ullapool)	3.03	0.03	0.1	-0.4	-0.2	0	0.03	4.6	-2.7
Broadford Bay (near Sconser) (± Ullapool)	3.2	0.2	0.3	0.2	0.1	-0.1	0.2	4.9	-2.85
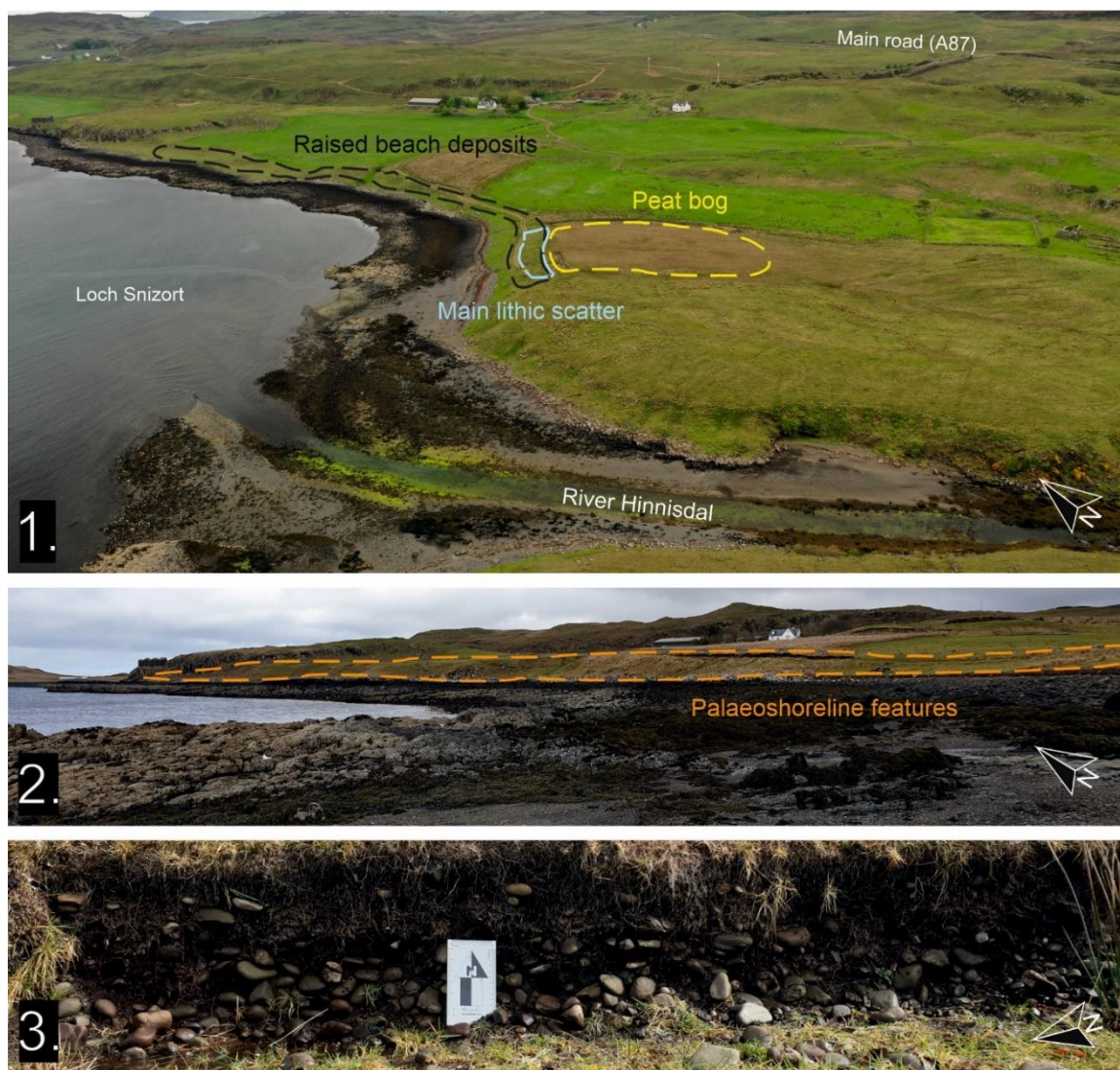
Figure 2.2. Site photos from South Cuidrach. A. (see Figure 1.3) Aerial drone photo showing the main features of interest, from Hardy et al., (2023). Main archaeological lithic scatter (blue) within raised beach deposits (black). The peat fen (yellow) is the focus of the palaeoenvironmental reconstruction. B. Palaeoshoreline features viewed from the modern beach at South Cuidrach, outlined in orange. C. Raised beach deposits, including 150 mm scale-card (not oriented northwards).

The Isle of Skye has well documented bedrock geology and is renowned for its Palaeocene igneous rocks and landforms (Williamson et al., 1994). Notably, the granitic 'red' Cuillins mountain range in the southeast in contrast with the 'black' Cuillins to their west which include largely mafic mineralogy, primarily gabbros. In areas in central and northern Skye, basaltic dykes, sills, and plutons evidence the Palaeocene volcanism that spanned across large areas of the North Atlantic (Anderson et al., 1966). The foreshore afront the field site (Figure 2.2 (B)) includes outcrops of basaltic and microgabbro bedrock associated with a Palaeocene lava field of central Skye (Williamson et al., 1994).

Superficial Quaternary deposits at South Cuidrach include the modern gravel/cobble/sand beach extending up to the high tide mark, marked by the lower vegetation limit. The beach is composed in part of black sands and alluvium from the Hinnisdal River. In the intertidal zone seaward of the field site there is a large flat bedrock outcrop which is submerged at MSL (Figure 2.2 (A)). Directly south of the site there is a small hilly headland with c. 5 m cliffs of the same basaltic origin. Topographical survey results and comments on the geomorphology of the site are found in the results section. Lithological descriptions of the peat fen at South Cuidrach are also found in the results section, along with the topography of the site and the bedrock topography from a Ground-Penetrating Radar (GPR) survey.

Along the seaward side of the largely level peat fen there are a series of sedimentary deposits which are c. 1 m above the surface of the fen at their peak, and c. 4 m above the vegetation high-tide mark. The well-sorted and rounded cobbles (Figure 2.2 (C)) and the proximity of these deposits to the coast, points to this feature being a raised beach (Smith et al., 2019). These deposits extend for around 500 m from the field site, northwards along the coast, at an approximately constant elevation.

2.1.2 Fieldwork Summary

Fieldwork at South Cuidrach was completed in two trips, the first in July 2021 conducted by Professor Natasha Barlow, Dr Adam Booth and Luis Rees-Hughes (each of the University of Leeds). In 2021, site photography, sedimentary descriptions and pilot analysis work were completed. The team investigated the geomorphology of the site using ground-penetrating radar (GPR). This geophysical technique was used to examine the bedrock topography beneath superficial sediment deposits, applying the methodology used by Rees-Hughes et al., (2021). Eleven sediment cores were taken using a combination of hand gouge and Russian corers, in tandem with the GPR data, both to examine the coastal stratigraphy within the sediment basin and to ground-truth the GPR results.

In March 2023, fieldwork was carried out by Professor Natasha Barlow, Dr Graham Rush, and myself. Elevation surveys were prioritised to define the previous GPR survey against Ordnance Datum. A transect of cores along the shore-facing side of the bedrock basin was taken to determine the elevation

of the lowest point of the sill, based on the methodology in isolation-based sea-level reconstructions e.g. Long et al., 2011; Brader et al., 2017. This defined the elevation above which the highest tides (HAT) must have reached if there was a marine ingression into the bedrock basin. Sediment cores were taken again in 2023, and photographed, providing samples for lab techniques. 2023 fieldwork included further site descriptions and photos, which aimed to improve the holistic understanding of the geomorphological and environmental history of the site.

2.2 Geophysical Survey

Initial sediment cores showed a topographic depression in the bedrock underlying the peat fen behind the raised beach feature (referred to as the 'bedrock basin'). A geophysical survey was designed to map this bedrock basin and determine; 1) the location and depth of the bedrock sill within the bedrock basin; 2) the point(s) of the greatest depth of sedimentary deposits from which to recover the best core samples for analysing stratigraphy.
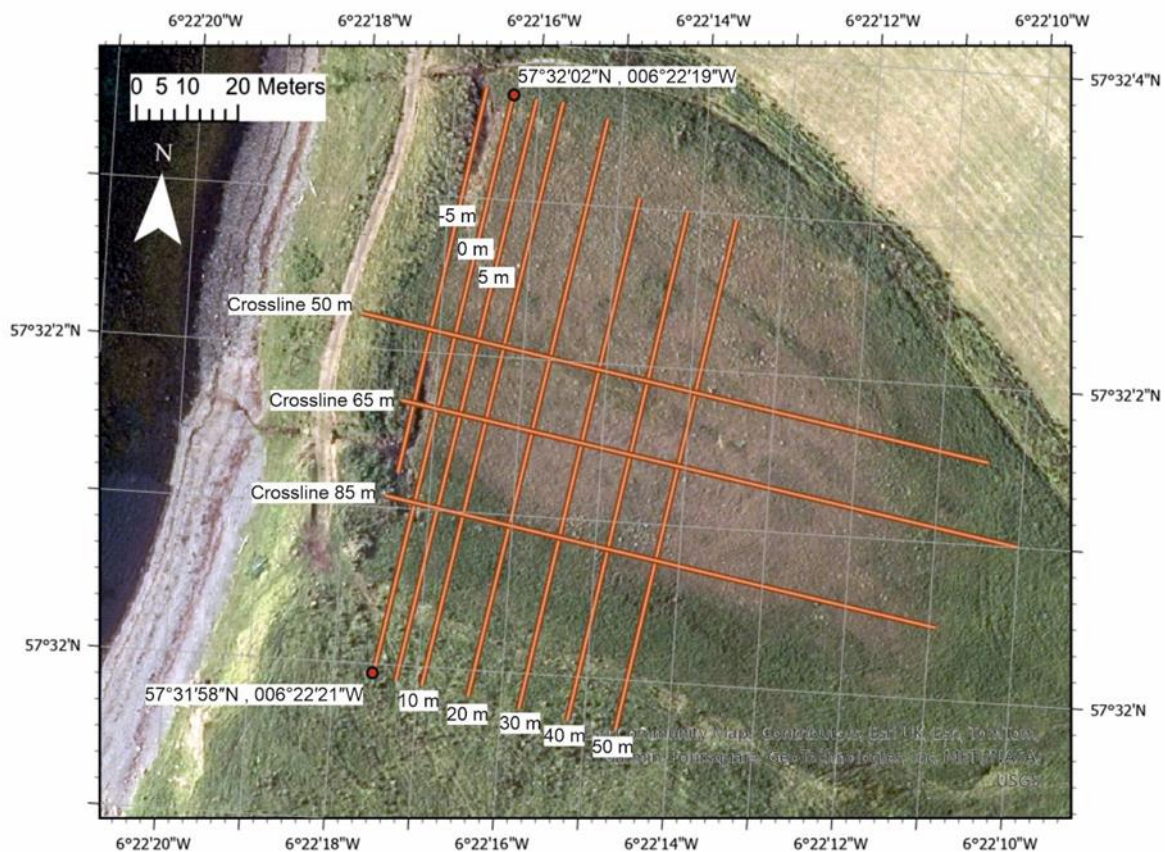
Figure 2.3. Locations and dimensions of GPR survey run-lines. Aerial photography from © Getmapping Ltd (2024).

This technique provides the ideal tool for near-surface terrestrial geophysical investigations on rough terrain. GPR was selected as a preferred method because: it is non-destructive and does not disturb the ground surface; GPR provides real-time data allowing users to alter survey plans in the field; GPR hardware is, relative to other techniques, easily transportable to inaccessible sites. GPR also offers continuous horizons that sediment coring alone cannot produce.

Positions of GPR runlines were recorded using a handheld dGPS, so that the 2023 differential dGPS survey could ground-truth the GPR data. To conduct the GPR survey, parallel lines were used at 5 m intervals on the seaward side of the basin running approx. north to south. Three crossline transects were taken at 50, 60 and 85 m from the origin point (noted 57°32′02″N, 006°22′19″W in Figure 2.3). There was a 5 m interval between the four lines on the seaward side of the peat fen. This higher horizontal resolution was essential for observing the seaward side of the basin, inland of which, a 10 m interval was found sufficient to identify the deepest points of the basin given the available time.

The pulse transmitter and receiver on the mobile GPR handset produce radargrams which show the two-way-time to reflective surfaces resulting from contrasting electromagnetic properties (permittivity and conductivity). Radargrams provide a 2D profile along the transects shown in Figure 2.3. Data processing sequence was conducted by Dr Adam Booth, using Sandmeier ReflexW (version 9.5.4), and interpolation using Mathworks Matlab software to apply a linear interpolation algorithm. The processing sequence was carried out as follows: Firstly, a Dewow filter was used to remove noise outside of the useful signal and identifiable diffraction hyperbola, applied within a window of 30 ns. Secondly, a bandwidth filter removed frequencies outside of the useful bandwidths of 20-40 MHz and 160-320 MHz. Thirdly, a static correction set 'time-zero' accurately in the radar traces, correcting reflectors to a -21 ns shift. Finally, gain-type processing was used to balance the amplitudes of radar signals and to increase the visibility of useful features in the radargram. The time delay of radar pulses was calculated in ReflexW based on the geometry of diffraction hyperbola, which allows travel-time radargrams to be used to estimate depth.

Horizons representing bedrock within the radargrams were then identified manually, which was the deepest strong visible reflector. I carried out further data analysis which was based on the interpolated dataset produced in Matlab. All GPR figures were produced using ArcGIS Pro. The interpolated grid from Matlab required a datum transformation for projection in British National Grid (BNG), automated in ArcGIS Pro (version 3.1.4).

2.3 Lithostratigraphy

The primary objective of this work was to collect samples from which to analyse the stratigraphy within the peat fen and provide material for lab-based palaeoenvironmental techniques. The deepest point was chosen based on the GPR results so that the fullest stratigraphic sequence was retrieved, with the oldest sediments likely preserved at the base of the core. The main sample core was taken at 57°32'01"N, 006°22'19"W. Sediment samples were taken from this point in 2021 (core SC-21-5) and 2023 (core SC-23-1).

Table 2.2. Sample list of sediment cores recovered from South Cuidrach in July 2021 and March 2023.

ID	Depth (cm)	Type
SC-23-1A	250 - 300	Russian (ø=60mm)
SC-23-1A	300 - 350	Russian
SC-23-1A	350 - 400	Russian
SC-23-1A	400 - 417	Gouge (ø=30mm)
SC-23-1B	380 - 480	Gouge
SC-23-1B	470 - 488	Gouge
SC-23-1C	395 - 495	Gouge
SC-21-5A	0 - 50	Russian
SC-21-5A	50 - 100	Russian
SC-21-5A	100 - 150	Russian
SC-21-5A	150 - 200	Russian
SC-21-5A	200 - 250	Russian
SC-21-5A	250 - 300	Russian
SC-21-5A	300 - 350	Russian
SC-21-5A	350 - 400	Russian
SC-21-5A	305 - 415	Russian
SC-21-5A	390 - 490	Gouge

Two types of hand-operated corers were used for sampling. The upper section of lithology is soft, water-logged peat, and was sampled using a Russian corer. This corer obtains 500 x 60 mm of sample cut horizontally, reducing the effects of contamination at the edges during coring. The gouge corer was

used beneath the peat section in the harder gyttja, silts and clays comprising the lower section of the basin. Samples taken using this equipment are 1000 x 30 mm diameter cores.

In 2021, the stratigraphy of 11 sediment cores were logged, 6 of which were along a transect perpendicular to the raised beach (Figure 2.6). Each of these 11 cores was stored at the University of Leeds. A full core sequence was collected at site SC-21-5, identified as the deepest point according to GPR results.

On the return site visit in 2023, additional material was sampled from the same point for all biostratigraphic techniques in the project. All core samples were stored in PVC tubing and cased in labelled transparent plastic before being transported to the University of Leeds and stored refrigerated at 4°C.

Figure 2.4. Photos of (A); Myself and Dr Graham Rush taking sediment core samples at South Cuidrach and (B); SC-23-1B Sediment core photo. Photos taken by Professor Natasha Barlow in March 2023.

All samples were photographed, alongside detailed lithological descriptions in the field, as changes in colouration can occur when core samples dry. Initial field observations of lithostratigraphy were taken using the Tröels-Smith (1955) standard system for describing unconsolidated sediments (Long et al., 1999). The method describes five characteristics of unconsolidated sediments: Darkness, stratification, elasticity, dryness, nature of contact (upper contact) and the components of the unconsolidated sediment in 25% units. Secondary Tröels-Smith descriptions were performed in the lab, to account for any change/decay due to drying in transport, and the limitations of field observations including weather conditions and time constraints. The Tröels-Smith system includes some subjectivity and dependence on the experience of the observer, which has been a cause for critique of the method. Additionally, the technique can make researchers prone to 'drift', where the lithology of a point of observation is repeatedly described relative to the previous point (Nelson, 2015). To minimise this risk, I compared different lithofacies to a Munsell Soil Colour Chart, providing a non-relative reference point for each observation, carried out in the lab.

2.4 Elevation Survey

Manual and digital elevation survey techniques were used at both Sconser and South Cuidrach. There were three objectives for the elevation survey work. 1) Record the lowest elevation of the sill above the bedrock basin. 2) Define the GPR survey work and the sediment logs against Ordnance Datum. 3) Characterise the surface topography of the peat fen. The positions of sediment cores taken in July 2021 were recorded using a handheld GPS and used to determine the sites for coring in March 2023. Elevations of lithological changes in the basin are not integral to the sea-level reconstruction aspect of this project, although they provide important contextual data. Elevation corrections for the GPR survey were used to determine the topography of the bedrock.

A Leica System 500 dGPS was used to measure the elevation of a temporary benchmark (TBM). I applied a post-processed kinematics (PPK) technique; applying ephemeris corrections from the Loch Carron Ordnance Survey base station (Ordnance Survey identifier: LCAR). All elevations are given in meters with reference to Ordnance Datum Newlyn, UK mainland (m OD). The Leica System 500 operated for 4 hours to improve precision. A TBM chosen at a prominent point provided good satellite coverage and made the point accessible for theodolite levelling measurements to various points (Figure 2.5).

Elevations were measured at the sediment core locations; the transect of cores along the bedrock sill of the basin; and at various points across the field site to characterise the surface topography. These techniques mean key morphological features are measured to a single reference point.

Alongside elevation results, error margins are calculated as the root sum of squares (RSS) of levelling survey error and dGPS error to two decimal places. This standard approach assumes a normal distribution of error from the dGPS process following Foster (2015).

Figure 2.5. Photos of the dGPS setup and levelling techniques used at South Cuidrach. A. Temporary benchmark (TBM) site and Leica System 500 dGPS setup. B. The theodolite level used to survey features from TBM.
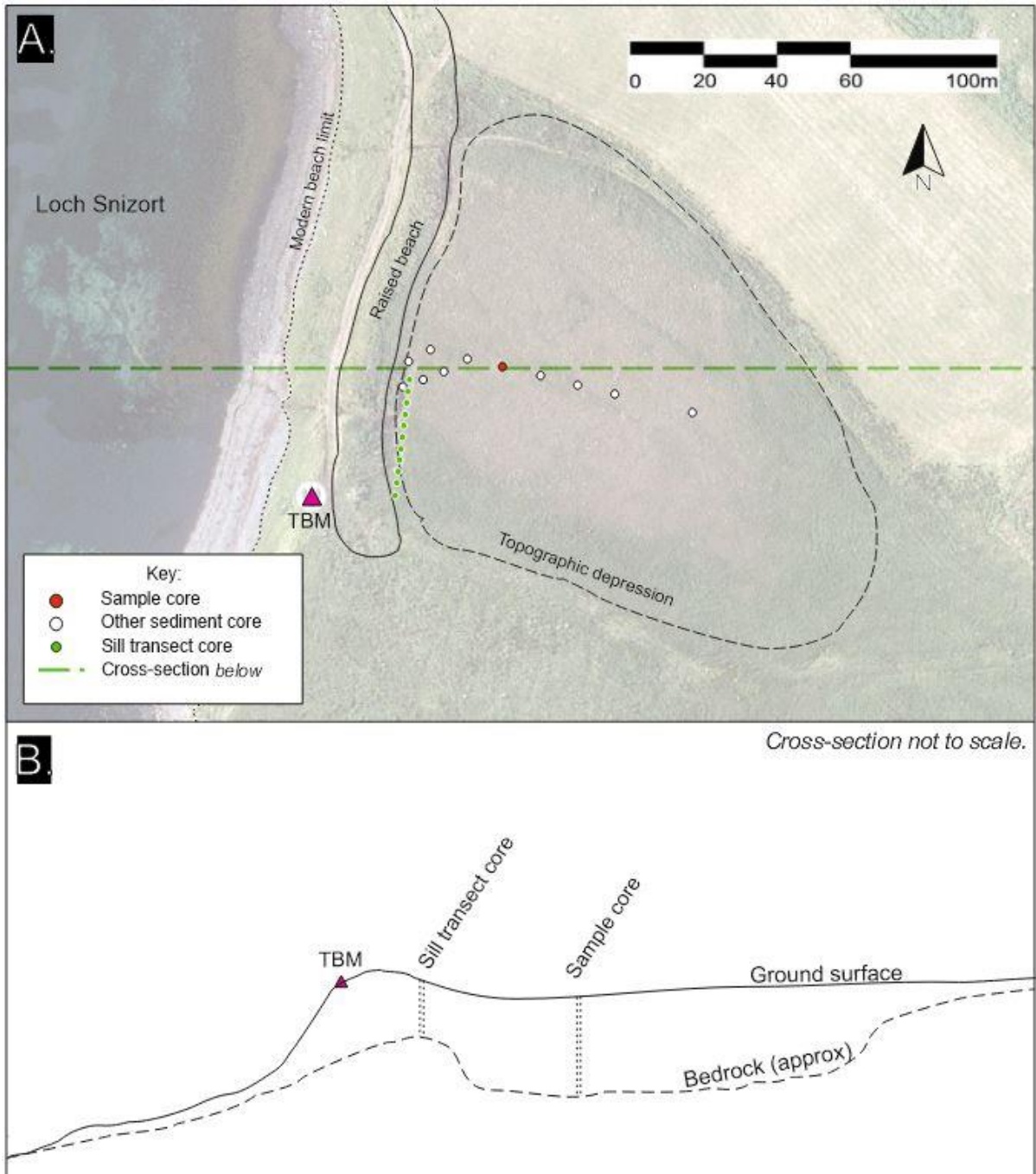
Figure 2.6. A. Diagram of survey objectives and sediment core locations used at South Cuidrach. 'Sample core' in red shows the locations of SC-21-5 and SC-23-1 cores. Aerial photography from © Getmapping Ltd (2024). B. Schematic cross-section diagram of the site, not to scale.

2.5 Microfossils

Using both diatom and pollen assemblage data from the sediment cores collected in South Cuidrach has helped build a holistic environmental reconstruction. Whilst diatom data is primarily used to understand changes in marine influence at the site, the pollen data contributed information about terrestrial vegetation changes.

2.5.1 Diatom Analysis

Diatom analysis followed the approach widely adopted in other Scottish isolation basin studies (Shennan et al., 2006; Selby et al., 2016). Initially, samples were taken at 8 cm intervals throughout the length of the deepest core (SC-23-1C). After this overview, resolution increased to 4 cm, then 2 cm where key changes were identified in either the litho- or biostratigraphy. The preparation of diatom slides followed standard techniques (Palmer and Abbott, 1986), modified for the laboratory equipment at the University of Leeds (Figure 2.7).

Microscope work was completed using a high-powered Leica microscope at 1000x magnifications, and a minimum of 250 diatom valves per slide were counted, following standard approaches for Scottish palaeo coastal analyses (e.g. Barlow et al., 2013, 2014). A total of 36 slides were counted. Visual identification of species was helped by various publications of reference material (Van der Werff et al., 1958; Hartley, 1996; Guiry et al., 2024). Species were differentiated by the morphology of their frustules, and identification required familiarisation with each species in turn.

The halobian diatom species classification scheme was used (Hemphill-Haley, 1993) to class diatom taxa into groups based on their salinity tolerance range. Species are presented as a percentage of the total count and grouped by their halobian classification. 'Percentage Abundance' is reported as the percentage of a specific taxa present in the total number of diatom valves counted at that sample depth, according to standard procedure (Smol et al., 2010). Plotting of the diatom data was undertaken in R using the Rioja package (Juggins, 2015).

I.	Approximately 0.5 cc of sediment was taken from core SC-23-1C at the sample depth (avoiding material which contacted the gouge corer during acquisition).
II.	Organics were then digested using 20% H_2O_2 (hydrogen peroxide) solution. Digestion was enhanced using in a water-bath at 50°C until all organics were dissolved.
III.	Samples were centrifuged at 4000 rpm for 4 minutes and supernatant was decanted to waste.
IV.	Samples were spotted onto coverslips on a hotplate at 100°C until fluid was evaporated.
V.	Coverslips are then mounted onto slides using Naphrax mountant, ready for diatom counting.

Figure 2.7. Flow chart of diatom preparation techniques. Based on the standard lab procedure at the University of Leeds, based on (Palmer and Abbott, 1986).

2.5.2 Pollen Analysis

Pollen sub-sampling was carried out on either side of key lithological/diatomological changes, and above these, at 30 cm resolution throughout SC-23-1. Twelve samples were taken in total, to give an overview of the vegetation changes. Sub-samples were also taken at the same depths as radiocarbon samples so that the pollen dataset is tied to the chronology established from diatom analysis. This aided correlation with existing pollen sequences from the Isle of Skye over the same period e.g. Selby (2004).

Pollen preparation followed the standard operating procedure at the University of Leeds, which is based on Moore et al., (1991), using density separation. Isolation of pollen from sediments requires the removal of inorganics, clastic material, and non-palynomorphs from samples. The same process

was carried out on each of the pollen samples, regardless of changes in lithology (SC-23-1) between basal clays / humified organics, and young peats at the top of the core.

I. Sub-sampling:

1 cm^3 of sediment measured from each sample depth using a volumetric sampler. *Lycopodium* marker spore tablet was added to each sample, which was used at counting stage to quantify concentrations of pollen, after Stockmarr et al., (1971).

II. Carbonate removal:

30 ml 7% HCl added to each sample, then sample was placed in 90 °C water bath for 20 minutes. Samples mixed using a glass rod, and centrifuged at 3000 rpm for 5 minutes, supernatant then decanted. Removal of HCl required topping sample up with deionised water and centrifuging again at 3000 rpm for 5 minutes.

III. Humic acid and fine sediment removal:

25 ml of 10 % NaOH added to each sample. Samples then placed in 90 °C water bath for 5 minutes. Samples sieved at 125 µm. Centrifuged at 3000 rpm for 5 minutes.

IV. Silicate removal

SPT (sodium polytungstate) prepared to a specific gravity of 1.9 g cm^3. 4 ml of SPT was added to each sample. Each sample was mixed using a glass rod and centrifuged at 1800 for 20 minutes without the brake applied. Supernatant fluid recovered and this process (X) was repeated, until samples were visibly clear. Samples were topped up with deionised water and placed in new sample tubes. Samples centrifuged at 3000 rpm for 5 mins, and the supernatant decanted for the recycling of SPT.

V. Acetolysis

Glacial acetic acid (CH$_3$COOH) was added to fill the sample tube and mixed using glass rod. Samples were placed in centrifuge at 3000 rpm for 5 minutes. Acetolysis mixture was combined 9 parts acetic anhydride with 1 part concentrated sulphuric acid. 5 ml of acetolysis mixture placed into each sample, and reaction was enhanced by placing in a water bath for 3 minutes. Reaction stopped using glacial acetic acid, and then samples were centrifuged at 3000 rpm for 5 minutes. Supernatant fluid was then decanted, and samples topped up with deionised water.

Figure 2.8. Flow chart of pollen preparation techniques. Based on the work of Moore (1991).

Slides were prepared using a glycerol mountant. Approximately 1 ml of glycerol was placed onto the slide, followed by a small amount of sample using a pipette. This mixture was spread out, and a cover slip was placed over the top. Slides were made up throughout the process of counting. Counting was undertaken using a Leica high-powered microscope at 400x magnifications initially. Individual samples were sometimes counted at 630x magnifications if required. To ensure robust identification, each new pollen group was photographed and logged. A minimum of 200 pollen grains were counted per sample, where 200 grains were identifiable. Identification of pollen grains was helped by Beug (2004) and Martin et al., (2017). Pollen concentrations were calculated using the methods of Stockmar (1971). A single tablet containing 2×10^4 Lycopodium spores was added to each sample, then the pollen concentrations were calculated by:

$$\text{Pollen concentration} = \frac{20,000}{\text{Total pollen count}} \times \text{Count of Lycopodium spores}$$

This approach allowed quantitative comparisons of pollen concentrations between samples.

2.6 Radiocarbon

Depths for radiocarbon sampling were determined by changes in the diatom taxa up-core. Establishing a chronology for the changes in marine influence is critical to meet the project objectives. Four samples for radiocarbon dating were taken from the SC-23-1 core sequence. Once the sample depth was established, ground plant macrofossils were selected from three of the four points. A minimum of 10 mg of material was taken from each depth, and contamination was avoided by removing the section of sediment which came into contact with the corer during retrieval. Where no macrofossils were available, bulk sediment samples were extracted instead.

Samples were submitted to Beta Analytic Inc. AMS laboratory for ^{14}C dating. Dates were calibrated using the IntCal20 calibration curve in OxCal version 4.4.4 (Ramsey, 2021).

2.7 Particle Size Analysis

Grain size is used in palaeoenvironmental research as an indication of relative energy (McLaren, 1981), to be used here in conjunction with other evidence to determine changes in the depositional setting at South Cuidrach and make inferences about RSL changes. Here, a laser particle size analysis (PSA) technique was used, selected as the most suitable grain size measurement technique for homogenous

silts/sands such as those found at the base of the sample core SC-23-1. PSA analysis was carried out using the Retsch Camsizer XT. X-Jet Module in the Sorby Laboratory Suite at the University of Leeds. The measurements were taken by Helena Brown, and the numerical analysis I completed myself. The Retsch Camsizer XT is a particle size and shape analyzer which uses dynamic imaging analysis. I used the Gradistat Program (Version 9.1) developed by Blott et al., (2001) for statistical analysis of the PSA results.

I.	Approximately 1 cc of sediment was taken from core SC-21-5A at the sample depth.
II.	Samples were dried at 60 °C for 24h.
III.	Carbonates were dissolved using ~20 ml of HCl for 24h / until the reaction was visibly complete. Samples were then topped up with deionised water and centrifuged at 3000 rpm for 4 minutes before the supernatant was decanted to waste.
IV.	Organics were then digested using 10% H_2O_2 (hydrogen peroxide) solution. Digestion was enhanced using in a water-bath at 50°C until all organics were dissolved. Samples were then topped up with deionised water and centrifuged at 3000 rpm for 4 minutes before the supernatant was decanted to waste.
V.	Samples were then dried again at 60 °C for 24h.

Figure 2.9. Flow chart of particle size analysis preparation techniques, prior to measurements undertaken using the Retsch Camsizer XT analyser.

2.8 Loss on Ignition

Loss on ignition methods followed the standard lab procedure of Plater et al., (2015) adapted to fit the standard operating procedure at the University of Leeds. A volume of approximately 5 – 10 g of

material was sampled from 2cm intervals along the core, between 321 – 477 cm depth. Upper and lower bounds of LOI sampling depths were determined by the diatom sampling depths. These were taken from cores SC-23-1A (300 - 350), SC-23-1A (350 - 400) and SC-23-1B (380 - 480) (Table 2.2). Samples were dried at 60°C overnight to remove all water and then ground using a pestle and mortar to create a homogenous sample. Porcelain crucibles were weighed (m_{cruc}) using a 4-place mass balance. Approximately 1 g of sample was weighed in crucibles to give $m_{initial}$. These were then placed into a furnace at 440°C overnight, a temperature which avoids the destruction of carbonates. Once cooled, samples were reweighed to give m_{final}.

LOI is a measure of the inorganic content within dry sediment that remains as a percentage of dry weight following ignition, here at 440°C, and was calculated by:

$$LOI \% = \frac{(m_{initial} - m_{cruc}) - m_{final}}{(m_{initial} - m_{cruc})} \times 100$$

The procedure assumed that change in mass which occur in mineral matter are negligible or nil, so that LOI is a representative measure of organic matter by weight ($LOI \%$). Plotting of LOI data was undertaken using the Rioja package in R (Juggins, 2015), some functions of which were adapted to suit this dataset.

2.9 Summary

To summarise, this chapter details the methods applied at South Cuidrach to reconstruct RSL changes and investigate the palaeoenvironment. The geomorphology of the site was measured using GPR and dGPS techniques, alongside qualitative observation methods. Internal stratigraphy of the isolation basin was observed using coring methods and the Tröels-Smith system for describing unconsolidated sediment. Diatom analysis was the main method for identifying changes in marine influence at the site and was conducted alongside pollen analysis, which was used to investigate vegetation changes. A chronological framework was built based on radiocarbon dates taken at key transitions in the diatom assemblages.

3. RESULTS

This chapter presents the results of the litho-, bio- and chrono-stratigraphic laboratory work and data analysis of the cores collected at South Cuidrach. Section 3.5 integrates and summarises the results from these various techniques. The results from work at Sconser are presented in Chapter 4.

3.1 Elevations and Geomorphology

Modelling the surface/bedrock topography and precisely measuring the geomorphological features at South Cuidrach was key to building a holistic understanding of environmental change at the site. Geophysical survey results are shown in Figure 3.2 and Figure 3.10. The term 'overburden thickness' is repeatedly used with reference to the GPR results, as this dataset does not account for changes in surface topography, as no dGPS survey was undertaken during the GPR work in 2021. The results of the elevation survey undertaken in March 2023 are shown in Table 3.1 and Table 3.2.

3.1.1 Elevation Survey Results

Some of the key results from the elevation survey include the following: the sample core SC-23-1 was taken at an elevation of 7.25 ± 0.028 m OD (57°32'01"N, 006°22'19"W); the elevations measured along the surface of the raised beach show a range of 0.65 m; and the lowest sill transect elevation was 4.47 ± 0.03 m OD (See Table 3.1 and Table 3.2).

Table 3.1. Sill transect and theodolite levelling data, used to determine the elevation of the basin sill.

Sill transect (Gouge corer)		Levelling survey		Elevations		
ID	Depth (m)	Backsight (m)	Foresight (m)	Surface elevation (m OD)	Bedrock elevation (m OD)	Notes
TBM		1.38		7.84		dGPS basestation site
1	1.34		1.97	7.26	5.92	
2	1.97		2.10	7.12	5.15	
3	2.15		2.16	7.06	4.91	
4	2.38		2.14	7.08	4.70	
5	2.59		2.13	7.09	4.50	
6	2.59		2.16	7.06	**4.47**	Deepest core (site used in lab analysis)
7	2.53		2.19	7.03	4.50	
8	1.22		2.11	7.11	5.89	
9	0.99		2.11	7.11	6.12	
10	2.51		2.14	7.08	4.57	
11	2.06		2.17	7.05	4.99	
TBM		1.37				

Table 3.2. Results of dGPS survey of key features at South Cuidrach; the TBM, SC-23-1 surface, and the raised beach surface.

ID	Elevation (m OD)	GPS error (m ±)	Levelling error (m ±)	RSS error margin (m ±)
TBM	7.84	0.03	0.01	0.03
SC-23-1	**7.29**	0.03	0.01	0.03
Raised-beach surface 1	7.94	0.03	0.01	0.03
Raised-beach surface 2	7.77	0.03	0.01	0.03
Raised-beach surface 3	7.41	0.03	0.01	0.03
Raised-beach surface 4	7.47	0.03	0.01	0.03
Raised-beach surface 5	7.65	0.03	0.01	0.03
Raised-beach surface 6	7.29	0.03	0.01	0.03
Raised-beach surface 7	7.51	0.03	0.01	0.03

3.1.2 Ground-Penetrating Radar

Two time slices which were used for the manual identification of the unconsolidated sediment/bedrock interface within the basin (identified as a 'continuous reflector') are shown in Figure 3.1. The low-frequency (20 – 40 MHz) data identifies a strong reflector created by the dielectric contrast at this interface. This is more pronounced than some smaller internal structures visible in the radargrams. Figure 3.1 (A) shows some evidence of internal stratification within superficial deposits at 23 - 75 m (horizontally from origin) and 50 – 150 ns return time. This may be due to signal attenuation caused by the increased thickness of the deposits (Neal, 2004) and these reflectors are not visible above the shallower bedrock. There is likely to be a dielectric contrast on either side of the water table in the basin, relating to the saturation depths noted in the lithology (3.2.1) at c. 361 cm in SC-23-1, another possible cause of the internal stratification in the radargrams.

The straight horizontal surfaces in the uppermost 0 – 50 ns of Figure 3.1 (A & B) represent the contrasting electromagnetic properties between the air and ground. The sediment/bedrock interface can be seen Figure 3.1, but is less visible in image A between c. 23 and 75 m horizontal distance. The depth penetration of the GPR system was limited to around 200 ns in each of the radargrams.

There are some diffraction hyperbolae visible in Figure 3.1 (B) which are found adjacent to the raised beach and therefore may represent a continuation of the raised beach deposits buried below the ground surface. Given the context, it is likely that these hyperbolae are beach cobbles. They are most numerous around 45 – 80 m from the origin point of Line -5 (Figure 3.1 (B)), beneath the landward side of the raised beach. These features weaken the signal of the underlying bedrock, however, the

continuous reflector of that sediment/bedrock interface is still clear. It is possible that where the raised beach deposits are densely packed, they appear as a single strong reflector, visible in the Crossline 50 radargram (Figure 3.1) at 0 – 10 m horizontal distance.
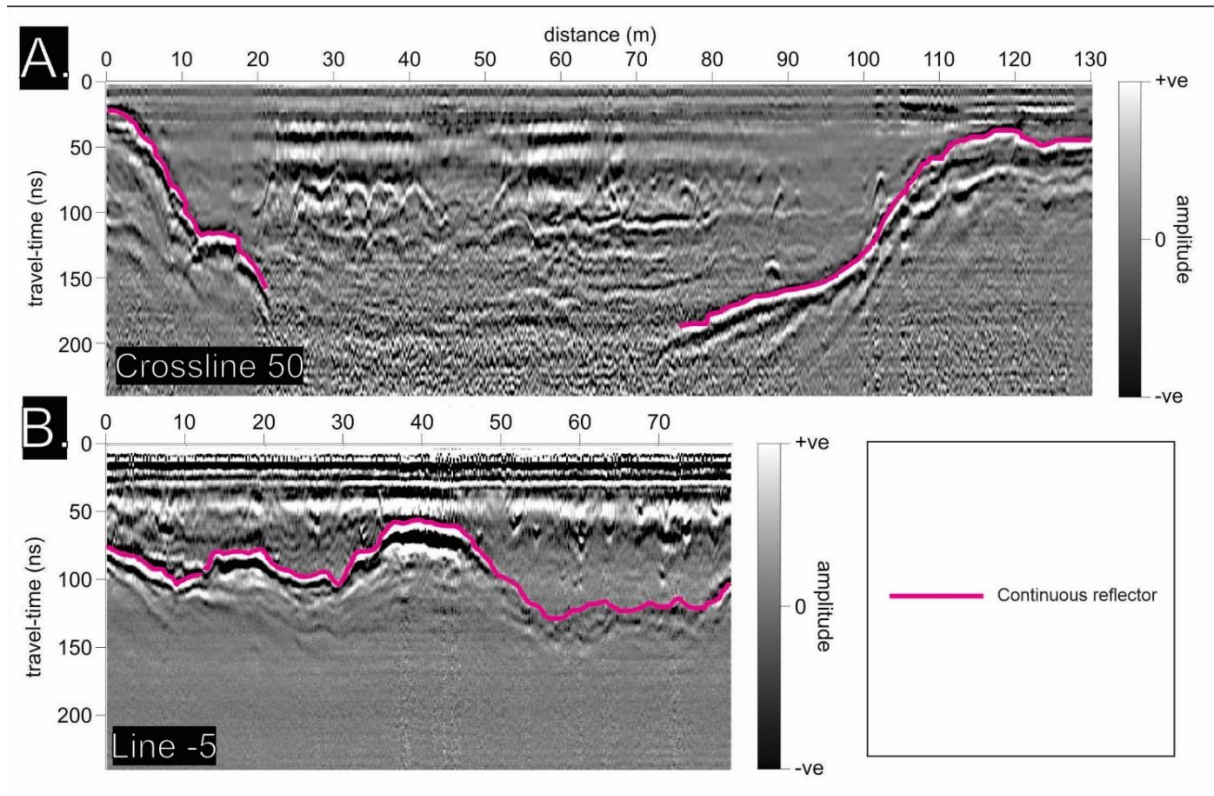
Figure 3.1. Manually identified continuous reflectors on GPR radargrams from the sediment basin at South Cuidrach. Data from (A.) Crossline at 50 m and (B.) The line at -5 m (identified in Figure 2.3 and Figure 3.2). The X-axis shows the distance (m) from the origin of each GPR run-line (0 distance = location of identifying label in Figure 3.2). Manual identification by Dr Adam Booth.
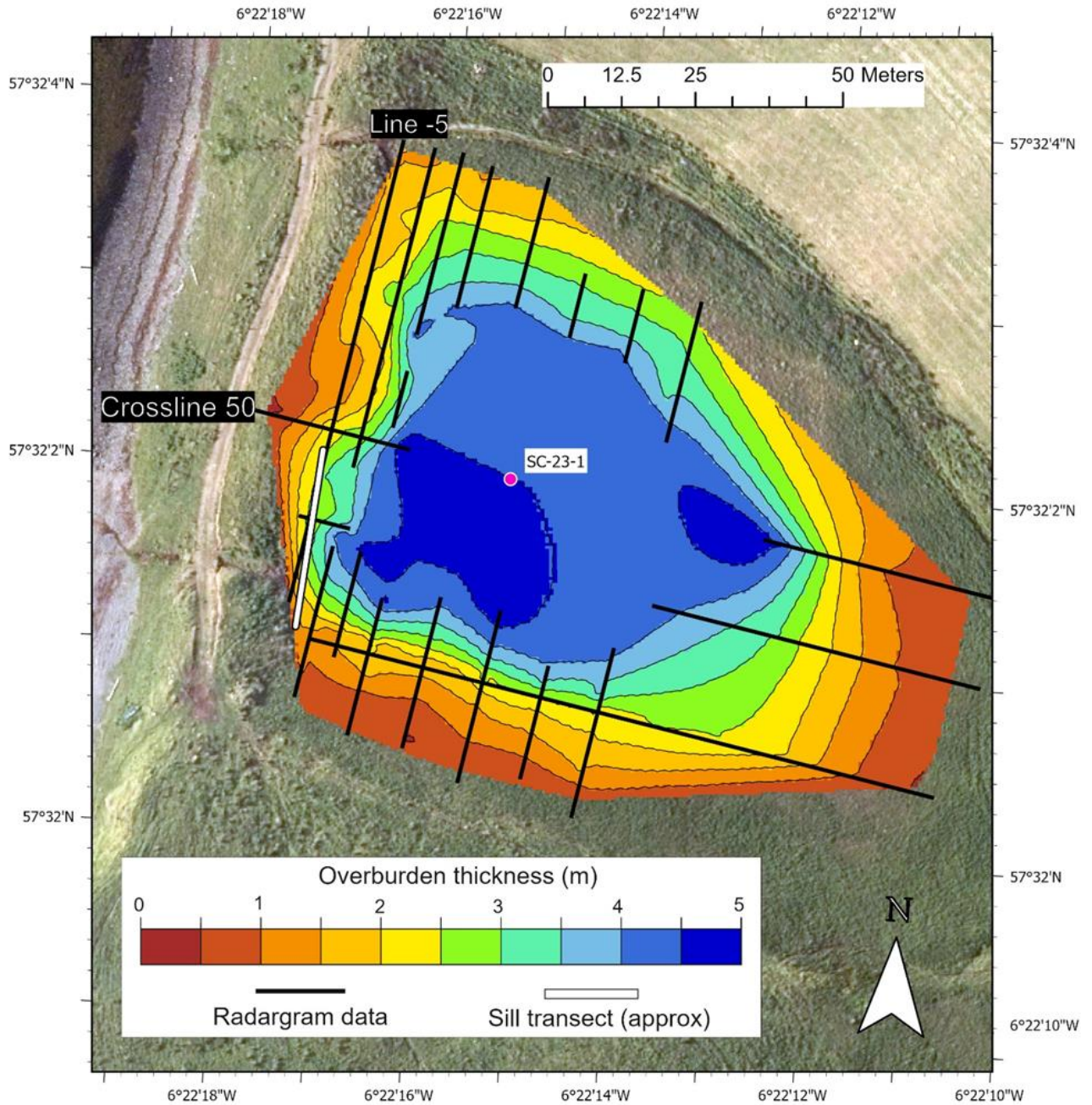
Figure 3.2. Overburden thickness from ground penetrating radar survey conducted in 2021 at 0.5 m resolution. The site of SC-23-1 sediment core is identified, alongside GPR lines 'Crossline 50' and 'Line -5' (identified in Figure 3.1). The transect of sediment cores designed to identify the basin sill is approximately located ('Sill transect (approx)'). The dataset is a linear-interpolated surface based on depths from GPR survey lines, identified in black, where the gap between the deepest part of the basin represents the limitations of the GPR to 'see' the deepest depths and therefore the bedrock elevation is interpolated. Aerial from © Getmapping Ltd (2024).

3.2 Sedimentology

This section presents the results of the sedimentological analysis of SC-23-1 and SC-21-5, including stratigraphic logging, PSA and LOI data from the cores.

3.2.1 Stratigraphic Log

A stratified sediment succession is found within the peat fen at South Cuidrach. Mainly minerogenic material is found within the deepest part of the deposits from within the basin, where the basal unit is a more homogenous green/grey clay observed below 455 cm (Figure 3.3). Above this, there is a darker layer containing mainly humified organics. The surface deposits consist of stratified layers of peat, with light-coloured sphagnum including many plant fragments at the top. Stratigraphy across these cores (see locations Figure 2.6) is grouped into six key units (Figure 3.3).

The following lithological description of core SC-23-1, the core selected for laboratory analysis, is also observed in core SC-21-5 very close by (Figure 3.3). The unit at the base of the core (495 – 455 cm) is made up of green/grey clays with small amounts of organic material. The unit above this (455 – 361 cm) is mostly dark grey clays and silts, with more organic content than the layer beneath. From 361 – 286 cm, there is further minerogenic material (clays and silts) intercalated with humified peat. The boundary between this unit and the one beneath is gradational, occurring across > 1 cm. There are several silt laminae (< 1 cm in width) in this unit (also identified in Figure 3.6), which are comprised of similar silts to the underlying layer. From 286 - 77 cm depth, the sediment is darker in colour and contains more organic content and visible plant macrofossils than the layer beneath. This part of the core is mostly comprised of humified organics beyond recognition, with occasional moss / herbaceous plant fragments. At 77 – 5 cm depth, light brown sphagnum peat is found, with lower concentrations of humified organics than the layers beneath. At the surface, the cores exhibit in-situ plant fragments, mosses, and roots of herbaceous plants (5 – 0 cm depth), reflecting the modern environment of a saturated peat fen. The whole core was saturated, but marginally less so below ~ 361 cm, attesting to the site being a fen peatland, rather than raised bog peatland (Joosten and Clarke, 2002).
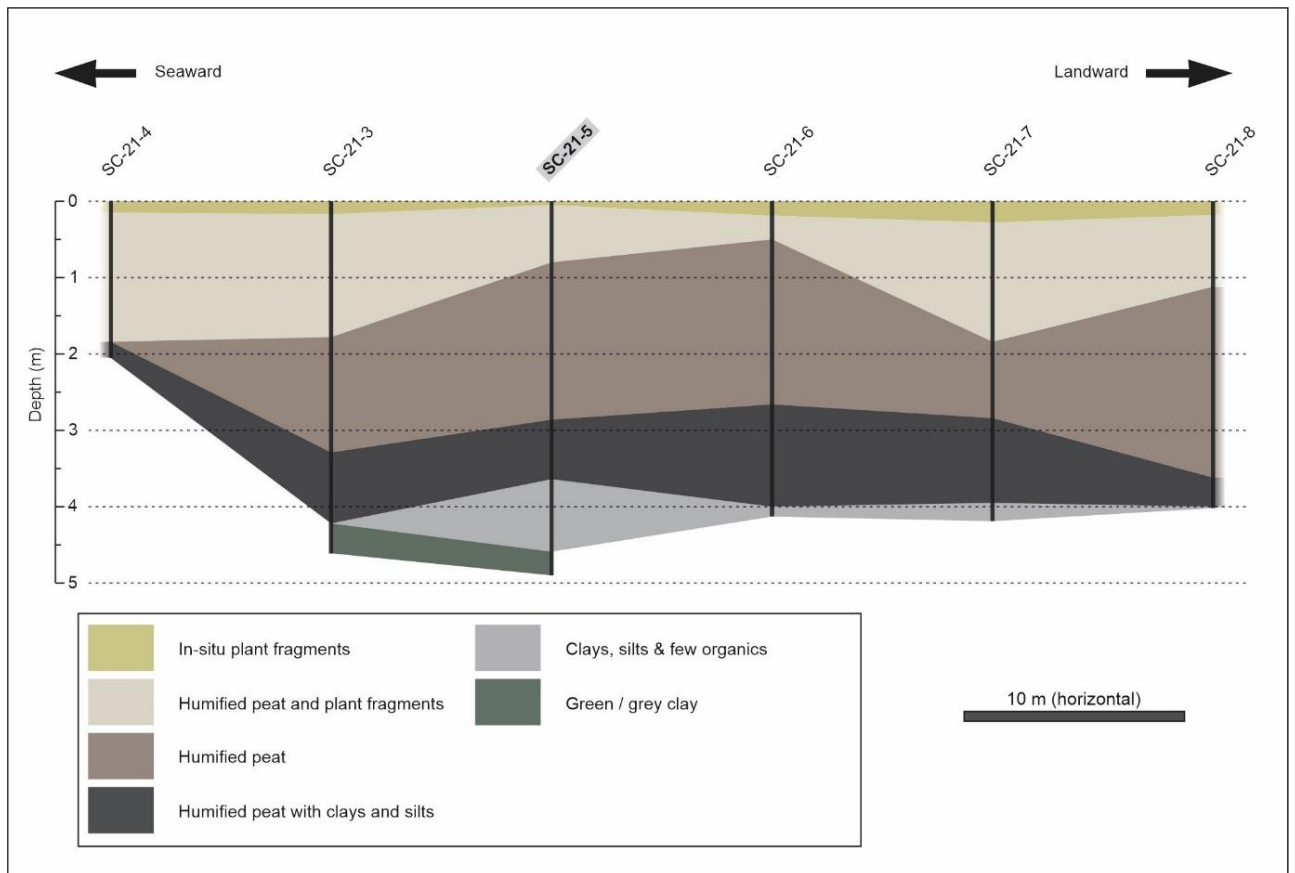
Figure 3.3. Lithostratigraphy within the isolation basin recorded at the six core sites (Figure 2.6) at South Cuidrach. Detailed litho- and bio-stratigraphy was conducted in the core collected at site SC-21-5 (highlighted grey), using the cores collected in 2023 (SC-23-1). At the deepest point of each sediment core is bedrock.

3.2.2 Particle Size Analysis and Loss on Ignition

PSA focussed on the minerogenic units in the basal c. 2 m of the cores. The grain size results (Figure 3.4) exhibit moderate to poor sorting throughout the sampling depths of 494 – 310 cm, sampled at 8 cm intervals (core SC-23-1). At the base of the core, from 494 – 350 cm, silts of varying class sizes are present, with small amounts of clays and sands. There is an increase in the proportion of medium–fine sands at 446 cm, followed by a sharp fall in the proportion of sand at 438 cm. These changes punctuate the bottom section of the core. Sorting throughout the base of the core remains moderate to poor until 350 cm. Above which, sediments are very poorly sorted where standard deviation (1 σ) is greater than 2, but for the top 3 samples, where sorting is moderate. The top three samples correspond to the depths of silt laminae found at 361 – 286 cm (3.2.1), and to the beginning of the section of SC-23-1 which is mostly humified peats.

A. Sediment type **B**. Sorting
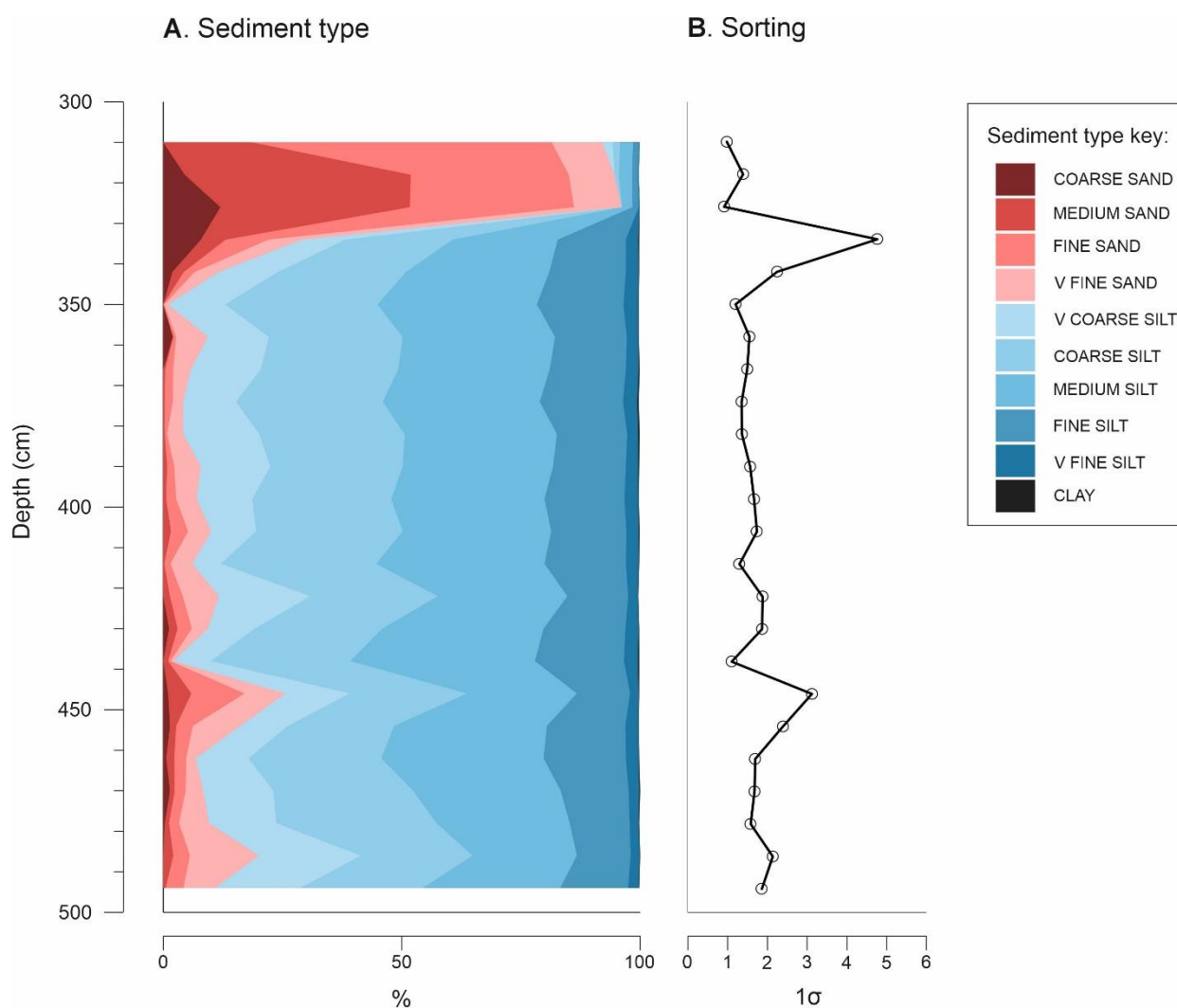
Figure 3.4. A. Sediment types stacked area plot from PSA, analysis follows Blott and Pye (2001). B. Standard deviation (1 σ) of particle size data for each sample, using the Folk and Ward (1957) method to quantify sorting (lower values equal greater degree of sorting). The Wentworth (1922) scale for classification of sediments is used.

Loss on ignition provides an overview of the organic content up core. The LOI results from SC-23-1 core are presented below in Figure 3.5, and again alongside a biostratigraphic and lithological summary in Figure 3.9. In between 477 cm and 347 cm, the mean LOI is 24%. In this section, there are low LOI % values at 469 to 463 cm (mean value of 11.6%). A spike in LOI occurs at 429 cm; of 52.7%. The lithology includes mostly minerogenic sediments with increasing humified peat as depth decreases. From 345 to 337 cm there is a sharp increase in organic matter (LOI increases from 47.1 to 76.8 %). A key change in lithology between mostly minerogenic and mostly organic material occurs at 361 cm, beneath the sharp increase in LOI. Above 335 cm, the mean LOI value is 82.6%. This section of higher organic matter content is found where the lithology is mostly humified peats. On either side of the transition from basal green/grey silts to darker grey silts at 455 cm, the mean LOI increases from 16.9% to 24.6%.
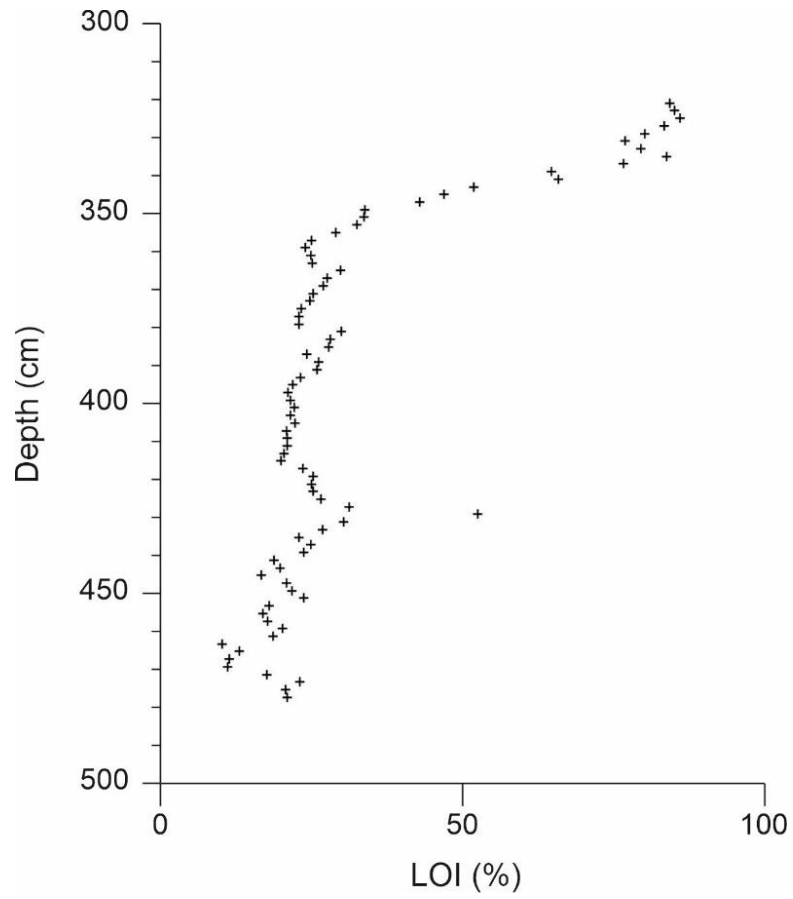
Figure 3.5. Results of LOI at 440 °C at the base of the SC-23-1 sediment core (LOI %).

3.3 Biostratigraphy

3.3.1 Diatoms

Diatom assemblage counts were obtained from 36 samples from the lower part of core SC-23-1, between 492 and 324 cm, with an average of 259 valves counted per sample. In total, 9,327 individual specimens were identified for these analyses.

The most evident change in diatom taxa throughout SC-23-1 (Figure 3.6) occurs between 440 cm and 438 cm depth, above which, halophobian taxa are less prevalent, and mesohalobian/polyhalobian taxa more prevalent. Below this depth (492 – 440 cm), there are no mesohalobian/polyhalobian taxa. Within this deepest section of SC-23-1, two key oligohalobian (freshwater, tolerates low salinity (Hemphill-Haley, 1993)) species dominate. *Staurosirella pinnata* and *Fragilaforma virescens* together make up 66.1% of the total count. *Nitzschia amphibia* is also abundant between 492 and 440 cm. The sharp cessation of halophobian species and the corresponding immediate introduction of poly/mesohalobian species means that the depth of the change in hydrological conditions from freshwater to brackish is identified at 440 – 438 cm. This sharp drop in halophobian species (*Eunotia praerupta* disappearance) is contrasted by the introduction of *Cocconeis scutellum*, and the gradual disappearance of *Fragilaforma virescens* and *Staurosirella pinnata*.

Above 438 cm, more salt-tolerant freshwater species are prevalent, and there are marine taxa present up to 328 cm. This section of SC-23-1 is dominated by three key species which are abundant throughout: *Cocconeis scutellum*, *Pseudostaurosira brevistriata* and *Pseudostaurosira elliptica*. *C. scutellum* is a marine diatom species with a wide salinity tolerance range, being found at various tidal levels in coastal environments (Sawai et al., 2016). *Pseudostaurosira* species comprise 53.3% of taxa at these depths in SC-23-1 (438 – 328 cm). These are typically highly abundant species where they are found, and are found in freshwater / brackish environments globally (Rzodkiewicz et al., 2017).

There is a change in taxa at 332 cm, where several *Navicula* species (*elegans, crucicula and crucifera*) appear in the dataset. These brackish and marine taxa are absent in the core below 332 cm. Furthermore, two new oligohalobian species are found between 332 cm and the top of the diatom preservation: *Navicula escambia* and *Amphora ovalis*. Key oligohalobian species *Pseudostaurosira brevistriata* and *P. elliptica* also disappear from the record at these depths. Poor preservation above 324 cm depth in the organic-rich peat is likely due to the dissolution of silicate diatom valves which can be caused by humic acids in peatland (Carballeira et al., 2020). At 446 cm, which was resampled twice (eliminating the possibility of a sampling error) no diatoms were found. Only one Oligohalobous

halophile (freshwater - stimulated at low salinity) species was identified; *Cyclostephanos dubius*, and in low numbers (<3% of total count). This category is not therefore included in Figure 3.6 and Figure 3.9.

Figure 3.6. Diatom assemblage data from SC-23-1, showing percentage abundance of species against depth. Counts of < 3 % of the total count have been removed. Radiocarbon ages and summary lithology of the SC-23-1 core are also shown.

Table 3.3. Halobian classification system used to identify salinity changes in diatom assemblage data, based on salinity tolerances of species (Hemphill-Haley, 1993). See Figure 3.6.

Classification	Salinity range (‰)	Environment
Polyhalobous	> 30	Marine
Mesohalobous	0.2 - 30	Brackish
Oligohalobous	< 0.2	Freshwater - stimulated at low salinity
Halophobous	0	Salt-intolerant

3.3.2 Pollen

Pollen counts through the core SC-23-1 (Figure 3.7) are dominated by *Alnus, Betula*, and grass species, but there are changes within their concentrations throughout SC-23-1. *Betula* is present from the base of the sequence (at 440 cm) upwards. The sample at this depth is atypical of the lowest part of this sequence. Several types of spores, ferns, mosses and shrubs are present, particularly *Sphagnum* moss, which is prevalent again only above 250 cm. *Ulmus* is present only at depths of 330 cm, immediately above 331 cm (one of the ^{14}C sample depths (Table 3.4)), whilst genera such as *Quercus* alongside *Larix* and *Pinus* are more common in lower parts of the core. *Sagina subulata*; a mat-forming perennial moss; is found today on exposed rocky surfaces, notably on the Trotternish peninsula on Skye (Harrold, 1978). *Sagina* pollen is found at depths of 420 and 370 cm, early in the sequence. *Poaceae* (grasses) pollen are present throughout the SC-23-1 sequence, increasing as a percentage of the count at depths of 300 and 270 cm. At these depths, total counts were below 100 specimens, however. *Calluna vulgaris* pollen is found at shallower depths (180 – 150 cm) in SC-23-1, as ferns, mosses and shrubs increase alongside. *Erica tetralix* and *Juniperis* species are also found. *Pinus* pollen is found at 440 cm alongside *Quercus*, and again at 350 cm, at percentage abundance of > 10 %.
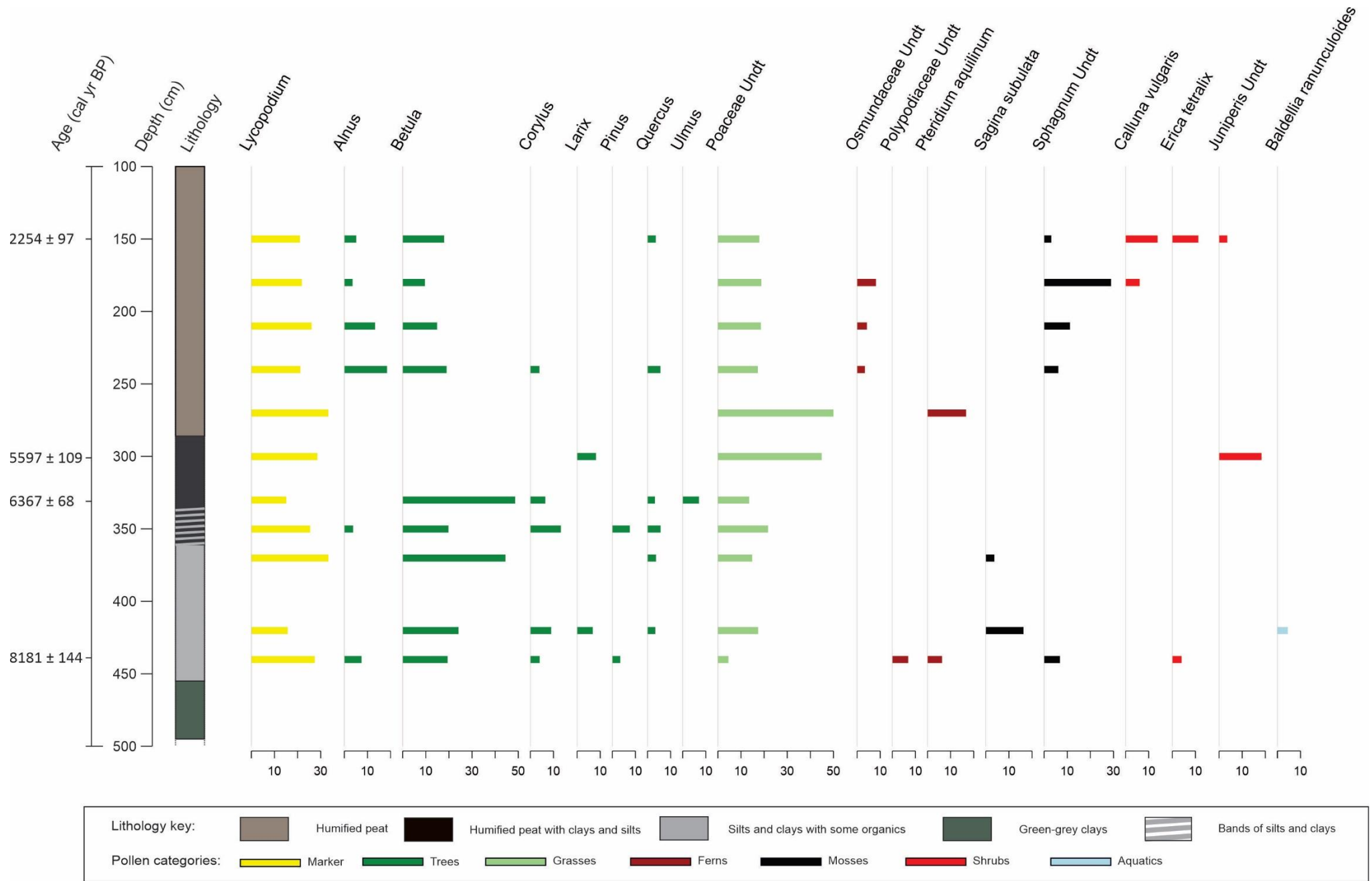
Figure 3.7. Pollen assemblages from SC-23-1 against lithology and radiocarbon results. Pollen is grouped into a vegetation classification based on data from Martin et al., (2017).

3.4 Chronology

3.4.1 Radiocarbon Results

Material for four radiocarbon dates was retrieved from the SC-23-1 & SC-21-5A cores, with the resulting ages ranging from 2254 ± 97 to 8181 ± 144 cal. BP, each falling within the Holocene. Each radiocarbon date is detailed Table 3.4, along with calibration plots and contextual details.

Table 3.4. [14]C dating summary table for SC-23-1. Table includes calibration plots for each date, produced in OxCal using the IntCal 2020 calibration curve (Reimer et al., 2020; Ramsey, 2021).

Depth (cm)	Lab ID	Material	14C Conventional age	± (1σ)	Calibration range (Cal BP)	Calibration median age (cal. BP)	± (2σ)	Calibration plot	Biostratigraphic context
150	SC-21-5A-150	Plant (Reeds)	2280	30	(51.8%) 2350 – 2300 (43.7%) 2245 - 2157	2254	97		Upper limiting date from within peat stratigraphy.
301	SC-23-1A-301	Plant (Reeds)	4880	30	(1.1%) 5705 – 5694 (91.7%) 5660 – 5580 (2.7%) 5504 – 5488	5597	109		Mass of surface herbaceous plant matter representing terrestrial limit.
331	SC-23-1A-331	Plant (Reeds)	5580	30	(1.5%) 6435 – 6428 (93.9%) 6405 – 6299	6367	68		Suitable material for 14C dating near diatomological change at 332 cm.
439	SC-23-1C-439	Organic sediment (bulk date)	7380	30	(74.1%) 8325 – 8162 (2.3%) 8136 – 8116 (19.1%) 8109 – 8037	8181	144		Transition from freshwater to brackish diatom assemblage.
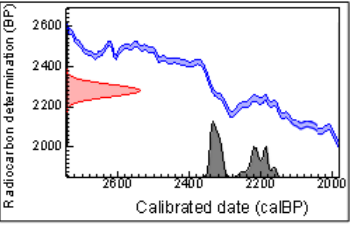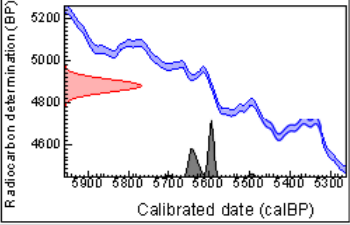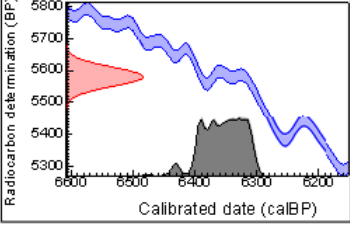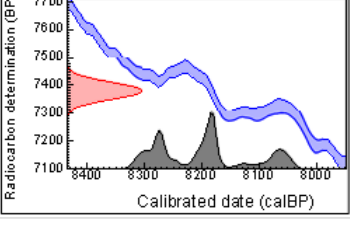
3.4.2 Age-Depth Model

An age-depth model is presented for the SC-23-1 core using the radiocarbon dates, produced to estimate the ages of events within the pollen data which occurred in between the radiocarbon sampling ages/depths. Using the OxCal P_Sequence model (Ramsey, 2021), Figure 3.8 shows the modelled 95.4% confidence limits on the estimated ages between the radiocarbon data points. This model is presented to allow estimations of the age of depths within the core at depths for which there is no direct dating control, with the noted caveat that the model is based on only four radiocarbon ages.
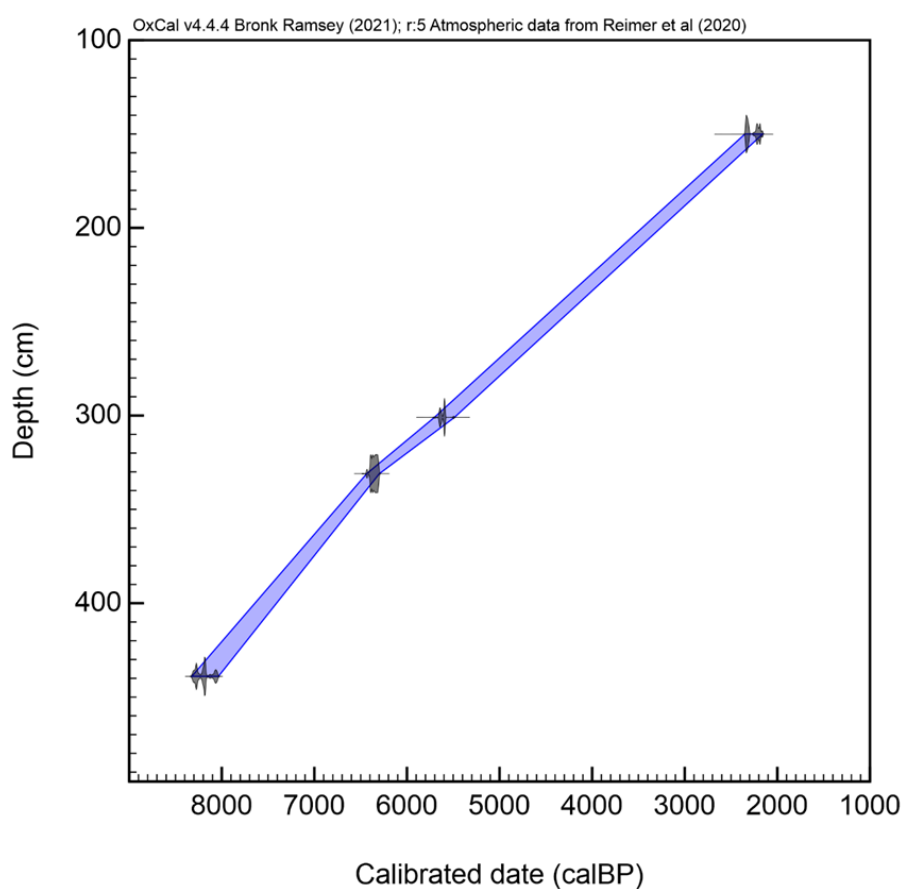
Figure 3.8. Age-depth model for the SC-23-1 core, using P-Sequencing in OxCal v4.4.4 Ramsey (2021) and the IntCal20 calibration curve (Reimer et al., 2020). The full length of the cores is shown (0 – 495 cm depth) on the y-axis, and the blue area shows 95.4% confidence limits on estimated age with depth.

3.5 Palaeoenvironmental Synthesis

This section includes my interpretation of the results from the analysis of the SC-23 and SC-21 cores.

3.5.1 Changing Marine Influence in SC-23-1

The lithology data shows a change at 455 cm, indicating varying energy input in the deposits. SC-23-1 includes fine green/grey sediment at its base which the PSA results show as mostly silts (Figure 3.9). At 455 cm (a gradual change of >1 cm), colouration becomes grey (Figure 3.3) and a small increase in organic matter is observed (Figure 3.5). Despite this change in colouration, PSA results classify most of the material on each side of this transition as silts, with a low proportion of sands. This indicates somewhat consistent low-energy conditions throughout this part of the core (455 - 361 cm) and an environment in which mostly fine particles fall out of suspension (Palmer et al., 2021). The lithological evidence supports the interpretation that this was a freshwater lake situated within the basin at South Cuidrach.

A clear change in the hydrological setting in the basin at South Cuidrach occurs above 455 cm. At 440 – 438 cm in SC-23-1 (439 cm is dated to 8181 ± 144 cal. BP), a hydrological change is identified by the introduction of polyhalobian (marine) and mesohalobian (brackish) diatom taxa (Figure 3.9). At 438 cm, halophobian (freshwater) species reduced from 16% to 0% of the total count at 440 cm. The sharp cessation of halophobian species and the corresponding immediate introduction of poly/mesohalobian species means that the depth of the change in hydrological conditions from freshwater to brackish is identified at 440 – 438 cm. *Fragilaforma virescens* (basonym: *Fragilaria virescens*) is one of the species found in high concentrations below 438 cm, which is known to inhabit freshwater lakes (Flower et al., 1996). This diatomological change occurs at the same depth as a small shift in particle size, above which there is a lesser proportion of sands.

As described above, the introduction of marine and brackish diatom taxa indicates increasing salinity within this coastal lacustrine setting. Alongside the marine/brackish taxa at depths <440 cm, saline-tolerant freshwater (oligohalobian) taxa are common (Figure 3.9). This indicates that the hydrological change is from freshwater to slightly brackish conditions, where all preserved diatom taxa inhabit salinities of > 0.2‰ (Hemphill-Haley, 1993; Selby and Smith, 2016). Clearly, following the diatom change at 8181 ± 144 cal. BP there is still a large proportion of freshwater input into the basin resulting in these assemblages. Selby and Smith (2016) associate similar diatom changes with marine influence from the very highest tides (from a coastal barrier formation nearby on Loch Snizort) such that if the South Cuidrach basin was inundated due to an RSL transgression, it would be indicative of the highest

tides at the time of ingression, not a waterbody permanently connected to the sea. This is supported by the lithological evidence showing a low-energy lacustrine environment, dissimilar to the sand/cobble beach found at around MSL at South Cuidrach in the modern environment (Figure 2.2).

Another lithological change which occurs at 361 cm; from mainly minerogenic silts to mainly humified peats; represents the start of peat formation in the basin. The Holocene epoch on Skye is typified by the post-glacial formation of peat in coastal wetlands (Walker and Lowe, 1990; Ballantyne, 1990), and this is seen in SC-23-1, marked by a sharp increase in organic matter (Figure 3.9 (B)). This change occurs beneath the top of the diatom preservation (324 cm), which is typical of isolation basins, where diatom assemblages continue to represent a marine environment later than corresponding lithological changes (Long et al., 2011).

An increase in brackish taxa at 332 cm indicates a hydrological change from a mostly freshwater setting to one with increased marine influence. The change is mostly taxonomic, as rather than a gradual change in the concentrations of preexisting species, several new species are found, particularly *Navicula crucicula* (synonymous with *Parlibellus Crucicula* (Genkal and Yarushina, 2017)) which inhabits a diverse range of freshwater and brackish environments. The proportion of brackish species is greater than that of freshwater species at 332 cm (Figure 3.9), leading to the interpretation that this assemblage reflects an increase in tidal influence within the basin and a greater influence than the very highest tides alone. Rather than just the highest tides, as in the strata beneath, at depths above 332 cm until preservation ceases at 324 cm, marine deposits are interpreted to represent a tidal level between HAT and MHWS. This change occurs at 6367 ± 68 cal. BP, a date retrieved from the nearest dateable material to this diatomological change at 332 cm (Table 3.4).

This interpretation suggests that the basin was a freshwater lake before 8181 ± 144 cal. BP, after which the lake became brackish. Diatom preservation ceases before the end of this brackish phase, but evidence from the peat stratigraphy and fragments of vegetation in SC-23-1 suggest a terrestrial limit. A radiocarbon date of 5597 ± 109 cal. BP was sampled using material from a mass of surface herbaceous plant matter at 301 cm, providing a terrestrial limiting data point given the absence of evidence of any marine influence at this point. Given these arguments, marine influence must have reduced or abated at some point between these dates, though the exact timing is uncertain, most likely due to the dissolution of diatom valves in humic acids. Using Calib Rev 8.1.0 and IntCal 20 (Stuiver and Reimer, 1993; Reimer et al., 2020), these two dates return a calibrated pooled mean value of 6049 ± 114 cal. BP. However, marine influence must have ended in the basin between the dates at 301 and 331 cm, and given the uncertainties discussed above it is most accurate to report the age of the end of marine influence in the basin as between 6435 and 5488 cal. BP at a depth of 316 ± 15 cm.

The evidence presented above gives some insight into the drivers of the sustained brackish conditions at South Cuidrach which started at 8181 ± 144 cal. BP and ceased by 5597 ± 109 cal. BP. This period is interpreted as having been caused by intermittent or temporary inundation of the site from the highest tides. The sustained nature of these conditions without reverting to a freshwater body is evidence that this marine influence was not the result of a tsunami or transient storm events, which would have only caused short-lived marine inundation (e.g. Storegga tsunami at c. 8150 cal. BP, which was a transient event (Woodroffe et al., 2023)). Sedimentological evidence (3.2.2) also supports this interpretation as no occasional high-energy events are observed.

To summarise, there is a brackish phase within this coastal lacustrine setting which occurs from 438 cm (8181 ± 144 cal. BP) until the top of the diatom preservation, indicative of the highest tides (HAT). A further increase in brackish diatom taxa at 332 cm (6367 ± 68 cal. BP) occurs and is maintained until diatom preservation ceases at 324 cm, indicative of a tidal level between HAT and MHWS. The lithological evidence suggests that isolation occurred at some point following the top of the diatom preservation, and before the terrestrial limit, which is dated to 5597 ± 109 cal. BP from a mass of herbaceous plant matter, a point at which the depositional setting changes from a low-energy coastal lake to a peat fen which is the contemporary environment at South Cuidrach.
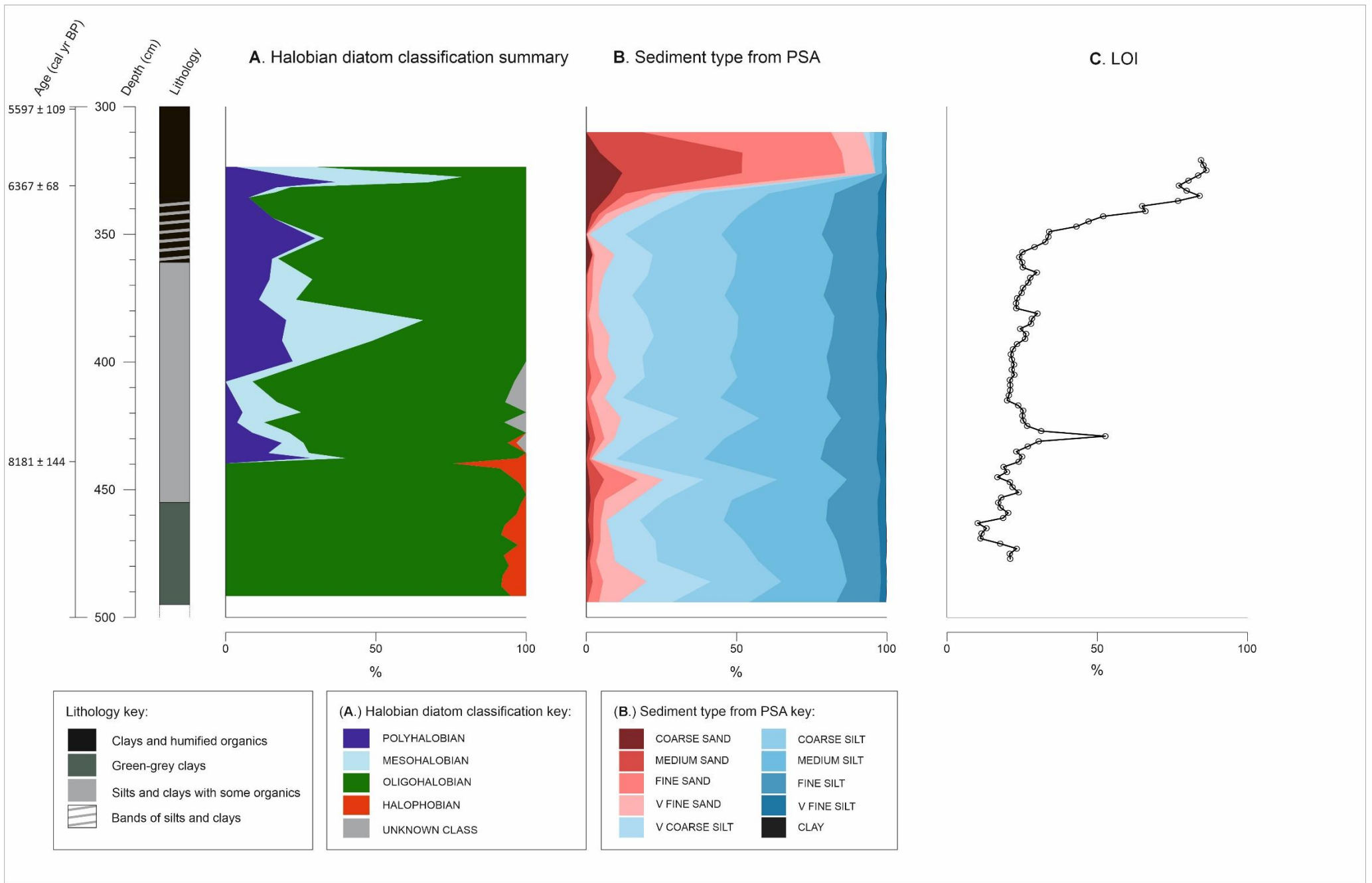
Figure 3.9. Summary of palaeoenvironmental datasets from SC-23-1, including the lithology and radiocarbon dates. A. Stacked area plot showing the Halobian classification summary of diatom assemblages (Figure 3.6). B. Stacked area plot of PSA results; grouped into sediment type. C. Loss on ignition (%) against depth.

3.5.2 Determining the Sill Elevation

Given the topography of the bedrock within the basin (3.1.2), any marine inundation into this coastal lake or lagoon would mean the sea levels surpassed the lowest possible ingression point; the 'sill elevation'. Identifying this was another objective of the GPR survey work. The results from the GPR Line -5 (Figure 3.10) show the overburden thickness along the seaward side of the basin edge to be southward along 59.2 m from the origin (57°32'02"N, 006°22'19"W) of Line -5, at a depth of 2.3 m (for location see Figure 3.2).
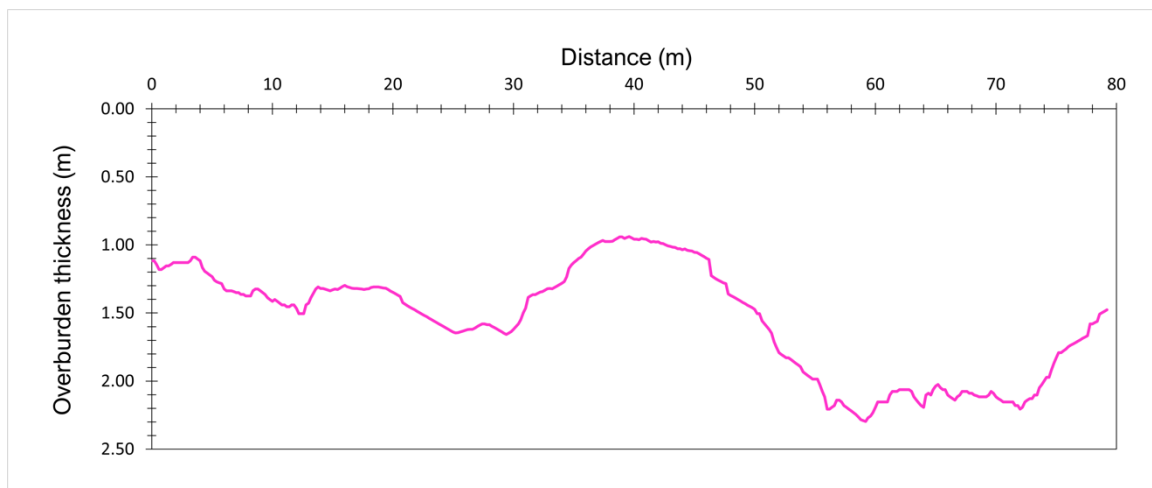
Figure 3.10. Overburden thickness along Line -5, which runs adjacent to the bedrock sill, on the landward side of the raised beach. Distance (m) = 0 shows the origin of the GPR Line -5 at 57°32'02"N, 006°22'19"W. Line -5 is identified in (Figure 3.2).

Figure 3.2 shows an overburden thickness of < 3 m at the edge of the dataset to the northeast, however, these are not seaward-facing, and there is an increase in surface elevation towards the cultivated land to the northeast. This considered, it is unlikely that the ingression point of the basin is found along the northeastern side of the basin. To the northwest of the GPR dataset also, the overburden thickness is low (1.5 – 1 m) at its edge. Also, there is another deep section (1.66 m at most) identified in Line -5 at 20 – 30 m from the origin (Figure 3.10). No surface elevation data was collected at the surface along Line -5 though the topography variation is estimated to be <0.5 m. Line -5 was located on the level surface of the peat fen, on the landward side of the surface of the raised beach deposits. Considering which, the point where the bedrock is deepest along Line -5 must represent the ingression point. The difference between the deepest point from Line -5 (2.3 m) and the deepest core

from the sill transect (2.59 m, see 'Sill transect 6' in Table 3.1) is 0.29 m. The root sum of squares of error estimates from dGPS, levelling and comparing GPR with the sill transect data (above) determines the sill elevation to be 4.47 ± 0.29 m OD.
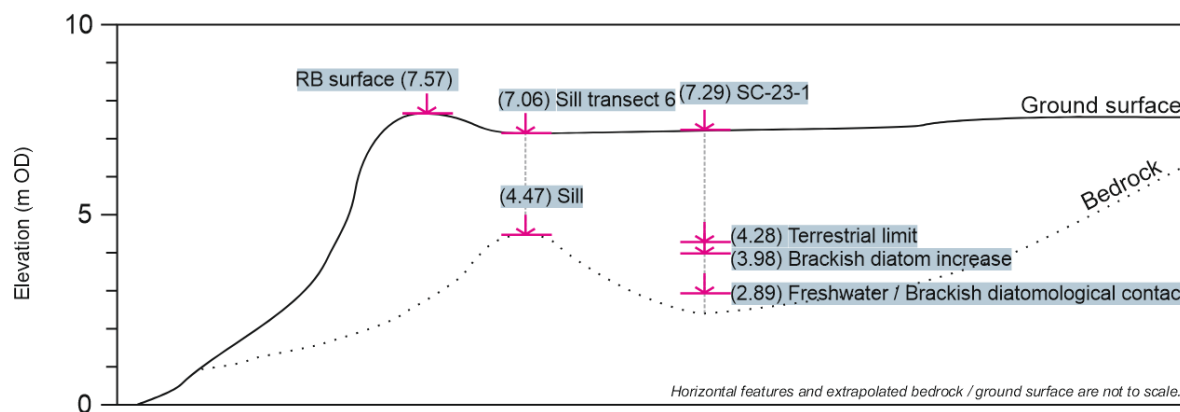
Figure 3.11. Elevations (m OD) of various geomorphological features at South Cuidrach. Table 3.1 lists elevation survey results in full. The point which controls the ingression of the basin is above the key diatom changes. The elevation of the raised beach surface (RB surface) is shown.

Diatom changes caused by a marine ingression in the basin are shown to be controlled by the lowest elevation of the basin sill (Figure 3.11), as the lithological and diatomological changes in the core occur at a lower elevation than the basin sill as identified through the fieldwork (Long et al., 2011). Both the ingression of the basin and the subsequent isolation are controlled by this elevation of 4.47 ± 0.29 m OD, therefore, this site is an isolation basin where the lithological and diatomological data (2.5.1) provide evidence that between c. 8181 ± 144 cal. BP and sometime before the terrestrial limit at 5597 ± 109 cal. BP, the basin was a small, brackish, low-energy lacustrine environment. On balance, the evidence suggests this brackish phase is caused by a change in RSL rather than a short-lived or extreme event. This isolation basin offers precise constraints on RSL changes at the site which are analysed in the following section.

3.5.3 New Empirical Constraints on Relative Sea Level from South Cuidrach

Firstly, a new sea level index point (SLIP) (Shennan et al., 2018) is identified from the ingression phase in the isolation basin. According to data from the UK Hydrographic Office (1993), HAT in Loch Snizort is 5.83 m CD, and the difference from CD to OD is + 2.7 m in Loch Snizort, meaning HAT is 3.13 m OD (Table 2.1). If we interpret the initial marine ingression at 8181 ± 144 cal. BP as coming from the highest tides (based upon modern tides), then HAT (the reference water level (RWL)) must have been at this elevation of 4.47 ± 0.29 m OD, and RSL was 1.34 ± 0.7 m above present (Sill elevation - HAT). Elevation

error is calculated as the 2σ uncertainty of the survey elevation error and the indicative range (0.2 m; see 'Isolation Basins', in Table 2 of Shennan et al., (2018)) following the methods of Shennan et al., (2015, 2018). At 8181 ± 144 cal. BP, RSL was 1.34 ± 0.7 m above present at South Cuidrach.

Secondly, another new SLIP is identified from the hydrological change within the brackish phase of the basin, where a small change in type and percentage abundance of brackish diatom taxa occurs (3.5.1) (See 'Brackish diatom increase' in Figure 3.11). This diatomological change at 331 cm is dated to 6367 ± 68 cal. BP. This index point represents a different RWL, as marine influence has increased. This index point also represents marine influence from near the highest tides, meaning a RWL between HAT and MHWS following the methods of Shennan et al., (2015, 2018). MHWS at South Cuidrach is presently 2.6 m OD (Table 2.1). The median value of present HAT and MHWS is 2.87 m OD. This change was also controlled by the basin sill (4.47 ± 0.29 m OD), meaning RSL was 1.6 ± 0.79 m above present. Elevation error is calculated as the 2σ uncertainty of the survey elevation error and the indicative range (0.27 m). In this instance, the indicative range is given as half of the difference between HAT and MHWS (HAT – MHWS / 2) after Shennan et al., (2018). At 6367 ± 68 cal. BP, RSL was 1.6 ± 0.79 m above present at South Cuidrach.

Finally, a new terrestrial limiting datapoint is identified using the mass of surface herbaceous plants at 301 cm in SC-23-1, with a radiocarbon age of 5597 ± 109 cal. BP (See 'Terrestrial limit' in Figure 3.11). The elevation of this point is 4.28 ± 0.29 m OD, meaning this point is possibly above the sill elevation given the error on the sill elevation of (4.47) ± 0.29 m OD (Figure 3.11). In this case, I use the same RWL of modern HAT (3.13 m OD), compared with the terrestrial limiting elevation of 4.28 ± 0.29 m OD. In the case of terrestrial limiting dates, the reference elevation is the maximum point RSL can have reached within the uncertainty range (Garrett et al., 2020). This means RSL at 5597 ± 109 cal. BP was less than 1.5 m higher than present, with a lower error estimate of - 0.7 m. The calculation is based on subtracting the RWL (3.13 m OD) from the elevation of the terrestrial limit (4.28 ± 0.29 m OD), resulting in a value of 1.15 ± 0.35 m. Elevation error is calculated as the 2σ uncertainty of the survey elevation error and the indicative range (0.2 m).

Two new SLIPs and a terrestrial limiting data point have been developed from the litho- and bio-stratigraphic evidence within this isolation basin. These data aim to contribute to the expanding database of postglacial RSL results in Scotland (Shennan et al., 2018) and global databases (Khan et al., 2019). A simplified version of the SLIP database spreadsheet from Shennan et al., (2018) is presented in Table 3.5.

Table 3.5. New sea level index points from South Cuidrach. Format adapted from Shennan et al., (2018).

Depth in SC-23-1 (m)	Type	Latitude	Longitude	Radiocarbon Age (14C a BP)	Radiocarbon age uncertainty (14C a)	Calibrated median age (cal. BP)	Age 2σ Uncertainty ± (cal. a)	Sample elevation (m MSL)	Sample elevation uncertainty + (m)	Sample elevation uncertainty - (m)	RSL (m)	RSL 2σ Uncertainty + (m)	RSL 2σ Uncertainty - (m)
4.39	Isolation basin	57.53	-6.37	7380	30	8181	144	4.47	0.29	0.29	1.34	0.7	0.7
3.31	Isolation basin	57.53	-6.37	5580	30	6367	68	4.47	0.29	0.29	1.6	0.79	0.79
3.01	Terrestrial limiting	57.53	-6.37	4880	30	5597	109	4.28	0.29	0.29	1.5	0	0.7

3.5.4 Holocene Vegetation Changes

Pollen results from SC-23-1 indicate several key changes in vegetation during the deposition of the sedimentary sequence outlined in Section 3.2.1. The deepest pollen sample at 440 cm (c. 8181 ± 144 cal. BP) includes both the arboreal pollen found in the subsequent four samples (ending at 330 cm (c. 6367 ± 68 cal. BP)) and low concentrations of ferns, mosses and shrubs. This is evidence of environmental change occurring following the basal sample of 440 cm (c. 8181 ± 144 cal. BP) which causes a subsequent reduction in these autochthonous spores and pollen from low-lying vegetation, with the sole exception of *Sagina subulata*, which is found at 420 cm depth. Given the diatomological evidence that this site was a small coastal lake at the time (3.5.1) containing mostly minerogenic sediment, the pollen suggests it was surrounded by heathland ferns and mosses found at 440 cm. There is a possibility that the surrounding environment was affected by the salinity and pH changes (Shennan et al., 1995) associated with the marine ingression into the basin. *Pinus* pollen is found at 440 cm alongside *Quercus*, and again at 350 cm, at percentage abundance of > 10 %, characterising a mixed woodland environment from the area surrounding South Cuidrach. Vegetation at depths of 420 – 330 cm appears to be *Corylus* and *Betula* dominated mixed woodland at South Cuidrach, with large

amounts of *Poaceae* (grasses) also present. Due to the radiocarbon ages, this stage is well constrained between approximately 8181 ± 144 cal. BP and 6367 ± 68 cal. BP (331 cm) At 420 cm, 8 grains of *Baldellia ranunculoides* (Lesser Water Plantain) were counted. This perennial herb grows in freshwater wetland environments (Kozlowski et al., 2008).

The Elm decline, which is observed widely in the Isle of Skye Holocene pollen record, is estimated to have occurred at 5036 ± 247 cal. BP (Parker et al., 2002). However, this event is not clearly identifiable in SC-23-1 as only one sample contains *Ulmus*. This count of *Ulmus* coincides with the mixed woodland assemblages throughout the lower part of the SC-23-1 pollen sequence, from its base to 330 cm. Genera such as *Quercus* alongside *Larix* and *Pinus* also indicate a developed mixed woodland, rather than a sparse post-glacial shrubland.

Subsequent samples at 270 and 300 cm (c. 5 ka BP from age/depth model) contained very few pollen grains*,* and insufficient data to conclude that this was a purely grassland environment. Although, they coincide with a general decrease in arboreal pollen at other sites on Skye (Selby, 2004). *Calluna vulgaris* (Heather), alongside these other shrubs are prevalent in the modern environment across Skye and at South Cuidrach. They increase following anthropogenic landscape clearances of the Late Holocene (Selby, 2004).

On Skye, an increase in *Sphagnum* spores typifies the acidification of soils associated with the development of heathland, commencing at the start of the late Holocene (Selby et al., 2004, 2023). This corresponds with an increased occurrence of *Calluna vulgaris* which is present at 180 – 150 cm in SC-23-1, also representative of a heathland environment (Edwards et al., 2019). *Sphagnum* spores commence at 240 cm depth, and the age-depth model in Section 3.4.2 provides an age of 4187 ± 239 cal. BP for the 240 cm sample. This model is presented with the caveat of its limited constraining radiocarbon dates at these depths. *Quercus* is persistent at this stage of the sequence (240 – 150 cm), alongside other key arboreal pollen in *Betula* and *Alnus*. This part of the sequence indicates the development of an environment with similar characteristics to the modern at South Cuidrach which seems to have changed little during much of the Late Holocene. This is clear from the large variety of shrubs and mosses such as those that are observed in (first section methodology), alongside small concentrations of arboreal pollen (*Quercus, Betula*). There is a reduction in arboreal pollen after the age of 6367 ± 68 cal. BP (331 cm), potentially caused by regional woodland clearance occurring on Skye at the start of the Late Holocene (Green and Edwards, 2009; Selby et al., 2023).

3.5.5 Summary

Based on the evidence from diatom and pollen assemblages, LOI, and PSA, the basin at South Cuidrach was once a small coastal lake and operated as an isolation basin during the Holocene, and was subject to sustained brackish hydrological conditions after 8181 ± 144 cal. BP, which ceased before 5597 ± 109 cal. BP. These brackish conditions are interpreted to be associated with the highest tides of a transgression in RSL at the site. Following c. 6367 ± 68 cal. BP, marine influence increases slightly, leading to the interpretation of a tidal level between HAT and MHWS at this time. Partial/intermittent marine inundation of the basin may have been caused when these highest tides exceeded 4.47 ± 0.29 m OD. Two new SLIPs and a new terrestrial limiting data point have been developed from this isolation basin, which are listed in Table 3.5.

The basin at South Cuidrach has experienced several changes in vegetation over the Middle and Late Holocene. Mixed woodland dominates the pollen assemblages at the base of the core, which contract possibly due to anthropogenic landscape clearances of the Late Holocene. SC-23-1 preserves the onset of peat formation at this coastal site and the prevalence of grassland associated with the woodland clearances. The vegetation changes in response to marine inundation, with heathland ferns and mosses disappearing from the record after the basal sample. The implications of these new data in terms of the palaeoenvironment and RSL changes at South Cuidrach continue to be explored in Chapter 5.

4. SCONSER

4.1 Sconser Methodology

Twenty presently submerged and intertidal stone circles between 3 and 5 m in diameter are dispersed on the foreshore at Sconser, Isle of Skye, identified by Professor Karen Hardy as possible LUP huts (Bailey and Hardy, 2021). Site investigations within this project focussed on an elevation survey to precisely define these artefacts against Ordnance Datum and build an approximate chronology for their construction from modelled RSL curves. A digital earth model (DEM) created from a photogrammetry drone survey (McCarthy, 2023) was then corrected to the elevation survey, to visualise the palaeo-shoreline positions based upon modelled RSL data.

4.1.1 Site Description

The area denoted in this report as Sconser (Figure 4.1) is a large, north-facing tidal flat near the village of Sconser, Skye. It lies to the east of the entrance of Loch Sligachan, on the opposite shore to Peinachorrain.

Figure 4.1. Ordnance Survey map showing the location of the Sconser study site. Projected British National Grid (BNG) and displaying BNG coordinate system (Ordnance Survey, 2024).

The mountain peak Glamaig is located 3 km southwest of the site and is part of the Red Cuillin range. Another name is given for the foreshore area of Rubha Garbh (translated as rough point). This expansive foreshore is exposed to the north following the Narrows of Raasay between the isles of Skye and Raasay, and to the east following Caol Mòr between Raasay and Scalpay. Chart data from the UKHO records that the offshore approaches to Loch Sligachan are 52 m at their deepest (© British Crown and OceanWise, 2024). The Isle of Skye has an average windspeed of 11 knots (Met Office, 2024). The modern tidal range is around 4.9 m (Table 2.1), which exposes a particularly large foreshore during spring tides (Figure 4.3).

Various marine sedimentary deposits are found on the foreshore. Ranging from sands and silts through to boulder-sized deposits. It's these marine sands and gravels into which the stone circle artefacts are embedded (Hardy et al., 2021) (Figure 4.2). The artefacts are dispersed throughout the intertidal zone at Sconser (Figure 4.3). Due to the artefact's submersion, it is not possible to get a direct date for their construction, nor is there any material available for direct dating.

Figure 4.2. Photo taken from the Sconser field site looking north. The foreground shows one of the stone circle artefacts with a 3 m stave for scale. The peak of Ben Tianavaig is in the background. Photographed in March 2023.
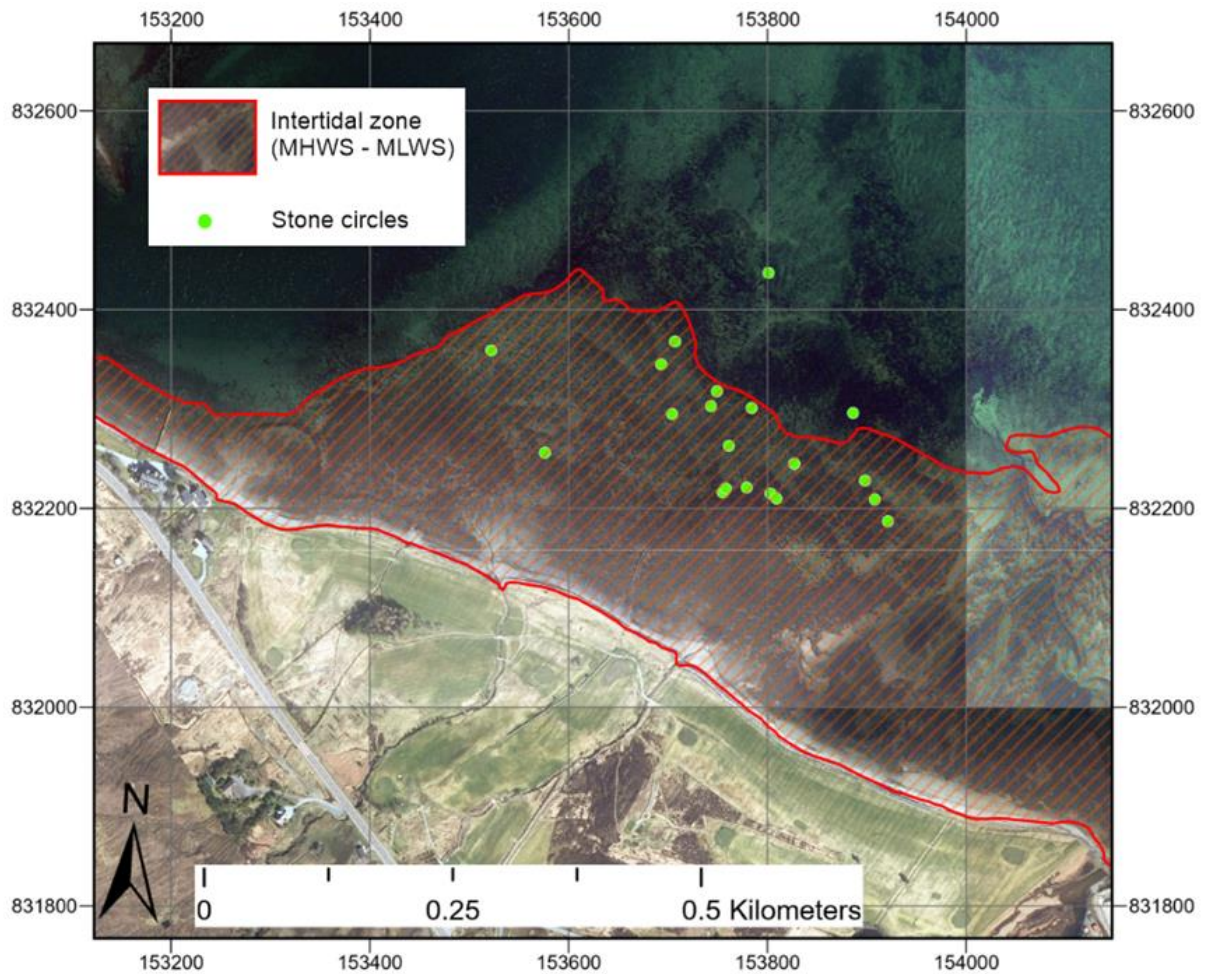
Figure 4.3. The intertidal zone (modern MHWS – MLWS) at Sconser, and the locations of stone circle artefacts identified by Hardy et al., (2021). Locations of artefacts are shown again with results in Figure 4.5. Tidal data from Ordnance Survey. Coordinates are British National Grid. Aerial photography from © Getmapping Ltd (2024).

4.1.2 Bathymetry

In 2021, a photogrammetry drone survey was completed by local volunteer Jamie Booth in association with Professor Karen Hardy (University of Glasgow) and Dr John McCarthy (University of Flinders). This was essential data for the aims of the work I carried out at Sconser, precisely defining the relative elevations of the artefacts and the surrounding bathymetry. The georeferenced photos and elevation data were collected at low tide during spring tides in March 2023 and were constrained by the lower tidal limit. A DEM was constructed using photogrammetry techniques at Flinders University from drone images. It achieved a horizontal resolution of 10 cm^2 across an area within Figure 4.3 of around 600 by 450 m.

4.1.3 Elevation Survey

Model outputs predict that RSL was lower than present during the postglacial and early Holocene (Figure 1.9) (Bradley et al., 2011; Ward et al., 2016; Scourse et al., 2024). Therefore, to overcome the lack of chronology for these sites, I used modelled RSL as a method to constrain the potential time scale in which these artefacts could have been built, under the assumption that they must have been built above the high-tide mark (Hardy et al., 2021; Bailey and Hardy, 2021). Tidal corrections for the GIA model export data from MSL to HAT were applied using data from the UKHO (Table 2.1). This therefore required establishing their elevations with respect to an elevation datum, to then compare to the elevations of palaeo sea levels. This elevation survey was achieved using a dGPS survey at Sconser in March 2023, carried out by myself, Professor Natasha Barlow and Dr Graham Rush. To 'tie in' the Flinders University drone data to the elevation survey, prominent control points were surveyed which were easily identifiable on the DEM. These points were also photographed.
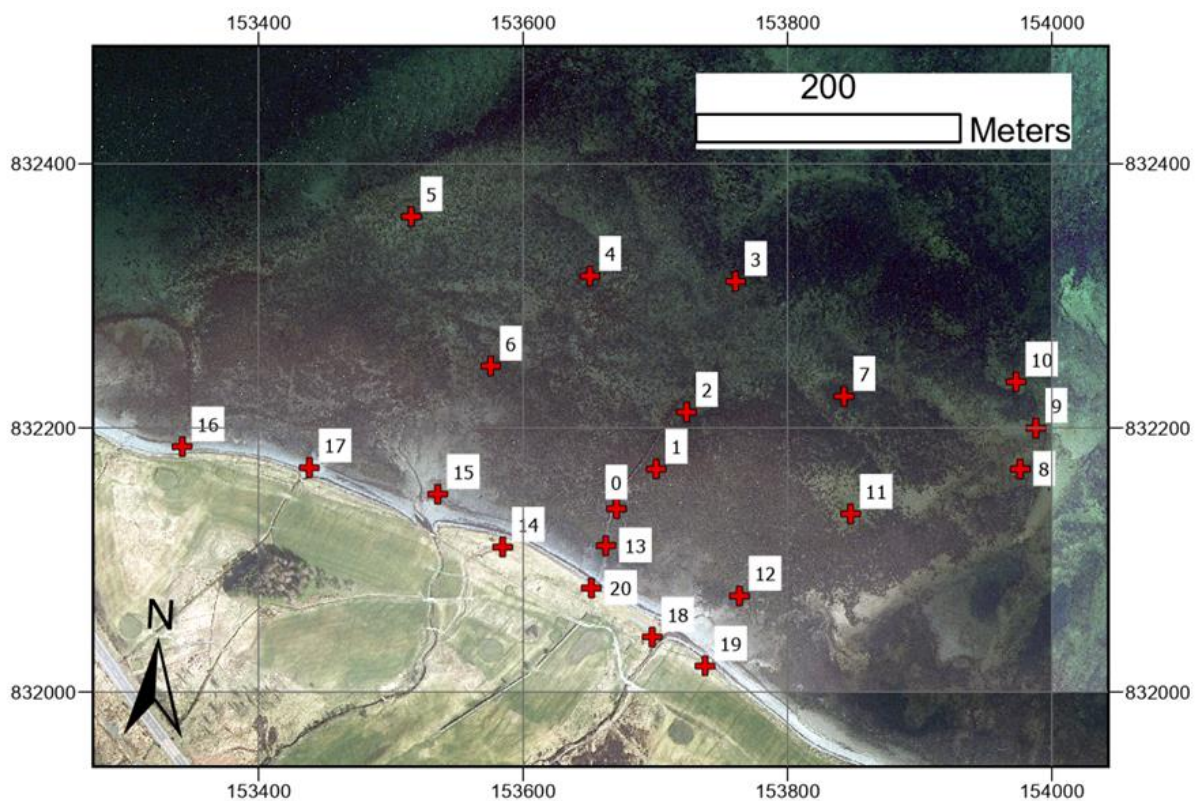
Figure 4.4. The 20 elevation control points surveyed at Sconser, Isle of Skye. Coordinates are British National Grid. Aerial photography from © Getmapping Ltd (2024).

Twenty locations were surveyed, following the criteria of being easily identifiable in the drone survey data, and widely spatially dispersed, as well as possible to reach given time constraints against the

rising tide. Elevations were measured using a theodolite level from a TBM situated at site 20 (Figure 4.4). The operation of dGPS and the levelling survey was identical to that described in Section 2.4. Photos were taken at each elevation control point for reference and used in identifying equivalent locations manually on the DEM. To supplement this approach, a GPS lat-long measurement was taken at each location, using a Garmin 12 XL handheld GPS.

Elevation corrections were applied to the drone survey DEM in ArcGIS Pro Version 3.1.4, after the manual identification of control points using the site photos and dGPS described above. An estimate of the elevation of RSL was acquired from the PALTIDE data portal tool (Ward et al., 2016; Scourse et al., 2024), which sources RSL estimates from the BRADLEY 2011 GIA model (Bradley et al., 2011).

4.2 Sconser Results

This section presents the results of the investigation at Sconser, including the bathymetric survey and approximate age of the artefacts based upon the position of the palaeoshoreline.

4.2.1 Bathymetry and Palaeoshoreline at Sconser

Results from the elevation-corrected DEM show a gently sloping intertidal zone upon which the artefacts are situated (Figure 4.5). The DEM shows a c. 5 m change between MSL and the lowest seaward extents of the dataset. The approximate average gradient in the DEM of 0.3% between modern MSL and the depths to the northeast. Coverage was limited by the elevation of lowest tides at the time of surveying. The data has been clipped, removing areas where the drone survey data was noisy and failed to precisely measure the bathymetry. The clipped areas were manually identified on the basis that features of the seabed such as small boulders were not clearly visible.
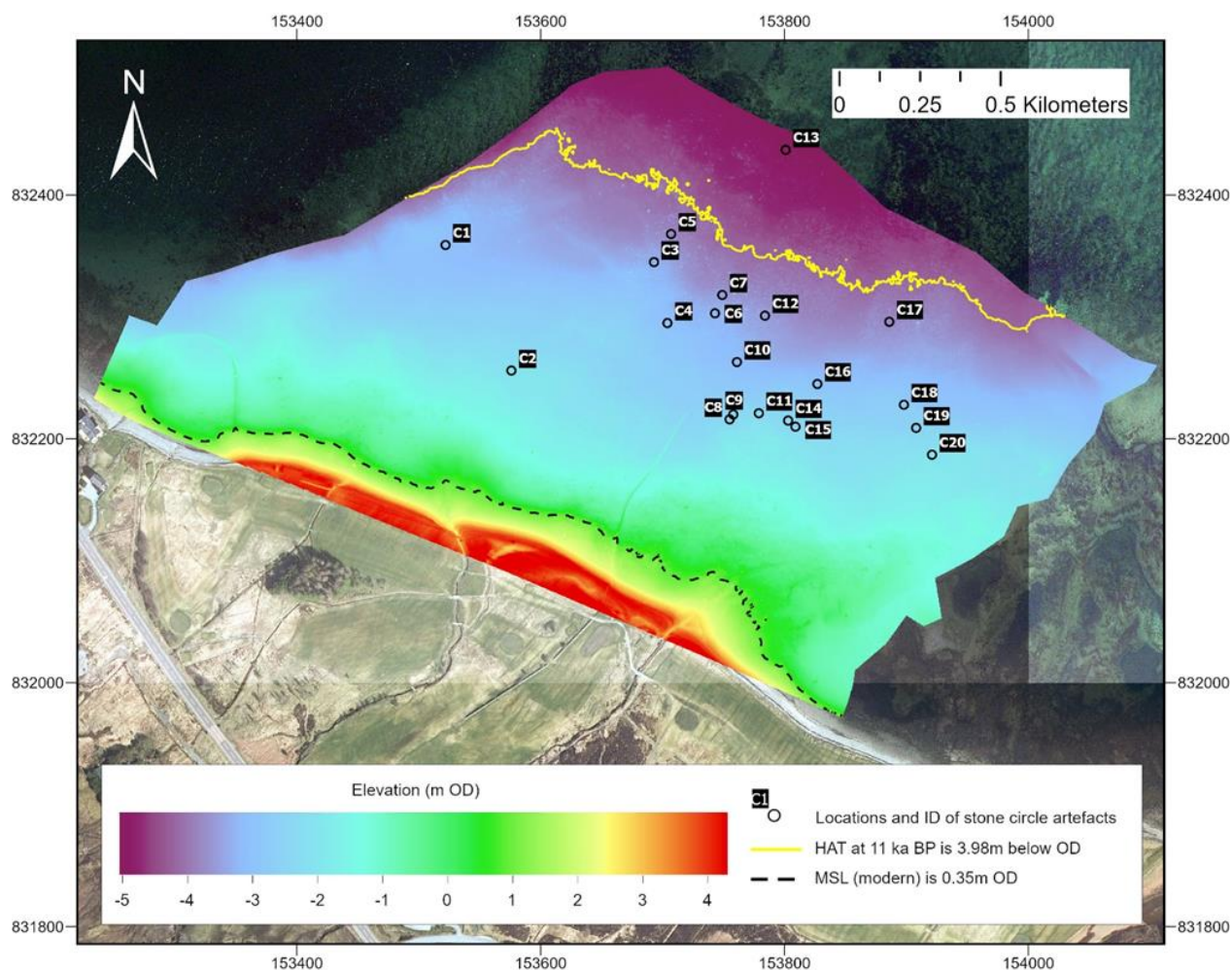
Figure 4.5. Bathymetry of the intertidal zone at Sconser, measured using photogrammetry by John McCarthy in 2021, elevation corrected in this project. Includes locations of stone circle artefacts and estimates of HAT from a GIA model (Bradley et al., 2011; Scourse et al., 2024). Artefacts are listed in Table 4.1 alongside their elevations. Aerial photography from © Getmapping Ltd (2024).

The pattern of RSL change since the Last Glacial is described in detail in Chapter 1, and model outputs for Sconser show a similar pattern to other sites in northern Skye (e.g. South Cuidrach) including an RSL low stand at the start of the Holocene. These estimates (Figure 1.9) show that at 10 ka BP, RSL was at -2.46 m; at 11 ka BP, -7.13 m; and at 12 ka BP, -3.26 m. Data from the UKHO (1993) reports that HAT at Broadford Bay is 3.15 m OD (0.2 m CD) (Table 2.1), representing the nearest secondary port to the Sconser field site, around 12 km southeast of Sconser.

Table 4.1. Stone circle artefacts located as green dots in Figure 4.5 and their elevation. These artefacts are identified as potentially Late Upper Palaeolithic huts (Hardy et al., 2021).

ID	Elevation (m OD)	Relative elevation below modern MSL (0.35 m OD)	x (British National Grid)	y (British National Grid)
C1	-3.04	-2.69	153522	832359
C2	-2.19	-1.84	153576	832256
C3	-3.24	-2.89	153693	832345
C4	-2.96	-2.61	153704	832295
C5	-3.59	-3.24	153707	832368
C6	-3.2	-2.85	153743	832303
C7	-3.47	-3.12	153749	832318
C8	-2.42	-2.07	153755	832216
C9	-2.5	-2.15	153758	832220
C10	-3.08	-2.73	153761	832263
C11	-2.41	-2.06	153779	832221
C12	-3.42	-3.07	153784	832301
C13	-4.49	-4.14	153801	832437
C14	-2.45	-2.1	153803	832215
C15	-2.44	-2.09	153809	832210
C16	-2.99	-2.64	153827	832245
C17	-3.66	-3.31	153886	832296
C18	-2.75	-2.4	153898	832228
C19	-2.58	-2.23	153908	832209
C20	-2.18	-1.83	153921	832187

Assuming modern tidal ranges, the following estimates of the elevation of HAT at each 1 ka time interval are as follows: 10 ka BP, HAT = 0.69 m OD; 11 ka BP, HAT = -3.98 m OD; and 12 ka BP, HAT = -0.11 m OD. These values are calculated using the modern difference between MSL and HAT at Sconser. Around 11 ka BP is the only time since the LGM at which sea levels are modelled to have fallen below

the lowest elevations of the artefacts at -3.66 m OD (excluding artefact C13), as demonstrated by the contour line on the DEM shown in Figure 4.5 (HAT at -3.98 m OD). Figure 4.5 demonstrates how at modern MSL, each of the artefacts is submerged, ranging between 1.83 and 4.14 m below MSL. Hardy et al., (2021) compare these structures with Late Palaeolithic huts (Kuznetsov, 2013), based on their morphology.

4.2.2 Summary

By surveying the elevations of presently intertidal stone circle artefacts on the foreshore at Sconser, Skye, we can approximately post-date the artefacts to 11 ka (± 1 ka) based on the modelled elevations of palaeo RSL. My findings suggest that these artefacts were constructed in the LUP or Mesolithic period, during a low-stand in RSL after the LLS which pre-dates rising sea levels associated with a rapid increase in global meltwater input during the early Holocene (Smith et al., 2011).

5. DISCUSSION

This chapter is structured around the research objectives presented in Chapter 1 to answer the overarching research question: **How did relative sea level and environmental changes on the Isle of Skye affect the migrations of Late Upper Palaeolithic and Mesolithic humans?** The sub-sections of this discussion chapter address each research objective systematically.

5.1 Relative Sea Level changes at South Cuidrach

This section is written to demonstrate how I have met the first research objective: **Reconstruct changes in RSL during the Postglacial and Holocene at South Cuidrach.** The implications of these results for the archaeological findings at South Cuidrach are discussed in the subsequent Section (5.4).

5.1.1 Comparisons with Modelled Relative Sea Level Predictions

To understand the drivers of the RSL changes at South Cuidrach, the data is compared with outputs of a GIA model (Figure 5.1). At 8 ka BP, the BRADLEY2011 model (Bradley et al., 2011) predicts RSL as -0.97 m, compared with 1.34 ± 0.7 m at 8181 ± 144 cal. BP from the South Cuidrach data. At 6 ka BP, the GIA model predicts RSL was 2.76 m, whereas RSL is reconstructed as 1.6 ± 0.79 m above present at 6367 ± 68 cal. BP. Here, the PALTIDE GIA model outputs predict RSL 0.37 m above the maximum error margin of the South Cuidrach RSL data point. Model predictions, given the uncertainties here, estimate a similar timing and magnitude of the mid-Holocene highstand, however, there are some key differences. The isolation basin data from South Cuidrach indicates that RSL rose to the index point at 1.34 ± 0.7 m at 8181 ± 144 cal. BP, which is > 1 ka earlier than the modelled dataset predicts the equivalent RSL rise. Also, the terrestrial limit at 5597 ± 109 cal. BP sits below the modelled dataset, as the model over-predicts RSL this time (Figure 1.9). GIA models are improved by making iterative changes to fit empirical data (Bradley et al., 2011; Whitehouse, 2018; Bradley et al., 2023), and this data will contribute to that field.
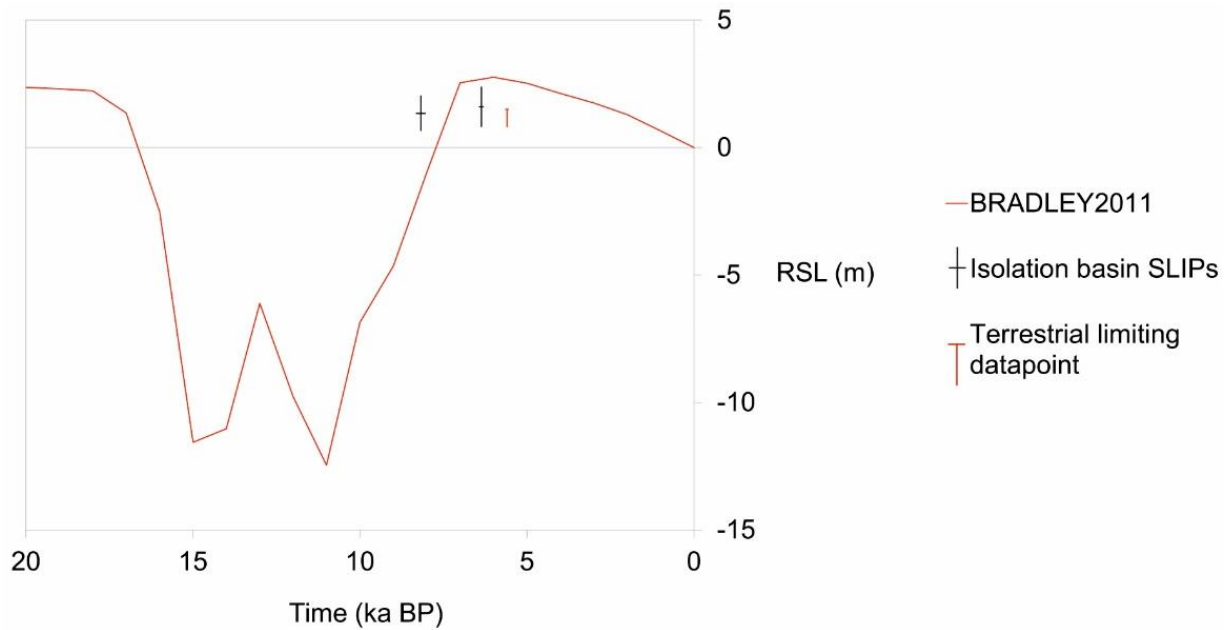
Figure 5.1. Two new sea level index points and a terrestrial limiting datapoint from South Cuidrach are compared with GIA-modelled RSL outputs for South Cuidrach extracted using PALTIDE (Ward et al., 2016; Scourse et al., 2024) from the BRADLEY2011 model (Bradley et al., 2011). See also Figure 1.9.

Another local site also suggests an earlier mid-Holocene rise in RSL. 3 km southwest of South Cuidrach, at Lyndale House on Loch Snizort (Selby and Smith, 2016), bio and litho-stratigraphic evidence from a coastal barrier system indicates marine influence after 8205–8386 cal. BP, until 6498–6716 cal. BP at 1.04 – 1.91 m OD (0.71 – 1.58 m above MSL (Table 2.1)) is identified. Sediment compaction was not quantified at the Lyndale House site in this study. Isolation basin RSL indicators are not influenced by sediment compaction, which is what makes them such excellent indicators of sea-level change (Long et al., 2011). Nevertheless, this data from Lyndale house falls within the error bounds of the RSL data points from South Cuidrach of 1.34 ± 0.07 m and within the chronology of between 8181 ± 144 cal. BP and 6435 - 5488 cal. BP (the ages of ingression and isolation of the basin, respectively). Considering this, South Cuidrach RSL data points and the Lyndale house coastal barrier system corroborate well on the timing of RSL rises in Loch Snizort.

Following the mid-Holocene highstand, which resulted in the inundation of the isolation basin at South Cuidrach, the BRADLEY2011 model predicts that RSL fell continually until present levels. The new empirical dataset presented in this thesis highlights that the GIA model predicts RSL rise later and higher in the Holocene than recorded in the South Cuidrach basin.

5.1.2 Drivers of Relative Sea Level Changes at South Cuidrach

Overall, the RSL changes at South Cuidrach appear closely related to major changes in RSL that occurred along the Scottish west coast (Shennan et al., 2018; Best et al., 2022; Simms et al., 2022). The RSL rise at South Cuidrach c. 8000 BP occurs during a period of rapid barystatic sea-level rise driven by the final decay of the LGM ice sheets and most notably the input of meltwater from proglacial lakes (Lawrence et al., 2016). The release of freshwater from the drainage of Lake Agassiz-Ojibway and the subsequent collapse of the Hudson Bay Ice Saddle caused this pattern of stages of RSL rise and north Atlantic cooling (Rush et al., 2023) around the period of the 8.2 ka climate event (Barber et al., 1999; Daley et al., 2011). Lawrence et al., (2016) present an empirical RSL record for southern Scotland from estuarine and salt marsh deposits, which identifies stages of the rapid sea-level changes occurring prior to the 8.2 ka climate event. The latest of these stages at 8323 - 8218 cal. BP happened around the time of the ingression process at South Cuidrach (8181 ± 144 cal. BP).

The rapid rise in the early / mid-Holocene represents a period in which barystatic sea-level rises outpaced the GIA process in northern Skye, and RSL rose to a mid-Holocene highstand which peaked at c. 6 – 7 ka BP (Selby and Smith, 2016; Shennan et al., 2000, 2018). The new SLIP at 6367 ± 68 cal. BP. (1.6 ± 0.79 m) represents the highest of the data points from South Cuidrach, but is notably lower than the maximum mid-Holocene RSL data points from Southern Skye (Selby et al., 2000) or from many sites on the Scottish mainland (Hamilton et al., 2015). A site on Loch Eishort, at a site 50 km south of South Cuidrach, data from an isolation basin shows RSL 3.22 m above present at 6240 BP (Selby et al., 2000). The difference in RSL change between northern and southern Skye illustrates the variable impact of regional isostasy driven by the primary LGM and LLS ice load over the Cuillins and mainland Scotland (Sissons, 1981), as spatial variation in the barystatic component from north to south Skye will be sub-decimetre scale (Shennan et al., 2018). RSL then fell at South Cuidrach into the late Holocene, due to reduced global meltwater input (Smith et al., 2019) which was outpaced by glacial isostatic uplift (Selby and Smith, 2016; Shennan et al., 2018).

The drivers of RSL change here appear to be these large-scale GIA and barystatic changes, rather than isolated and abrupt changes like tsunami events (Woodroffe et al., 2023). This has been discussed using sedimentological and diatomological evidence in the previous chapter (3.5). It appears most likely that the sustained marine inundation of the basin at South Cuidrach was caused by the major RSL events outlined above, and that this site offers important new constraints on the timing and magnitude of these changes for northern Skye. The implications of these findings for the archaeological artefacts discovered in the raised beach deposits are discussed in Section 5.4.1.

Given all the available sample material and methods used at South Cuidrach, I expect that no further evidence of RSL changes can be extracted from this isolation basin. The site is limited by the large error margins on the sill elevation, which is due to its burial by raised beach deposits. Further nearby sites could still improve constraints on RSL change in northern Skye, and this new data should be used to inform future nearby site investigations. Palaeoenvironmental findings are discussed in the following section.

5.2 Palaeoenvironmental Change at South Cuidrach

Here, I address the second research objective: **Investigate how the environment has changed over the Postglacial and Holocene at South Cuidrach.** Environmental changes on the Isle of Skye over these periods are well understood and there is an extensive pollen record available (e.g. Walker and Lowe, 2019). The results from South Cuidrach provide a localised reconstruction of environmental change, which gives essential context for the archaeological inhabitants of the site. Geomorphological changes over these periods provide supporting evidence for the RSL changes detailed in the previous section.

5.2.1 Raised Beach Formation and Relative Sea Level Changes

A succession of in-situ Mesolithic artefacts deposited beneath reworked LUP artefacts was discovered within a raised beach afront the isolation basin at South Cuidrach. Radiocarbon dates from in-situ Mesolithic artefacts from the raised beach reveal that the lowest part of the raised beach was formed before 7028 - 6853 cal. BP (Appendix A) and therefore the upper section of the raised beach must have formed subsequently. The top of the raised beach has a mean elevation of 7.58 m OD (Table 3.2). The elevation of the radiocarbon dates for the in-situ Mesolithic artefacts is approximately 1 m below the upper part of the raised beach, at c. 6.5 m OD. Evidence from the isolation basin data suggests that at most, RSL at the site rose to 1.6 ± 0.79 m at c. 6 – 7 ka BP, and a tidal level of HAT to MHWS was found at 4.47 ± 0.29 m OD. Given that the upper section of the raised beach was formed after 7028 - 6853 cal. BP, it must have formed in the mid-Holocene at around the time of this RSL highstand. The elevation of the raised beach (c. 5 to 8 m OD), and the cobble sized clasts of which it is comprised indicate that it was formed by high-energy/storm events during the mid-Holocene (Goslin and Clemmensen, 2017).

Mid-Holocene raised beach deposits are found throughout Scotland and have been regularly used to constrain isobases of RSL change (Smith et al., 2006; Firth et al., 2018). Although raised beach deposits can sometimes be used to infer indicative range (Smith, 2005), such datapoints have wider error

margins than isolation basins, and RSL changes were best constrained at this site from the isolation basin. The radiocarbon evidence above suggests this raised beach formed during this period of marine inundation of the isolation basin (c. 7 ka BP). This chronology means that the raised beach formed in front of the shallow coastal lake at the site, and inundation must have continued to occur following the formation of the raised beach. The evidence for sustained marine inundation of the coastal lake means that seawater repeatedly passed through the permeable raised beach deposits, as the blocking of the isolation basin by the formation of the raised beach did not prevent such marine ingressions. De la Vega Leinert et al., (2012) investigate an analogous palaeoenvironment, where the litho- and biostratigraphy from a coastal lagoon, not directly connected to the sea, are analysed to reconstruct RSL changes.

The lithics discovered within the beach were redistributed by this beach-building storm process, as transported artefacts are found throughout the upper section of the beach. A discussion of the redistribution of these LUP lithics into the upper section of the beach, and the Mesolithic lithics found in situ beneath these, are discussed in Section 5.4.1.

5.2.2 Vegetation Changes as Environmental Context for Prehistoric Settlers

The vegetational change which occurred at South Cuidrach over the Holocene can be used to indicate the environment which hosted prehistoric human visitors to South Cuidrach (those of the LUP (c. 14 – 10.5 ka BP), and the Mesolithic (c. 10.5 – 5.5 ka BP)). The new pollen data from the isolation basin commences at a radiocarbon age of 8181 ± 144 cal. BP, and so this analysis is placed in the context of pre-existing palaeoenvironmental research conducted on Skye (e.g. Selby, 2004; Brooks et al., 2012; Walker and Lowe, 2019). The LUP visitors to South Cuidrach (c. 12 – 11 ka BP) would have experienced the coldest temperatures which occurred during the latter stages of the LLS (Walker and Lowe, 2019).

During the LLS, evidence from nearby on Skye at Loch Ashik shows a decrease in arboreal *Betula* and *Pinus* pollen and grasses and sedges, whilst heather and shrubs such as *Empetrum* increase in concentration (Walker and Lowe, 2019). LUP inhabitants would have had to make adaptations to their technology and methods of mobility for subsistence in the harsh periglacial environment (Mithen et al., 2015; Hardy et al., 2024). As the LLS cold period abated, this pattern reversed and Skye was recolonised with grasses and trees (Walker and Lowe, 2019). There was a transition from the periglacial environment associated with cool temperatures of the LLS, after which there is evidence of the settlement of Mesolithic populations at South Cuidrach (Hardy and Ballin, 2024). The culture which occupied Skye following the LLS was vastly different in technology and lifestyle to the LUP cultures

(Spikins et al., 2008), and was much more widespread due to changes in key environmental constraints on migration (5.4.2).

Subsequent settlers inhabited a vastly different environment from the LUP period. Pollen data from South Cuidrach begins at c. 8 ka BP; in the Late Mesolithic (c. 9.5 – 5.5 ka BP). Key arboreal taxa which evidence the mixed woodland assemblage in SC-23-1 match the chronology of the Mesolithic. These arboreal taxa often have wide dispersal and are allochthonous to the site at South Cuidrach (e.g. *Betula* (Edwards et al., 2019)), however, they indicate a warmer climate, creating habitable conditions for Late Mesolithic inhabitants. Such conditions were sustained until mass anthropogenic landscape clearances of the Late Holocene (Selby, 2004).

5.2.3 Summary of the Palaeoenvironment at South Cuidrach

Rapid environmental changes on the Isle of Skye over the postglacial and Holocene provide insights into the environments inhabited by LUP and Mesolithic peoples. Around 10 °C of warming occurred following the LLS (Walker and Lowe, 2019), which enabled the development of mixed woodland found in the pollen stratigraphy at South Cuidrach. The pollen data does not oppose the interpretation of the site as a brackish coastal lake, allochthonous pollen dominates the stratigraphy during the sustained marine inundation of the site. The RSL rise during the mid-Holocene at South Cuidrach caused a marine ingression into the isolation basin at c. 8 ka BP. The raised beach was formed subsequently at c. 7 ka BP, but marine ingression continued as seawater passed through the permeable raised beach. The research objective of a palaeoenvironmental reconstruction for South Cuidrach has been met, given the available material. A higher resolution pollen analysis could be used to build a more detailed understanding of vegetation and RSL changes at the site in future, however, this work succeeds in placing South Cuidrach in the context of other palaeoenvironmental work on Skye (Brooks et al., 2012; Walker and Lowe, 2019).

5.3 Stone Circles at Sconser

The third and final research objective was: **Determine how changes in RSL impacted the construction of currently intertidal artefacts at Sconser, Isle of Skye.** This section discusses how this objective was met, and the efficacy of the method of using large-scale modelled RSL to determine the chronology of submerged artefacts.

5.3.1 Summary of Sconser Findings and Uncertainties

The artefacts on the foreshore at Sconser have been approximately post-dated using modelled RSL data in Chapter 4. At 10 ka, sea levels would have flooded the sites of these stone circle artefacts, meaning it is most likely that they formed at c. 11 ka (± 1 ka), a chronology which fits with the LUP (15.5 – 10.5 ka BP) or beginning of the EM (10.5 – 9.5 ka BP), supporting the Hardy et al., (2021) hypothesis that these artefacts are features from one of these periods.

The resultant estimates for the position of the HAT palaeo-shoreline over time are considered approximate because of various qualitative sources of uncertainty. The gentle gradient of the foreshore means that any changes which may have occurred to the bathymetry since the construction of these artefacts due to sedimentation/erosion will affect the position of the palaeo-shoreline for HAT at 11 ka BP in Figure 4.5. The resolution of the PALTIDE tool for extracting RSL data is a 1/24 degrees ocean model grid, meaning that this extracted modelled dataset is highly localised (c. 2.5 km grid spacing at 57° latitude) (Scourse et al., 2024). Although the BRADLEY2011 (Bradley et al., 2011) GIA model lacks empirical constraints in northern and central Skye, low RSL during the LLS which may have enabled the construction of these LUP artefacts is identified in several empirical datasets from Skye (e.g. Selby and Smith, 2016).

These estimates are made assuming the modern tidal range. Palaeotidal modelling data is available for this location (Ward et al., 2016; Scourse et al., 2024) which shows the change in the tidal amplitude of the M_2 constituent. However, these were not applied in this case for several reasons. Given the uncertainties arising from the drone survey, changes to the bathymetry of the site over time, and the spatial and temporal resolution of the GIA model data, these palaeotidal model predictions would have introduced a level of false precision to the estimates of HAT overtime at Sconser.

5.3.2 Additional Context and Chronological Constraints for Sconser

The ice margins for neighbouring Loch Sligachan offer some insights into the possible timing of the construction of Sconser artefacts. Nearshore subsea geophysical surveys (Dix and Duck, 2000) reveal offshore moraines between Skye and Scalpay, suggesting glacial extents during the LLS for the nearby Loch Ainort reached almost the opposite coast of Scalpay. Bickerdike et al., (2018) present maximum extents of the LLS Loch Sligachan glacier which reached a terminus seaward of the field site at Sconser (Figure 5.3). No precise date is available for this advance, but it occurred within the LLS at 12.9 – 11.7 ka BP. Given the chronology provided by the modelled RSL data (11 ± 1 ka), and under the assumption

that terrestrial ice prevented the construction of the stone circle artefacts, their construction could then have occurred between 11.7 and 10 ka BP. Again, these dates are subject to the large uncertainties described above but are based on the best available RSL and glacial ice reconstructions.

Due to the lack of tool/lithic artefacts at Sconser, it has not been possible to identify precisely which people group created the stone circles (Hardy et al., 2021). As previously noted, Ahrensburgian populations often inhabit sites immediately on the coast (Schmitt et al., 2009), and by the same method of using modelled RSL curves to estimate a chronology, a population at South Cuidrach identified as Ahrensburgian is likely to have occupied the shoreline. The estimate for South Cuidrach is marginally earlier (c. 12 – 11 ka BP) than for the Sconser visitors (c. 11.7 to 10 ka BP), and although these dates do overlap, there is no evidence at present that these two distinct locations are related, particularly given the broad scope of the timescale.

Given that these inhabitants were found on the periphery of a glaciated southern Skye, they are likely to have lived in an environment of periglacial tundra, depending on where within the large timespan proposed above these artefacts were constructed. Within this approximate chronology for the inhabitants of Sconser, significant environmental changes occurred on Skye. Data from Chironomid-inferred temperature estimates from the nearby Loch Ashik (Brooks et al., 2012) suggests there was c. 10 °C of warming between 11.7 and 10 ka BP. Arboreal pollen begins to dominate records on Skye with the onset of the Holocene at 11.7 ka BP (Walker and Lowe, 2019). This environmental data does not provide direct chronological constraints but can be used to understand the kind of environment these inhabitants may have found upon their post-glacial migration to Sconser. This site contributes to the expanding evidence for a widespread LUP presence in Scotland. How these populations accessed Scotland's western seaboard is another key question on which this palaeoenvironmental research provides insights.

5.3.3 Limitations and Directions for Future Research at Sconser

Following initial communication between coauthors of the manuscript in Appendix A, it had been hoped that these artefacts at Sconser may be able to provide some constraints on RSL change, however, no direct dating method was available for this approach. The new inferred chronology may not be to test future GIA models as this would introduce circularity into the models. Should future GIA models include increased spatial resolution, this may improve estimates for the timing of the construction of these artefacts. In this case, the PALTIDE tool (Scourse et al., 2024) is built by integrating different palaeotidal and GIA models (Bradley et al., 2011; Ward et al., 2016) to the same grid resolution, resulting in a lower resolution overall. Nevertheless, large uncertainties on the results of

this work would likely remain, and future archaeological investigations will be helped by the results of this study.

5.4 Archaeological Implications

Whilst the previous sections have addressed the specific research objectives, this section explores the implications of this work for archaeology, answering the overarching research question: **How did relative sea level and environmental changes on the Isle of Skye affect the migrations of Late Upper Palaeolithic and Mesolithic humans?** Much of this work is included in the unpublished work found in Appendix A.

5.4.1 Lithics in the Raised Beach

The distribution of lithics within the raised beach and the surrounding bathymetry reveals the intriguing prospect of a presently submerged archaeological site at South Cuidrach. Enabled by the large, shallow intertidal and subtidal area afront the isolation basin (Figure 1.5), a low point in RSL at c. 12 – 11 ka of c. 10 m occurred. This would have exposed a large area shoreward of South Cuidrach, extending around 200 m from the present shoreline into Loch Snizort. This likelihood, coupled with the redistributed Ahrensburgian lithics, and the known practise of Ahrensburgian populations inhabiting shore-side spots (Schmitt et al., 2009), supports the following explanation for the redistributed lithics.

As sea levels rose during the mid-Holocene, forming the raised beach, the Mesolithic population which inhabited South Cuidrach left behind these artefacts on the then surface of a cobble beach. As sea levels rose further, post 7028 - 6853 cal. BP, the LUP artefacts were likely redistributed from a now-submerged source on the large gently sloping intertidal and subtidal area (Figure 1.5) which was exposed during the late-glacial period of low RSL at c. 12 - 11 ka (Figure 1.9) conforming with the timing of the Ahrensburgian inhabitation of Scotland (Appendix A). This process explains the distribution of LUP artefacts above Mesolithic artefacts within the raised beach and provides excellent prospects for future archaeological research into the intertidal and subtidal areas at the site.

5.4.2 Environmental controls on Late Upper Palaeolithic migrations

The migratory routes of the palaeolithic populations can be estimated based on topography and available land space (Wygal and Heidenreich, 2014; Bell, 2020), which are both subject to ice-sheet

extents and RSL changes. In this section, the possible migration routes for the LUP inhabitants of South Cuidrach are explored, considering the work of this localised RSL reconstruction, and supplemented with RSL and ice-sheet reconstructions for postglacial Skye and Scotland. The Ahrensburgian is typified by 'broad-blade' technology (Saville et al., 2012; Appendix A) and this group inhabited large swathes of Northern Europe, including Denmark and northern Germany, around the LLS at c. 12.9 -11.7 ka BP (Wygal and Heidenreich, 2014). A migration across doggerland must have occurred for them to access Scotland (Walker et al., 2022), taking the approximate route proposed in Figure 5.2 (Appendix A).

The migrations of the LUP populations were made to several sites on the west coast of Scotland, including Sconser, and An Corran (Saville et al., 2012), from where the source material for the South Cuidrach lithics came. Another Ahrensburgian lithic assemblage is found at Shieldaig (Ballin and Saville, 2003). The technologies used by these populations match those found in continental Europe (Pedersen et al., 2022) and southern Scotland (Ballin, 2018). Therefore, it is possible that migratory routes crossed the Scottish mainland to gain access to the western coast (Appendix A). The mapping of possible migratory routes based on palaeoenvironmental constraints is essential to the discipline of prehistoric archaeology because these routes can guide researchers to new locations for study (Walker et al., 2022). Little is known about the transport methods used by LUP populations (Hamburgian, Federmesser and Ahrensburgian groups), and archaeological technology is not the subject of this work. However, Peeters and Momber (2014) suggest these groups were not capable of long-distance open-sea travel but likely transported themselves by a combination of short sea-crossings and on foot (Hardy et al., 2024). Questions remain about what possible routes these populations took to access the west coast of Scotland.

5.4.3 Late Upper Palaeolithic Migratory Routes

The Ahrensburgian population in northern Germany, Denmark and southern Scandinavia may have found a route to western Scotland by traversing across Doggerland (Gaffney et al., 2008; Mithen et al., 2015; Ballin, 2017), a region of the southern North Sea which was exposed during the LLS (Clark et al., 2022) (Figure 5.3). Doggerland once extended approximately as far north as the Lincolnshire coast, and the coastline stretched across the southern North Sea to Denmark. Ahrensburgian migrations did not pass through southern England, as there is no evidence of these groups found there. Rather, populations moved along the northern English coast into southern Scotland (Ballin, 2017). One isolated Ahrensburgian site in North Yorkshire (Killerby Quarry (Figure 5.2)) provides evidence of one route they may have taken (Hudson et al., 2023).

The route proposed by Hardy et al., (2024) (Figure 5.2) explains the migration of this population from the Northern European Plain to northern Britain, and on to western Scotland, which corroborates with the reconstructed palaeo-shoreline data (Clark et al., 2022) and maximum LLS ice extents (Bickerdike et al., 2018), and with the absence of Ahrensburgian presence in southern England.
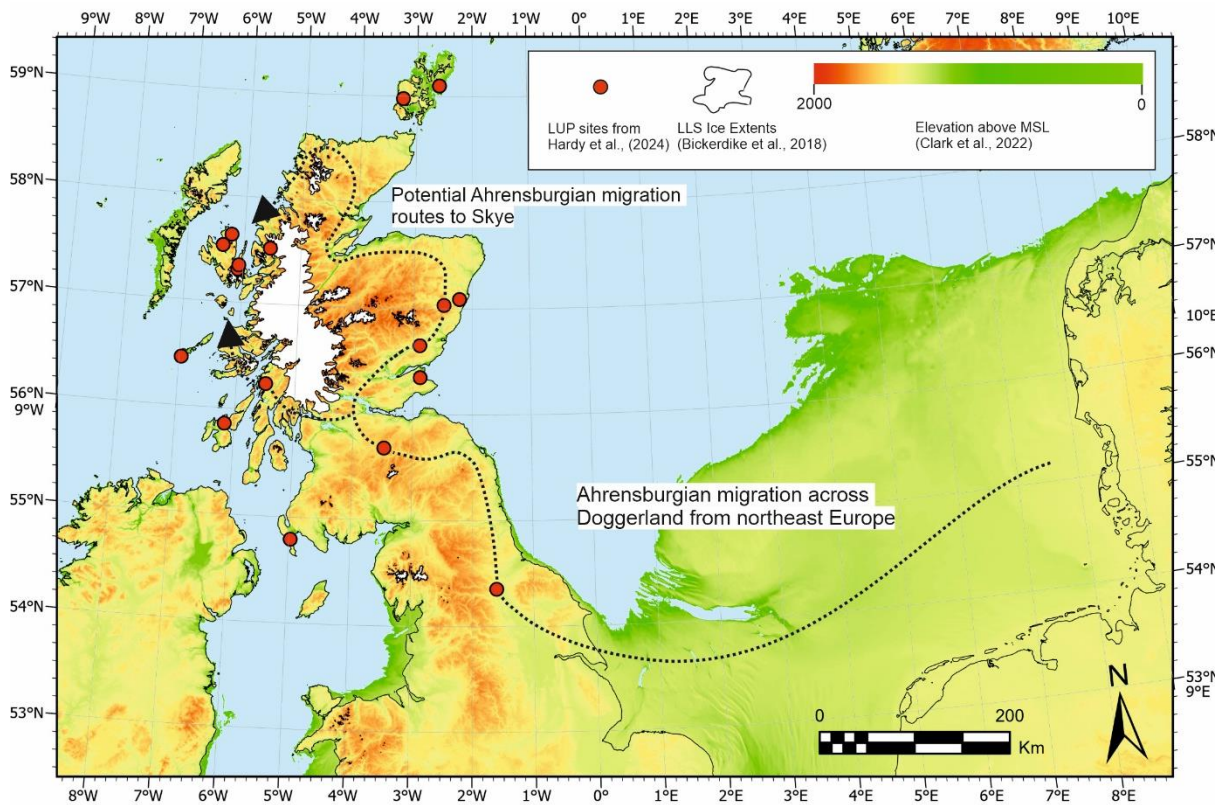
Figure 5.2. Possible migration routes for Ahrensburgian population routes across Doggerland and Scotland. Includes palaeo-shoreline and palaeotopography at 12 ka BP from Clark et al., (2022). Other LUP sites (groups besides the Ahrensburgian) are also shown. And maximum LLS ice extents from Bickerdike et al., (2018). Note non-linear scale of palaeotopography in key. Adapted from manuscript in Appendix A.

The West Highland Glacier Complex of the LLS (Figure 5.2) would have been an obstacle to terrestrial migrations of these LUP people, as was the dramatic topography of the Grampian mountains. There is a wide distribution of LUP sites in Scotland, most of which are situated in the lowlands and near the coast (Figure 1.2). These sites broadly follow the pattern of potential migration routes in Figure 5.2. To access the western seaboard of Scotland including Skye, migration must either have taken place across the highlands before/after the maximum extent of the LLS ice sheet, or around its periphery as proposed in Figure 5.2 (Appendix A).
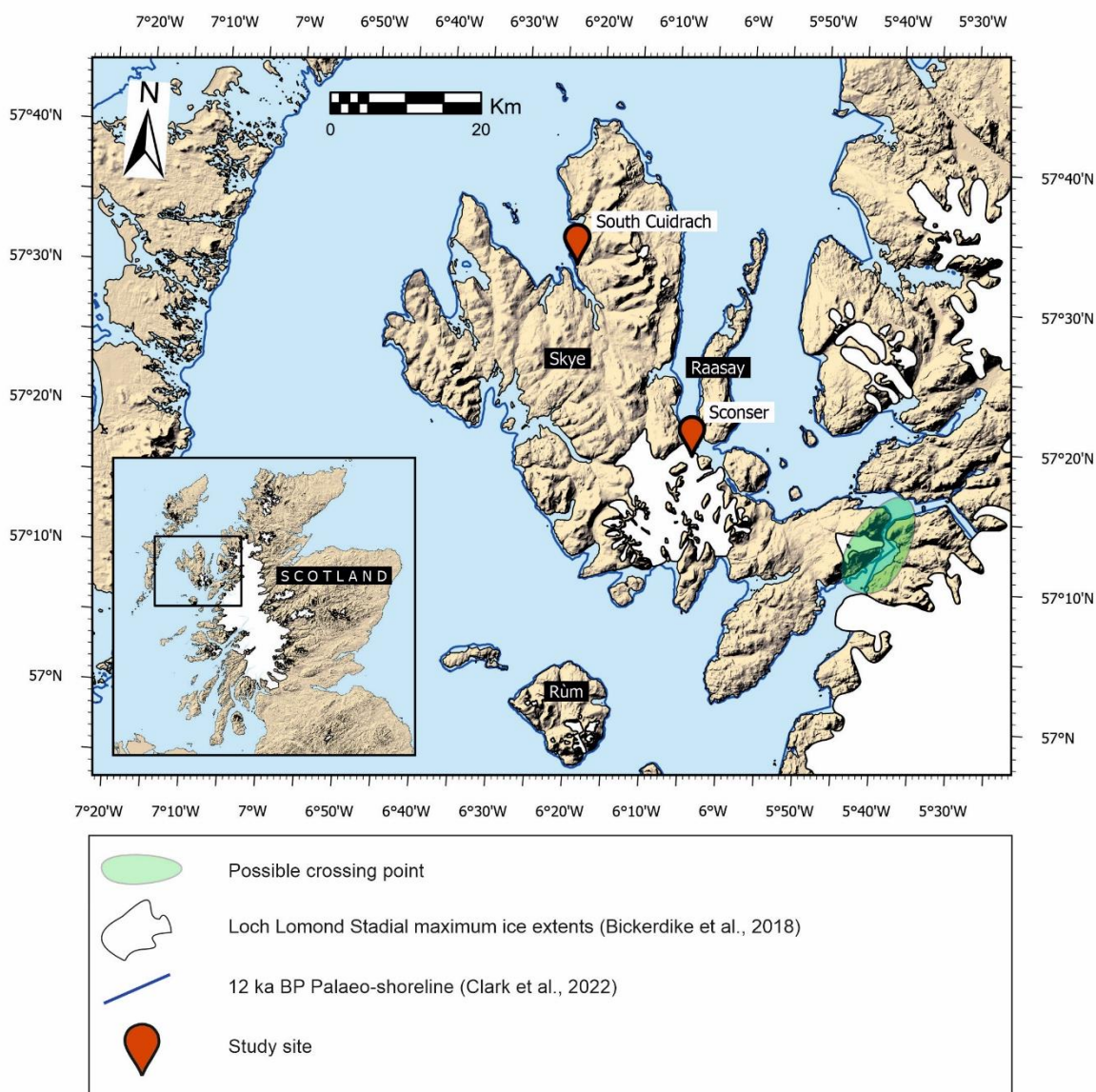
Figure 5.3. Map of Isle of Skye with maximum LLS ice extents (Bickerdike et al., 2018) and 12 ka BP palaeo-shoreline estimated using GIA modelling in Clark et al., (2022), revealing exposed lowland routes around the Cuillin ice-field created by lower-than-present RSL. Hill shade topography from Ordnance Survey (2024) exaggerated 1.5 times. Adapted from manuscript in Appendix A.

Once the Scottish west coast was accessed, Skye and the surrounding islands show sparse, but widespread evidence of LUP inhabitation/visitation. Lithic assemblages besides South Cuidrach are found on Raasay (Ballin et al., 2015), Tiree and Islay (Mithen et al., 2015) (Figure 5.2). Possible routes for access to Skye from the mainland can also be identified using RSL and ice sheets as constraints. As previously discussed, the pattern of RSL change on Skye (Figure 1.9) includes a low point at c. 12 – 11 ka BP. This could have been a controlling factor in migrations between Skye and the mainland. Marine charts for the UK (© British Crown and OceanWise, 2024) suggest that the Kylerhea Narrows could

have been exposed by a fall in sea levels of c. 10 m (Figure 5.3). This identifies the Kylerhea Narrows as a potential crossing point. Lower-than-present RSL could also have created land bridges between Skye, Raasay and Scalpay, which would have extended beyond the LLS glacial limit and been navigable by foot for LUP migrants (Figure 5.3). The LLS Cuillin ice field may also have formed a barrier to migration, but evidence from Sconser and GIA model predictions estimate lower than present RSL along Skye's east coast around this time (Figure 5.3), leaving open the possibility of terrestrial access to northern Skye and the sites of An Corran and South Cuidrach during the LLS.

At present, the best estimates for the routes taken by Late Upper Palaeolithic settlers from northern Europe are constrained by state-of-the-art reconstructions of relative sea level, palaeotopography and ice sheet margins (Clark et al., 2022; Hardy et al., 2024). New chronologies and environmental context for settlers at South Cuidrach and Sconser have proved vital in advancing our understanding of the migratory routes they may have taken.

6. CONCLUSIONS

This project represents the only palaeoenvironmental reconstruction for the archaeological field site at South Cuidrach and provides vital context for understanding the sequence of lithic deposits at the site, which is the northernmost example of an Ahrensburgian population in Britain. Here, I summarise the key findings and give recommendations for future research.

At Sconser, the timing of the construction of presently intertidal stone circle artefacts is determined as between 11.7 and 10 ka BP, fitting with the established chronology for the Late Upper Palaeolithic period in Scotland. This approximate age is supported by evidence from GIA model predictions of RSL and by ice-margin estimates during the Loch Lomond Stadial. This data is crucial to understanding the origins of these artefacts to identify which people group constructed them and to link them to other sites in Scotland. Findings will contribute to a growing literature on the Late Upper Palaeolithic in Scotland and add further evidence to the proposed route of human migration along the eastern coast of the Isle of Skye enabled by low relative sea levels during the Loch Lomond Stadial.

New empirical constraints on relative sea level from an isolation basin at South Cuidrach have been established for the mid-Holocene. The site was inundated from c. 8 – 6 ka BP, a period during which relative sea levels were above 1.34 ± 0.7 m higher than present. This change appears closely related to major trends in RSL which occurred along most of the western Scottish coastline during the mid-Holocene. This period of higher-than-present RSL happened when barystatic sea level rises outpaced the glacio-isostatic rebound in northern Skye, a pattern which is clearly simulated in large-scale GIA models. The isolation basin data suggests a mid-Holocene highstand of a lower magnitude than is found in field data from sites in Southern Skye. Given the limitations of the site, no further evidence of relative sea level change is likely to be extracted from South Cuidrach.

The raised beach at South Cuidrach was formed during the mid-Holocene highstand and the sequence of lithics found throughout the deposits give evidence of an intertidal or subtidal source nearby. The gently sloping bathymetry seaward of the South Cuidrach isolation basin may have hosted Late Upper Palaeolithic settlers when RSL was lower-than-present during the Loch Lomond Stadial. This new prospect incentivises further field archaeological investigations at South Cuidrach, which should prioritise a high-resolution bathymetric survey to identify larger artefacts or highlight potential submerged lithic findspots. New Late Upper Palaeolithic migration routes outlined in this thesis (and associated publication in Appendix A) offer suggestions for where researchers are likely to find new sites in future. These routes extend to the north and south of the West Highland Glacier Complex, close to the ice sheet margins.

This project, which has analyzed two sites in northern Skye, carries significant implications for both archaeology and palaeo sea-level research. Most importantly, the work at South Cuidrach begins to address the research gap identified by Best et al. (2022), which highlighted the need for empirical constraints on RSL in northern Skye.

BIBLIOGRAPHY

Anderson, F.W. and Dunham, K.C. 1966. *The geology of Northern Skye*. Edinburgh: HM Stationery Office.

Bailey, G. and Hardy, K. 2021. Coastal prehistory and submerged landscapes: Molluscan resources, shell-middens and underwater investigations. *Quaternary International*. **584**, pp.1–8.

Ballantyne, C.K. 1990. The Late Quaternary glacial history of the Trotternish Escarpment, Isle of Skye, Scotland, and its implications for ice-sheet reconstruction. *Proceedings of the Geologists' Association*. **101**(3), pp.171–186.

Ballantyne, C.K. 1989. The Loch Lomond Readvance on the Isle of Skye, Scotland: Glacier reconstruction and palaeoclimatic implications. *Journal of Quaternary Science*. **4**(2), pp.95–108.

Ballantyne, C.K. and Benn, D.I. 1994. A Loch Lomond Readvance Glacier in Duirinish, NW Skye. *Scottish Journal of Geology*. **30**(2), pp.183–186.

Ballantyne, C.K. and Small, D. 2019. The Last Scottish Ice Sheet. *Earth and Environmental Science Transactions of the Royal Society of Edinburgh*. **110**(1–2), pp.93–131.

Ballin, T.B. 2018. *Reindeer hunters at Howburn Farm, South Lanarkshire*. Cambridge: Archaeopress Publishing Ltd.

Ballin, T.B. 2017. Rising waters and processes of diversification and unification in material culture: the flooding of Doggerland and its effect on north-west European prehistoric populations between ca. 13 000 and 1500 cal BC. *Journal of Quaternary Science*. **32**(2), pp.329–339.

Ballin, T.B. and Bjerck, H.B. 2016. Lost and found twice: Discussion of an early post-glacial single-edged tanged point from Brodgar on Orkney, Scotland. *Journal of Lithic Studies*. **3**(1), pp.31–50.

Ballin, T.B. and Saville, A. 2003. An ahrensburgian-type tanged point from shieldaig, Wester Ross, Scotland, and its implications. *Oxford Journal of Archaeology*. **22**(2), pp.115–131.

Ballin, T.B., White, R., Richardson, P. and Neighbour, T. 2015. An Early Mesolithic stone tool assemblage from Clachan Harbour, Raasay, Scottish Hebrides. *The Journal of the Lithic Studies Society*. **31**, pp.94–104.

Barber, D.C., Dyke, A., Hillaire-Marcel, C., Jennings, A.E., Andrews, J.T., Kerwin, M.W., Bilodeau, G., McNeely, R., Southon, J., Morehead, M.D. and Gagnon, J.-M. 1999. Forcing of the cold event of 8,200 years ago by catastrophic drainage of Laurentide lakes. *Nature*. **400**(6742), pp.344–348.

Barlow, N.L.M., Long, A.J., Saher, M.H., Gehrels, W.R., Garnett, M.H. and Scaife, R.G. 2014. Salt-marsh reconstructions of relative sea-level change in the North Atlantic during the last 2000 years. *Quaternary Science Reviews*. **99**, pp.1–16.

Barlow, N.L.M., Shennan, I., Long, A.J., Gehrels, W.R., Saher, M.H., Woodroffe, S.A. and Hillier, C. 2013. Salt marshes as late Holocene tide gauges. *Global and Planetary Change*. **106**, pp.90–110.

Bell, M. 2020. *Making One's Way in the World: The Footprints and Trackways of Prehistoric People* [Online]. Oxbow books. [Accessed 24 July 2024]. Available from: https://www.torrossa.com/it/resources/an/4914451.

Benjamin, J., Rovere, A., Fontana, A., Furlani, S., Vacchi, M., Inglis, R.H., Galili, E., Antonioli, F., Sivan, D., Miko, S., Mourtzas, N., Felja, I., Meredith-Williams, M., Goodman-Tchernov, B., Kolaiti, E., Anzidei, M. and Gehrels, R. 2017. Late Quaternary sea-level changes and early human societies in the central and eastern Mediterranean Basin: An interdisciplinary review. *Quaternary International*. **449**, pp.29–57.

Best, L., Simms, A.R., Brader, M., Lloyd, J., Sefton, J. and Shennan, I. 2022. Local and regional constraints on relative sea-level changes in southern Isle of Skye, Scotland, since the Last Glacial Maximum. *Journal of Quaternary Science*. **37**(1), pp.59–70.

Beug, H. 2004. *Leitfaden der Pollenbestimmung für Mitteleuropa und angrenzende Gebiete.* Munich: Verlag Dr. Friedrich Pfeil.

Bickerdike, H.L., Evans, D.J.A., Stokes, C.R. and Ó Cofaigh, C. 2018. The glacial geomorphology of the Loch Lomond (Younger Dryas) Stadial in Britain: a review. *Journal of Quaternary Science*. **33**(1), pp.1–54.

Bickerdike, H.L., Ó Cofaigh, C., Evans, D.J.A. and Stokes, C.R. 2017. Glacial landsystems, retreat dynamics and controls on Loch Lomond Stadial (Younger Dryas) glaciation in Britain. *Boreas*. **47**(1), pp.202–224.

Blott, S.J. and Pye, K. 2001. GRADISTAT: a grain size distribution and statistics package for the analysis of unconsolidated sediments. *Earth Surface Processes and Landforms*. **26**(11), pp.1237–1248.

Brader, M.D., Lloyd, J.M., Barlow, N.L.M., Norðdahl, H., Bentley, M.J. and Newton, A.J. 2017. Postglacial relative sea-level changes in northwest Iceland: Evidence from isolation basins, coastal lowlands and raised shorelines. *Quaternary Science Reviews*. **169**, pp.114–130.

Bradley, S.L., Ely, J.C., Clark, C.D., Edwards, R.J. and Shennan, I. 2023. Reconstruction of the palaeo-sea level of Britain and Ireland arising from empirical constraints of ice extent: implications for regional sea level forecasts and North American ice sheet volume. *Journal of Quaternary Science*. **38**(6), pp.791–805.

Bradley, S.L., Milne, G.A., Shennan, I. and Edwards, R. 2011. An improved glacial isostatic adjustment model for the British Isles. *Journal of Quaternary Science*. **26**(5), pp.541–552.

Bradwell and Stoker 2015. Submarine sediment and landform record of a palaeo-ice stream within the British–Irish Ice Sheet. *Boreas*. **44**(2).

Bradwell, T., Fabel, D., Clark, C.D., Chiverrell, R.C., Small, D., Smedley, R.K., Saher, M.H., Moreton, S.G., Dove, D., Callard, S.L., Duller, G.A.T., Medialdea, A., Bateman, M.D., Burke, M.J., McDonald, N., Gilgannon, S., Morgan, S., Roberts, D.H. and Cofaigh, C. ó 2021. Pattern, style and timing of British–Irish Ice Sheet advance and retreat over the last 45 000 years: evidence from NW Scotland and the adjacent continental shelf. *Journal of Quaternary Science*. **36**(5), pp.871–933.

© British Crown and OceanWise, 2024. Digimap Marine Collection. Digimap. [Online]. [Accessed June 2024]. Available from https://digimap.edina.ac.uk/marine.

Bromley, G., Putnam, A., Hall, B., Rademaker, K., Thomas, H., Balter-Kennedy, A., Barker, S. and Rice, D. 2023. Lateglacial Shifts in Seasonality Reconcile Conflicting North Atlantic Temperature Signals. *Journal of Geophysical Research: Earth Surface*. **128**(1).

Brooks, S.J., Matthews, I.P., Birks, H.H. and Birks, H.J.B. 2012. High resolution Lateglacial and early-Holocene summer air temperature records from Scotland inferred from chironomid assemblages. *Quaternary Science Reviews*. **41**, pp.67–82.

Carballeira, R. and Pontevedra-Pombal, X. 2020. Diatoms in Paleoenvironmental Studies of Peatlands. *Quaternary*. **3**(2), p.10.

Chen, X., Zhang, X., Church, J.A., Watson, C.S., King, M.A., Monselesan, D., Legresy, B. and Harig, C. 2017. The increasing rate of global mean sea-level rise during 1993–2014. *Nature Climate Change*. **7**(7), pp.492–495.

Clark, C.D., Ely, J.C., Hindmarsh, R.C.A., Bradley, S., Ignéczi, A., Fabel, D., Ó Cofaigh, C., Chiverrell, R.C., Scourse, J., Benetti, S., Bradwell, T., Evans, D.J.A., Roberts, D.H., Burke, M., Callard, S.L., Medialdea,

A., Saher, M., Small, D., Smedley, R.K., Gasson, E., Gregoire, L., Gandy, N., Hughes, A.L.C., Ballantyne, C., Bateman, M.D., Bigg, G.R., Doole, J., Dove, D., Duller, G.A.T., Jenkins, G.T.H., Livingstone, S.L.,

Clark, J.G.D. 1936. The Mesolithic of Northern Europe: A study of the Food-Gathering Peoples of Northern Europe during the early Post-Glacial Period. *Cambridge University Press*. **12**(47), pp.379–383.

Clark, P.U., Alley, R.B., Keigwin, L.D., Licciardi, J.M., Johnsen, S.J. and Wang, H. 1996. Origin of the first global meltwater pulse following the Last Glacial Maximum. *Paleoceanography*. **11**(5), pp.563–577.

Daley, T.J., Thomas, E.R., Holmes, J.A., Street-Perrott, F.A., Chapman, M.R., Tindall, J.C., Valdes, P.J., Loader, N.J., Marshall, J.D., Wolff, E.W., Hopley, P.J., Atkinson, T., Barber, K.E., Fisher, E.H., Robertson, I., Hughes, P.D.M. and Roberts, C.N. 2011. The 8200 yr BP cold event in stable isotope records from the North Atlantic region. *Global and Planetary Change*. **79**(3), pp.288–302.

Deschamps, P., Durand, N., Bard, E., Hamelin, B., Camoin, G., Thomas, A.L., Henderson, G.M., Okuno, J. and Yokoyama, Y. 2012. Ice-sheet collapse and sea-level rise at the Bølling warming 14,600 years ago. *Nature*. **483**(7391), pp.559–564.

Dix, J.K. and Duck, R.W. 2000. A high-resolution seismic stratigraphy from a Scottish sea loch and its implications for Loch Lomond Stadial deglaciation. *Journal of Quaternary Science*. **15**(6), pp.645–656.

Edwards, K.J., Bennett, K.D. and Davies, A.L. 2019. Palaeoecological perspectives on Holocene environmental change in Scotland. *Earth and Environmental Science Transactions of the Royal Society of Edinburgh*. **110**(1–2), pp.199–217.

Fairbanks, R.G. 1989. A 17,000-year glacio-eustatic sea level record: influence of glacial melting rates on the Younger Dryas event and deep-ocean circulation. *Nature*. **342**(6250), pp.637–642.

Farrell, W.E. and Clark, J.A. 1976. On Postglacial Sea Level. *Geophysical Journal International*. **46**(3), pp.647–667.

Firth, C., Smith, D., Barlow, N., Bradley, S., Hall, A., Jordan, J. and Long, D. 2018. Quaternary sea level changes in Scotland. *Earth and Environmental Science Transactions of the Royal Society of Edinburgh*. **107**.

Flower, R.J., Jones, V.J. and Round, F.E. 1996. The Distribution and Classification of the Problematic Fragilaria (virescens V.) Exigua Grun./Fragilaria Exiguiformis (grun.) Lange-Bertalot: A New Species or a New Genus? *Diatom Research*. **11**(1), pp.41–57.

Folk, R.L. and Ward, W.C. 1957. Brazos River bar [Texas]; a study in the significance of grain size parameters. *Journal of Sedimentary Research*. **27**(1), pp.3–26.

Foster, J. 2015. 10. GPS and surveying *In*: *Handbook of sea-level research*. John Wiley & Sons, pp.157–170.

Gaffney, V., Fitch, S. and Smith, D. 2008. *Europe's Lost World: The Rediscovery of Doggerland*. York, UK: Council for British Archaeology.

Garrett, E., Melnick, D., Dura, T., Cisternas, M., Ely, L.L., Wesson, R.L., Jara-Muñoz, J. and Whitehouse, P.L. 2020. Holocene relative sea-level change along the tectonically active Chilean coast. *Quaternary Science Reviews*. **236**, p.106281.

Genkal, S.I. and Yarushina, M.I. 2017. On the morphology and taxonomy of Parlibellus Crucicula (Bacillariophyta). *Inland Water Biology*. **10**(4), pp.355–359.

© Getmapping Ltd. 2024. Digimap Aerial Photography Collection. Digimap. [Online]. [Accessed June 2024]. Available from https://digimap.edina.ac.uk/aerial.

Golledge, N.R. 2010. Glaciation of Scotland during the Younger Dryas stadial: A Review. *Journal of Quaternary Science*. **25**(4), pp.550–566.

Goslin, J. and Clemmensen, L.B. 2017. Proxy records of Holocene storm events in coastal barrier systems: Storm-wave induced markers. *Quaternary Science Reviews*. **174**, pp.80–119.

Green, F. and Edwards, K. 2009. 8.1 Palynological studies in northeast Skye and Raasay. *Scottish Archaeological Internet Reports*. **31**, pp.481–490.

Gregoire, L.J., Otto-Bliesner, B., Valdes, P.J. and Ivanovic, R. 2016. Abrupt Bølling warming and ice saddle collapse contributions to the Meltwater Pulse 1a rapid sea level rise. *Geophysical Research Letters*. **43**(17), pp.9130–9137.

Gregory, J.M., Griffies, S.M., Hughes, C.W., Lowe, J.A., Church, J.A., Fukimori, I., Gomez, N., Kopp, R.E., Landerer, F., Cozannet, G.L., Ponte, R.M., Stammer, D., Tamisiea, M.E. and van de Wal, R.S.W. 2019. Concepts and Terminology for Sea Level: Mean, Variability and Change, Both Local and Global. *Surveys in Geophysics*. **40**(6), pp.1251–1289.

Guiry, M.D., Guiry, G.M. 2024. AlgaeBase. *AlgaeBase*. [Online]. [Accessed 2 May 2024]. Available from: https://www.algaebase.org.

Hallmann, N., Camoin, G., Eisenhauer, A., Samankassou, E., Vella, C., Botella, A., Milne, G.A., Pothin, V., Dussouillez, P., Fleury, J., Fietzke, J. and Goepfert, T. 2020. Reef response to sea-level and

environmental changes in the Central South Pacific over the past 6000 years. *Global and Planetary Change*. **195**, p.103357.

Hamilton, C.A., Lloyd, J.M., Barlow, N.L.M., Innes, J.B., Flecker, R. and Thomas, C.P. 2015. Late Glacial to Holocene relative sea-level change in Assynt, northwest Scotland, UK. *Quaternary Research*. **84**(2), pp.214–222.

Hardy and Ballin 2024. South Cuidrach. *Proceedings of the Society of Antiquaries of Scotland*. **153**.

Hardy, K. 2016. Variable Use of Coastal Resources in Prehistoric and Historic Periods in Western Scotland. *The Journal of Island and Coastal Archaeology*. **11**(2), pp.264–284.

Hardy, K., Ballin, T. and Bicket, A. 2021. Rapidly changing worlds. Finding the earliest human occupations on Scotland's north-west coastline. *Quaternary International*. **584**, pp.106–115.

Hardy, K., Barlow, N.L.M., Taylor, E., Bradley, S.L. 2024. [Forthcoming] At the far end of everything: An Ahrensburgian presence in the far north of the Isle of Skye, Scotland. *Journal of Quaternary Science*.

Hardy, K. and Wickham-Jones, C. 2002. Scotland's First Settlers: the Mesolithic seascape of the Inner Sound, Skye and its contribution to the early prehistory of Scotland. *Antiquity*. **76**(293), pp.825–833.

Harrold, P. 1978. A glabrous variety of Sagina subulata (Sw.) C. Presl in Britain. *Transactions of the Botanical Society of Edinburgh*. **43**(1), pp.1–5.

Hartley, B. 1996. *An atlas of British diatoms*. Bristol: Biopress.

Head, M.J., Pillans, B., Zalasiewicz, J.A. 2021. Formal ratification of subseries for the Pleistocene Series of the Quaternary System. *Episodes Journal of International Geoscience*. **44**(3), pp.241–247.

Hemphill-Haley 1993. Taxonomy of recent and fossil (Holocene) diatoms (Bacillariophyta) from northern Willapa Bay, Washington. *U.S. Geological Survey*.

Hudson, S.M., Waddington, C., Pears, B., Ellis, N., Parker, L., Hamilton, D., Alsos, I.G., Hughes, P. and Brown, A. 2023. Lateglacial and Early Holocene palaeoenvironmental change and human activity at Killerby Quarry, North Yorkshire, UK. *Journal of Quaternary Science*. **38**(3), pp.403–422.

John P. Smol Eugene F. Stoermer 2010. *The Diatoms: Applications for the Environmental and Earth Sciences* 2nd ed. Cambridge: Cambridge University Press.

Joosten, H. and Clarke, D. 2002. *Wise use of Mires and Peatlands*. Totnes, Devon, UK: International Mire Conservation Group (IMCG) and International Peat Society (IPS).

Juggins, S. 2015. Rioja: Analysis of Quaternary Science Data.

Kemp, A.C., Horton, B.P. and Engelhart, S.E. 2013. SEA-LEVELS, LATE QUATERNARY | Late Quaternary Relative Sea-Level Changes at Mid-Latitudes *In*: S. A. Elias and C. J. Mock, eds. *Encyclopedia of Quaternary Science (Second Edition)* [Online]. Amsterdam: Elsevier, pp.489–494. [Accessed 15 July 2024]. Available from: https://www.sciencedirect.com/science/article/pii/B9780444536433001400.

Khan, N.S., Ashe, E., Shaw, T.A., Vacchi, M., Walker, J., Peltier, W.R., Kopp, R.E. and Horton, B.P. 2015. Holocene Relative Sea-Level Changes from Near-, Intermediate-, and Far-Field Locations. *Current Climate Change Reports*. **1**(4), pp.247–262.

Khan, N.S., Horton, B.P., Engelhart, S., Rovere, A., Vacchi, M., Ashe, E.L., Törnqvist, T.E., Dutton, A., Hijma, M.P. and Shennan, I. 2019. Inception of a global atlas of sea levels since the Last Glacial Maximum. *Quaternary Science Reviews*. **220**, pp.359–371.

Kozlowski, G., Andrew Jones, R. and Nicholls-Vuille, F.-L. 2008. Biological Flora of Central Europe: *Baldellia ranunculoides* (Alismataceae). *Perspectives in Plant Ecology, Evolution and Systematics*. **10**(2), pp.109–142.

Kuchar, J., Milne, G., Hubbard, A., Patton, H., Bradley, S., Shennan, I. and Edwards, R. 2012. Evaluation of a numerical model of the British–Irish ice sheet using relative sea-level data: implications for the interpretation of trimline observations. *Journal of Quaternary Science*. **27**(6), pp.597–605.

Kuznetsov, O.V. 2013. Ethnoarchaeology of Evenki reindeer hunters in Siberia: an application to late paleolithic settlements and habitation structure analysis. *Ethnoarchaeology: Current Research and Field Methods*. **13**(Conference Proceedings, Rome, Italy), pp.146–152.

Lambeck, K., Rouby, H., Purcell, A., Sun, Y. and Sambridge, M. 2014. Sea level and global ice volumes from the Last Glacial Maximum to the Holocene. *Proceedings of the National Academy of Sciences*. **111**(43), pp.15296–15303.

Langdon, P.G. and Barber, K.E. 2005. The climate of Scotland over the last 5000 years inferred from multiproxy peatland records: inter-site correlations and regional variability. *Journal of Quaternary Science*. **20**(6), pp.549–566.

Lawrence, T., Long, A.J., Gehrels, W.R., Jackson, L.P. and Smith, D.E. 2016. Relative sea-level data from southwest Scotland constrain meltwater-driven sea-level jumps prior to the 8.2 kyr BP event. *Quaternary Science Reviews*. **151**, pp.292–308.

Lawson, J.A., Saville, A. and Engl, R. 2023. A Time of Change: Mesolithic occupation at Cramond, Edinburgh during the 9th millenium BC. *SAIR*. (103).

Lin, Y., Hibbert, F.D., Whitehouse, P.L., Woodroffe, S.A., Purcell, A., Shennan, I. and Bradley, S.L. 2021. A reconciled solution of Meltwater Pulse 1A sources using sea-level fingerprinting. *Nature Communications*. **12**(1), p.2015.

Llovel, W., Balem, K., Tajouri, S. and Hochet, A. 2023. Cause of Substantial Global Mean Sea Level Rise Over 2014–2016. *Geophysical Research Letters*. **50**(19).

Lloyd, A.J., Crawford, O., Al-Attar, D., Austermann, J., Hoggard, M.J., Richards, F.D. and Syvret, F. 2024. GIA imaging of 3-D mantle viscosity based on palaeo sea level observations – Part I: Sensitivity kernels for an Earth with laterally varying viscosity. *Geophysical Journal International*. **236**(2), pp.1139–1171.

Long, A. 2001. Mid-Holocene sea-level change and coastal evolution. *Progress in Physical Geography: Earth and Environment*. **25**(3), pp.399–408.

Long, A.J., Innes, J.B., Shennan, I., Tooley, M.J., Long, A.J., Innes, J.B., Shennan, I. and Tooley, M.J. 1999. Coastal stratigraphy; a case study from Johns River, Washington, U.S.A. *Technical Guide - Quaternary Research Association*. **7**, pp.267–286.

Long, A.J., Woodroffe, S.A., Roberts, D.H. and Dawson, S. 2011. Isolation basins, sea-level changes and the Holocene history of the Greenland Ice Sheet. *Quaternary Science Reviews*. **30**(27–28), pp.3748–3768.

Martin, A. C. and Harvey, W. J. 2017. The Global Pollen Project: a new tool for pollen identification and the dissemination of physical reference collections. *Methods Ecol Evol*. **8**, pp.892–897.

McCarron, S., Moreton, S., Pollard, D., Praeg, D., Sejrup, H.P., Van Landeghem, K.J.J. and Wilson, P. 2022. Growth and retreat of the last British–Irish Ice Sheet, 31 000 to 15 000 years ago: the BRITICE-CHRONO reconstruction. *Boreas*. **51**(4), pp.699–758.

McCarthy, J. 2023. Sconser Digital Earth Model pers comms.

McLaren, P. 1981. An interpretation of trends in grain size measures. *Journal of Sedimentary Research*. **51**(2), pp.611–624.

Met Office 2024. Skye: Prabost (Highland) UK climate averages. *Skye: Prabost UK climate averages*. [Online]. [Accessed 2 January 2024]. Available from: https://www.metoffice.gov.uk/research/climate/maps-and-data/uk-climate-averages/gf5wbt9v5.

Milne, G.A., Long, A.J. and Bassett, S.E. 2005. Modelling Holocene Relative Sea-Level Observations from the Caribbean and South America. *Quaternary Science Reviews*. **24**(10–11).

Milne, G.A. and Mitrovica, J.X. 2008. Searching for eustasy in deglacial sea-level histories. *Quaternary Science Reviews*. **27**(25), pp.2292–2302.

Mithen, S., Wicks, K., Pirie, A., Riede, F., Lane, C., Banerjea, R., Cullen, V., Gittins, M. and Pankhurst, N. 2015. A Lateglacial archaeological site in the far north-west of Europe at Rubha Port an t-Seilich, Isle of Islay, western Scotland: Ahrensburgian-style artefacts, absolute dating and geoarchaeology. *Journal of Quaternary Science*. **30**(5), pp.396–416.

Moore, P.D. 1991. *Pollen analysis* Second edition. Oxford ; Blackwell Scientific Publications.

Naughton, F., Sánchez-Goñi, M.F., Landais, A., Rodrigues, T., Riveiros, N.V. and Toucanne, S. 2023. Chapter 6 - The Bølling–Allerød Interstadial *In*: D. Palacios, P. D. Hughes, J. M. García-Ruiz and N. Andrés, eds. *European Glacial Landscapes* [Online]. Elsevier, pp.45–50. [Accessed 25 June 2024]. Available from: https://www.sciencedirect.com/science/article/pii/B9780323918992000152.

Neal, A. 2004. Ground-penetrating radar and its use in sedimentology: principles, problems and progress. *Earth-Science Reviews*. **66**(3), pp.261–330.

Nelson, A.R. 2015. Coastal Sediments *In*: *Handbook of sea-level research*. Chichester, West Sussex : John Wiley & Sons, Ltd. : American Geophysical Union, pp.47–65.

Nield, G.A., Whitehouse, P.L., van der Wal, W., Blank, B., O'Donnell, J.P. and Stuart, G.W. 2018. The impact of lateral variations in lithospheric thickness on glacial isostatic adjustment in West Antarctica. *Geophysical Journal International*. **214**(2), pp.811–824.

Norris, S., Tarasov, L., Monteath, A., Gosse, J., Hidy, A., Margold, M. and Froese, D. 2021. Rapid retreat of the southwestern Laurentide Ice Sheet during the Bølling-Allerød interval. *Geology*. **50**.

Ordnance Survey. 2024. OS Terrain®50. *Ordnance Survey*. [Online]. [Accessed June 2024]. Available from: https://osdatahub.os.uk/downloads/open/Terrain50

Palmer, A.J.M. and Abbott, W.H. 1986. Diatoms as indicators of sea-level change *In*: O. van de Plassche, ed. *Sea-Level Research: a manual for the collection and evaluation of data* [Online]. Dordrecht: Springer Netherlands, pp.457–487. [Accessed 28 May 2024]. Available from: https://doi.org/10.1007/978-94-009-4215-8_16.

Palmer, A.P., Matthews, I.P., Lowe, J.J., MacLeod, A. and Grant, R. 2020. A revised chronology for the growth and demise of Loch Lomond Readvance ('Younger Dryas') ice lobes in the Lochaber area, Scotland. *Quaternary Science Reviews*. **248**, p.106548.

Palmer, A.P., Matthews, I.P., MacLeod, A., Abrook, A., Akkerman, K., Blockley, S.P.M., Candy, I., Francis, C., Hoek, W.Z., Kingston, F., Maas, D., El-Hady, S.R., Gulliford, R., Lincoln, P., Perez-Fernandez, M. and Staff, R.A. 2021. The Late Quaternary sediment successions of Llangorse Lake, south Wales. *Proceedings of the Geologists' Association*. **132**(3), pp.284–296.

Parker, A.G., Goudie, A.S., Anderson, D.E., Robinson, M.A. and Bonsall, C. 2002. A review of the mid-Holocene elm decline in the British Isles. *Progress in Physical Geography: Earth and Environment*. **26**(1), pp.1–45.

Pedersen, J.B., Poulsen, M.E. and Riede, F. 2022. Jels 3, a New Late Palaeolithic Open-Air Site in Denmark, Sheds Light on the Pioneer Colonization of Northern Europe. *Journal of Field Archaeology*. **47**(6), pp.360–378.

Peeters, J.H.M. and Momber, G. 2014. The southern North Sea and the human occupation of northwest Europe after the Last Glacial Maximum. *Netherlands Journal of Geosciences - Geologie en Mijnbouw*. **93**(1–2), pp.55–70.

Peltier, W.R. 2005. On the hemispheric origins of meltwater pulse 1a. *Quaternary Science Reviews*. **24**(14), pp.1655–1671.

Peltier, W.R. 1998. Postglacial variations in the level of the sea: Implications for climate dynamics and solid-Earth geophysics. *Reviews of Geophysics*. **36**(4), pp.603–689.

Peltier, W.R. and Andrews, J.T. 1976. Glacial-Isostatic Adjustment—I. The Forward Problem. *Geophysical Journal International*. **46**(3), pp.605–646.

Plater, Kirby, Boyle, Shaw, and Mills 2015. 21. Loss on ignition and organic content *In*: *Handbook of Sea Level Research*. John Wiley & Sons, pp.312–330.

Pollard, O.G., Barlow, N.L.M., Gregoire, L.J., Gomez, N., Cartelle, V., Ely, J.C. and Astfalck, L.C. 2023. Quantifying the uncertainty in the Eurasian ice-sheet geometry at the Penultimate Glacial Maximum (Marine Isotope Stage 6). *The Cryosphere*. **17**(11), pp.4751–4777.

Ramsey, C. 2021. OxCal 4.4. 4 calibration program. *Website: https://c14. arch. ox. ac. uk/oxcal/OxCal. html*.

Rees-Hughes, L., Barlow, N.L.M., Booth, A.D., West, L.J., Tuckwell, G. and Grossey, T. 2021. Unveiling buried aeolian landscapes: reconstructing a late Holocene dune environment using 3D ground-penetrating radar. *Journal of Quaternary Science*. **36**(3), pp.377–390.

Reimer, P.J., Austin, W.E.N., Bard, E., Bayliss, A., Blackwell, P.G., Ramsey, C.B., Butzin, M., Cheng, H., Edwards, R.L., Friedrich, M., Grootes, P.M., Guilderson, T.P., Hajdas, I., Heaton, T.J., Hogg, A.G., Hughen, K.A., Kromer, B., Manning, S.W., Muscheler, R., Palmer, J.G., Pearson, C., Plicht, J. van der, Reimer, R.W., Richards, D.A., Scott, E.M., Southon, J.R., Turney, C.S.M., Wacker, L., Adolphi, F., Büntgen, U., Capano, M., Fahrni, S.M., Fogtmann-Schulz, A., Friedrich, R., Köhler, P., Kudsk, S., Miyake, F., Olsen, J., Reinig, F., Sakamoto, M., Sookdeo, A. and Talamo, S. 2020. The IntCal20 Northern Hemisphere Radiocarbon Age Calibration Curve (0–55 cal kBP). *Radiocarbon*. **62**(4), pp.725–757.

Rovere, A., Raymo, M.E., Vacchi, M., Lorscheid, T., Stocchi, P., Gómez-Pujol, L., Harris, D.L., Casella, E., O'Leary, M.J. and Hearty, P.J. 2016. The analysis of Last Interglacial (MIS 5e) relative sea-level indicators: Reconstructing sea-level in a warmer world. *Earth-Science Reviews*. **159**, pp.404–427.

Rush, G., Garrett, E., Bateman, M.D., Bigg, G.R., Hibbert, F.D., Smith, D.E. and Gehrels, W.R. 2023. The magnitude and source of meltwater forcing of the 8.2 ka climate event constrained by relative sea-level data from eastern Scotland. *Quaternary Science Advances*. **12**, p.100-119.

Rzodkiewicz, M., Gąbka, M., Szpikowska, G. and Woszczyk, M. 2017. Diatom assemblages as indicators of salinity gradients: a case study from a coastal lake. *Oceanological and Hydrobiological Studies*. **46**(3), pp.325–339.

Saville, A. and Ballin, T.B. 2009. Upper Palaeolithic evidence from Kilmelfort Cave, Argyll: a re-evaluation of the lithic assemblage.

Saville, A., Hardy, K., Miket, R., Ballin, T.B., Bartosiewicz, L., Bonsall, C., Bruce, M., Carter, S., Cowie, T., Craig, O., Hallén, Y., Holden, T.G., Kerr, N.W., Miller, J., Milner, N. and Pickard, C. 2012. An Corran, Staffin, Skye. *Scottish Archaeological Internet Reports*. **51**, pp.1–101.

Sawai, Y., Horton, B.P., Kemp, A.C., Hawkes, A.D., Nagumo, T. and Nelson, A.R. 2016. Relationships between diatoms and tidal environments in Oregon and Washington, USA. *Diatom Research*. **31**(1), pp.17–38.

Schmitt, L., Larsson, S., Burdukiewicz, J., Ziker, J., Svedhage, K., Zamon, J. and Steffen, H. 2009. Chronological insights, cultural change, and resource exploitation on the West Coast of Sweden during the Late Palaeolithic/Early Mesolithic transition. *Oxford Journal of Archaeology*. **28**, pp.1–27.

Scourse, J., Ward, S., Wainwright, A., Bradley, S., Wilson, J.K. and Guo, J. 2024. An interactive visualization and data portal tool (PALTIDE) for relative sea level and palaeotidal simulations of the

northwest European shelf seas since the Last Glacial Maximum. *Journal of Quaternary Science*. **n/a**(n/a).

Selby, K.A. 2004. Lateglacial and Holocene vegetation change on the Isle of Skye: new data from three coastal locations. *Vegetation History and Archaeobotany*. **13**(4), pp.233–247.

Selby, K.A. and Smith, D.E. 2016. Holocene Relative Sea-Level Change on the Isle of Skye, Inner Hebrides, Scotland. *Scottish Geographical Journal*. **132**(1), pp.42–65.

Selby, K.A., Smith, D.E., Dawson, A.G. and Mighall, T.M. 2000. Late Devensian and Holocene relative sea level and environmental changes from an isolation basin in southern Skye. *Scottish Journal of Geology*. **36**(1), pp.73–86.

Selby, K.A., Wheeler, J. and Derrett, S. 2023. Disentangling Holocene Climate Change and Human Impact from Palaeoenvironmental Records from the Scottish West Coast. *Quaternary*. **6**(1), p.2.

Shennan, I. 1999. Global meltwater discharge and the deglacial sea-level record from northwest Scotland. *Journal of Quaternary Science*. **14**(7), pp.715–719.

Shennan, I. 2015. Handbook of sea-level research: framing research questions *In*: *Handbook of Sea-Level Research*., pp.3–24.

Shennan, I., Bradley, S.L. and Edwards, R. 2018. Relative sea-level changes and crustal movements in Britain and Ireland since the Last Glacial Maximum. *Quaternary Science Reviews*. **188**, pp.143–159.

Shennan, I., Hamilton, S., Hillier, C., Hunter, A., Woodall, R., Bradley, S., Milne, G., Brooks, A. and Bassett, S. 2006. Relative sea-level observations in western Scotland since the Last Glacial Maximum for testing models of glacial isostatic land movements and ice-sheet reconstructions. *Journal of Quaternary Science*. **21**(6), pp.601–613.

Shennan, I., Hamilton, S., Hillier, C. and Woodroffe, S. 2005. A 16000-year record of near-field relative sea-level changes, northwest Scotland, United Kingdom. *Quaternary International*. **133–134**, pp.95–106.

Shennan, I. and Horton, B. 2002. Holocene land- and sea-level changes in Great Britain. *Journal of Quaternary Science*. **17**(5–6), pp.511–526.

Shennan, I., Innés, J.B., Long, A.J. and Zong, Y. 1995. Holocene relative sea-level changes and coastal vegetation history at Kentra Moss, Argyll, northwest Scotland. *Marine Geology*. **124**(1), pp.43–59.

Shennan, I., Innes, J.B., Long, A.J. and Zong, Y. 1994. Late Devensian and Holocene relative sealevel changes at Loch nan Eala, near Arisaig, northwest Scotland. *Journal of Quaternary Science*. **9**(3), pp.261–283.

Shennan, I., Innes, J.B., Long, A.J. and Zong, Y. 1993. Late Devensian and Holocene relative sea-level changes at Rumach, near Arisaig, northwest Scotland. *Norsk Geologisk Tidsskrift*. **73**, 161 174.

Shennan, I., Lambeck, K., Horton, B., Innes, J., Lloyd, J., McArthur, J., Purcell, T. and Rutherford, M. 2000. Late Devensian and Holocene records of relative sea-level changes in northwest Scotland and their implications for glacio-hydro-isostatic modelling. *Quaternary Science Reviews*. **19**(11), pp.1103–1135.

Simms, A.R., Best, L., Shennan, I., Bradley, S.L., Small, D., Bustamante, E., Lightowler, A., Osleger, D. and Sefton, J. 2022. Investigating the roles of relative sea-level change and glacio-isostatic adjustment on the retreat of a marine based ice stream in NW Scotland. *Quaternary Science Reviews*. **277**, p.107366.

Simpson, J.B. 1934. XXIV.—The Late-Glacial Readvance Moraines of the Highland Border West of the River Tay. *Earth and Environmental Science Transactions of The Royal Society of Edinburgh*. **57**(3), pp.633–646.

Sissons, J.B. 1981. The last Scottish ice-sheet: facts and speculative discussion. *Boreas*. **10**(1), pp.1–17.

Smith, D., Fretwell, P., Cullingford, R. and Firth, C. 2006. Towards improved empirical isobase models of Holocene land uplift for mainland Scotland, UK. *Philosophical transactions. Series A, Mathematical, physical, and engineering sciences*. **364**, pp.949–72.

Smith, D.E. 2005. Evidence for Secular Sea Surface Level Changes in the Holocene Raised Shorelines of Scotland, UK. *Journal of Coastal Research*. **42**, pp.26–42.

Smith, D.E., Barlow, N.L.M., Bradley, S.L., Firth, C.R., Hall, A.M., Jordan, J.T. and Long, D. 2019. Quaternary sea level change in Scotland. *Earth and Environmental Science Transactions of The Royal Society of Edinburgh*. **110**(1–2), pp.219–256.

Smith, D.E., Harrison, S., Firth, C.R. and Jordan, J.T. 2011. The early Holocene sea level rise. *Quaternary Science Reviews*. **30**(15), pp.1846–1860.

Spikins, P. 2008. Mesolithic Europe : glimpses of another world *In*: G. Bailey and P. Spikins, eds. *Mesolithic Europe*. New York: Cambridge University Press, pp.1–17.

Stockmar, J. 1971. Tablets with Spores used in Absolute Pollen Analysis. *Pollen et Spores*. **13**, pp.615–621.

Stuiver, M. and Reimer, P.J. 1993. CALIB rev. 8.

Terberger 2006. From the First Humans to the Mesolithic Hunters in the Northern German Lowlands - Current Results and Trends *In*: *Across the western Baltic*. Sydsjællands Museums.

Tierney, J.E., Zhu, J., King, J., Malevich, S.B., Hakim, G.J. and Poulsen, C.J. 2020. Glacial cooling and climate sensitivity revisited. *Nature*. **584**(7822), pp.569–573.

Troels-Smith, J. 1955. Karakterisering af løse jordarter. *Danmarks Geologiske Undersøgelse IV. Række*. **3**(10), pp.1–73.

UKHO 1993. Admiralty tide tables. v.1: European waters, including Mediterranean Sea.

Van der Werff A, Huls H. 1958. *Diatomeeenflora van Nederland*. De Hoef: The Netherlands: Published privately.

de la Vega Leinert, A.C., Smith, D.E. and Jones, R.L. 2012. Holocene Coastal Barrier Development at Bay of Carness, Mainland Island, Orkney, Scotland. *Scottish Geographical Journal*. **128**(2), pp.119–147.

Walker, J., Gaffney, V., Fitch, S., Harding, R., Fraser, A., Muru, M. and Tingle, M. 2022. The archaeological context of Doggerland during the final Palaeolithic and Mesolithic *In*: V. Gaffney and S. Fitch, eds. *Europe's Lost Frontiers: Volume 1* [Online]. Context and Methodology. Archaeopress, pp.63–88. [Accessed 1 August 2024]. Available from: https://www.jstor.org/stable/jj.15135930.12.

Walker, M., Head, M.J., Berkelhammer, M., Björck, S., Cheng, H., Cwynar, L., Fisher, D., Gkinis, V., Long, A., Lowe, J., Newnham, R., Rasmussen, S.O. and Weiss, H. 2018. Formal ratification of the subdivision of the Holocene Series/Epoch (Quaternary System/Period): two new Global Boundary Stratotype Sections and Points (GSSPs) and three new stages/subseries. *Episodes Journal of International Geoscience*. **41**(4), pp.213–223.

Walker, M. and Lowe, J. 2019. Lateglacial environmental change in Scotland. *Earth and Environmental Science Transactions of the Royal Society of Edinburgh*. **110**(1–2), pp.173–198.

Walker, M. and Lowe, J. 1990. Reconstructing the environmental history of the last glacial-interglacial transition: Evidence from the Isle of Skye, Inner Hebrides, Scotland. *Quaternary Science Reviews*. **9**(1), pp.15–49.

Ward, S.L., Neill, S.P., Scourse, J.D., Bradley, S.L. and Uehara, K. 2016. Sensitivity of palaeotidal models of the northwest European shelf seas to glacial isostatic adjustment since the Last Glacial Maximum. *Quaternary Science Reviews*. **151**, pp.198–211.

Wentworth, C.K. 1922. A Scale of Grade and Class Terms for Clastic Sediments. *The Journal of Geology*. **30**(5), pp.377–392.

Whitehouse, P.L. 2018. Glacial isostatic adjustment modelling: historical perspectives, recent advances, and future directions. *Earth Surface Dynamics*. **6**(2), pp.401–429.

Williamson, I.T. and Bell, B.R. 1994. The Palaeocene lava field of west-central Skye, Scotland: Stratigraphy, palaeogeography and structure. *Earth and Environmental Science Transactions of The Royal Society of Edinburgh*. **85**(1), pp.39–75.

Woodroffe, S.A., Hill, J., Bustamante-Fernandez, E., Lloyd, J.M., Luff, J., Richards, S. and Shennan, I. 2023. On the varied impact of the Storegga tsunami in northwest Scotland. *Journal of Quaternary Science*. **38**(8), pp.1219–1232.

Woodroffe, S.A. and Horton, B.P. 2005. Holocene sea-level changes in the Indo-Pacific. *Journal of Asian Earth Sciences*. **25**(1), pp.29–43.

Woodroffe, S.A., Long, A.J., Punwong, P., Selby, K., Bryant, C.L. and Marchant, R. 2015. Radiocarbon dating of mangrove sediments to constrain Holocene relative sea-level change on Zanzibar in the southwest Indian Ocean. *The Holocene*. **25**(5), pp.820–831.

Wygal, B.T. and Heidenreich, S.M. 2014. Deglaciation and Human Colonization of Northern Europe. *Journal of World Prehistory*. **27**(2), pp.111–144.

APPENDIX

Appendix A: Publication submitted to Journal of Quaternary Science in August 2024. Documents is available on request. Referenced as follows:

Hardy, K., Barlow, N.L.M., Taylor, E., Bradley, S.L. 2024. [Forthcoming] At the far end of everything: An Ahrensburgian presence in the far north of the Isle of Skye, Scotland. *Journal of Quaternary Science*.